Changes in terrestrial ecosystem across the Cretaceous-Paleogene boundary in western Canada inferred from plant wax lipid distributions and isotopic measurements

Robert D. Bourque[1], Peter M. J. Douglas[1], Hans C. E. Larsson[2]

[1] Department of Earth and Planetary Sciences, Geotop Research Centre, McGill University, 3450 University Street H3A 0E8, Montreal, Quebec, Canada.

[2] Redpath Museum, McGill University, 859 Sherbrooke Street West H3A 0C4, Montreal, Quebec, Canada.

Abstract

Changes in terrestrial environments across the Cretaceous-Paleogene boundary, including plant ecology and carbon and water-cycling, remain poorly defined. Fluvial sediments spanning the Cretaceous-Paleogene (K-Pg) boundary of southern Saskatchewan, Canada contain well preserved plant wax *n*-alkanes that provide a means of reconstructing changes to plant ecology and carbon and water cycling during this mass extinction event. We measured *n*-alkane carbon ($\delta^{13}C$) and hydrogen ($\delta^{2}H$) isotope ratios in two sedimentary sections and applied established fractionation factors to estimate the isotopic compositions of precipitation and bulk sedimentary organic matter sources. We also analyzed the distribution of *n*-alkanes as an indicator of the relative abundance of aquatic and terrestrial plants. We find a consistent shift towards a greater relative abundance of longer-chain *n*-alkanes across the boundary, implying a persistent increase in the relative abundance of terrestrial plants in the sedimentary basin. This is consistent with an increase in birch and elm palynomorphs immediately above the boundary. We hypothesize the extinction of all large herbivores at the boundary may have facilitated this transition to a terrestrial angiosperm dominated flora immediately after the boundary. We also find that the

region was characterized by isotopically light precipitation, with δ^2H values between -95‰ to -160‰ but do not observe evidence for major millennial-scale changes in regional precipitation isotopic composition spanning the boundary. *n*-Alkanes derived from both aquatic and terrestrial plants at one site display an upward trend in $\delta^{13}C$ values of approximately 2‰ across the K-Pg boundary. This suggests millennial-scale local or global carbon-cycle variability altering either plant carbon isotope fractionation or the carbon isotope composition of dissolved inorganic carbon and atmospheric CO_2. Overall our results suggest that carbon and water cycle changes associated with the K-Pg impact in terrestrial environments in western Canada were short-lived, but ecological shifts in plant communities were longer-lasting.

Keywords: plant wax lipids; carbon isotopes; hydrogen isotopes; mass extinction; compound specific isotope analysis; paleohydrology

1. Introduction

The Cretaceous-Paleogene (K-Pg) boundary is the most recent mass extinction event in Earth's history, with an estimated 75% of all plant and animal species on the planet having gone extinct at the time (Norris et al., 1999; Labandeira et al., 2002; Vajda et al., 2001; Wolfe and Upchurch, 1986). The primary driver of the extinction has been linked to an asteroid impact (Alvarez et al., 1980; Smit and Hertogen, 1980) that occurred near the present-day Yucatán Peninsula, Mexico (Hildebrand et al., 1991). However, identifying the cause of the extinction event is complicated by evidence of large shifts in global climate (Wilf et al., 2003; Petersen et al., 2016-a) and large-scale volcanism from the Deccan Traps of present day India occurring across the K-Pg boundary (Schoene et al., 2019; Sprain et al., 2019). A range of hypotheses has

been put forth on the effects such an impact would have caused to the Earth system, none mutually exclusive from each other, which have ranged from the release of a large enough volume of aerosols to create an extended period of darkness (Pope et al., 1994), short-term global cooling on the order of tens to hundreds of years (Vellekoop et al., 2014; Vellekoop et al., 2016), and warming that lasted for several millennia (MacLeod et al., 2018; Vellekoop et al., 2018). The K-Pg boundary is marked by an iridium-rich clay layer which has been mostly been associated with the fallout of an impact (Alvarez et al., 1980). In addition, a negative carbon isotope excursion (CIE) is one of the defining features of the extinction event (Arens and Jahren, 2000), and implies a global change in carbon cycling and a net input of ^{13}C depleted carbon to the atmosphere, although the duration, magnitude, and cause of this CIE remains subject to debate (Renne et al., 2013).

However, these data alone do not sufficiently resolve the large number of processes that could have altered the global carbon cycle. The isotopic signal of bulk sedimentary organic carbon, which is primarily used to infer the CIE in terrestrial sediments as well as some marine strata, is a complex mixture of multiple carbon-cycle processes as it represents a mixed signal of all sedimentary organic carbon sources, and does not account for differential carbon isotope fractionation by different primary producers, or the effects of subsequent decomposition and diagenesis (Sepúlveda et al., 2019). Most research on carbon cycle changes associated with the impact has come from marine records, where studies have shown a decoupling of the deep ocean and surface ocean carbon reservoirs and diminished transport of organic matter from the surface to the deep ocean. This shutdown of the biological pump has been estimated to last hundreds of thousands of years (D'Hondt et al., 1998, Alegret and Thomas, 2009). Despite this long-term reduction in transport of carbon to the deep ocean, surface ocean primary productivity is

estimated to have recovered within a period of 10,000 years (Alegret and Thomas, 2009), with some groups of planktonic organisms closer to shorelines and in the upper reaches of the deep ocean having shown evidence of also having recovered on even shorter time spans (Sepúlveda et al., 2019). A similarly rapid recovery is inferred to have occurred in terrestrial ecosystems (Vajda et al., 2001). In contrast with the relatively detailed studies of carbon-cycle changes, there are few data that constrain the effects the impact had on global or regional water cycling. This is important as changes in the water cycle strongly affect terrestrial ecosystem productivity and function, which could have potentially exacerbated ecological or carbon-cycle changes caused by the impact (Moore et al., 2007; Setegn et al., 2011).

The pre-impact climate was in the midst of cooling of approximately 5-8 °C that has been documented for the last 100,000 years of the Maastrichtian, following a period of warming of 2.5-5 °C over the preceding 150,000-300,000 years (Petersen et al., 2016-a). This warming event has been linked to eruption (Barnet et al., 2018) or degassing (Hull et al., 2020) associated with Deccan Traps volcanism that was occurring in the late Maastrichtian, and which is suggested to been an early driver of extinctions before the impact (Petersen et al., 2016-a). High-resolution reconstructions of global temperatures and carbonate $\delta^{13}C$ values indicate a cooling of approximately 2 °C over the 200,000 years preceding the K-Pg boundary and a dramatic drop in $\delta^{13}C$ at the boundary, with carbon isotope recovery in marine systems not occurring until nearly 1 Myr later (Hull et al. 2020). Combining the estimated temperatures and carbonate isotopes with modeling, Hull et al. (2020) suggested that Deccan Trap outgassing would not have been responsible for boundary CIE and suggested instead that biological processes were responsible. It is important to note that the CIE preserved in terrestrial sediments is estimated to have been much shorter in duration, lasting approximately 5,000 to 10,000 years (Renne et al., 2013).

Constraints on ecosystem recovery provided an important framework for understanding possible changes in the terrestrial carbon and water cycles. There is evidence that plant communities recovered in a fairly short amount of time, taking as little as 10 years to recover (Lomax et al., 2001; Maruoka et al., 2007). Along with changes to climate, changes to plant ecology across the extinction event have been inferred, with pollen studies indicating key trends in plant group abundance (Braman and Sweet, 1999; Sweet et al., 1999; Vajda et al., 2001). For example, studies from southwestern Canada show highly diverse angiosperm communities before the impact (McIver, 1999; McIver 2002). The impact was directly followed by several spikes in fern pollen, which is observed on a global level (Vajda et al., 2001), followed by the repopulation of angiosperms and gymnosperms, with angiosperm recovery slightly earlier and dominating the relative abundance of woody plant pollens (Sweet and Braman, 1992; Braman and Sweet, 1999; Sweet et al., 1999). It has also been demonstrated that while angiosperms and gymnosperms recovered relatively quickly over only a few thousand years (McIver, 1999; Vajda and Rained, 2003; Vajda and McLoughlin, 2007), biodiversity for these two groups of plants remained low for over one million years (McElwain and Punyasena, 2007).

The objective of this study was to perform measurements of plant wax *n*-alkane distributions and carbon and hydrogen isotopes, alongside measurements of bulk sediment organic matter (OC) carbon isotopes, across the K-Pg boundary to infer changes to the carbon and water cycles and to plant ecology before and after the impact. *n*-Alkane measurements can provide insights into the carbon isotope compositions of atmospheric CO_2 and the hydrogen isotope composition of precipitation, providing a unique means of examining changes to carbon and water cycling (Sachse et al., 2012; Diefendorf and Freimuth, 2017). Additionally, indices of the relative abundance of *n*-alkanes of different chain lengths can be used as an indicator of

changes in the sources of the plant waxes, and thus changes the relative abundance of different plant groups (Ficken et al., 2000; Liu et al., 2019).

2. Methodology

2.1 Study area and stratigraphic sections

The samples analyzed in this study were taken from a pair of sites in southern Saskatchewan, Canada. The two specific sampling locations were Chambery Coulee (CC) and Highway 37 (HW37, Figure 1), located at 49°N, 108°W and 49°35'28.03"N, 108°42'57.50"W respectively. Coordinates for CC are approximate in agreement with the wishes of the private landowners. These sites were chosen because of the exceptional preservation of the K-Pg boundary (McIver et al., 2002; Bamforth et al., 2014; Jerrett et al., 2015; Redman et al., 2015) as well as for the presence of sedimentary units of both the uppermost Frenchman and lowermost Ravenscrag formations.

The Frenchman Formation is a unit of latest Cretaceous aged strata that is contiguous with the Hell Creek Formation of Montana. Both the Hell Creek and Frenchman formations have similar fauna and are composed of latest Cretaceous sediments leading up to and including the K-Pg boundary. The Frenchman Formation is composed of sand and clay lithosome units (Kupsch, 1957) which can further be categorized into broader sandstone and mudstone units that cycle through fining upward sequences (Bamforth, 2013). Magnetostratigraphy of sections from Grasslands National Park, which are 100-150 km from the sites in this study, show that the upper Frenchman Formation spans approximately 300,000 to 500,000 years (Bamforth, 2013). Based on an average thickness of the upper Frenchman Formation of 35 meters, this implies an

approximate average sedimentation rate of 8,500 to 14,000 years per meter, although it is likely that sedimentation rates varied substantially within the formation and there may be unconformities. Magnetostratigraphic analyses of the Frenchman Formation have confirmed that the K-Pg boundary occurs at the top of the formation (Bamforth, 2013). The K-Pg boundary is marked by a thin layer of tonstein, a sedimentary rock primary composed of kaolinite clay, that has been found globally and is thought to be related to fallout from the Chicxulub impact (Alvarez et al., 1980; Smit and Hertogen, 1980).

The overlying Ravenscrag Formation is earliest Paleocene in age and is predominantly composed of silt. The lowest layers of the Ravenscrag Formation are composed of the Ferris coal seam, which overlies the iridium-rich boundary clay layer (McIver, 1989). A recent study estimated that the potential rate of peat accumulation that formed the Ferris Coal seam would have been 0.4 mm/yr with the total duration of the coal seam (~20 cm) lasting as long as 75,000 years (Jerrett et al., 2015). At the time of sediment deposition these sites were located at a paleolatitude similar to their current latitude, between 49° and 52° N (Bamforth, 2013). The sites were also within 1000 km of the Western Interior Seaway (WIS), a large seaway that flooded the interior basin of North America during the Late Cretaceous period (Berry, 2017), and the Frenchman Formation has been described as forming in a coastal floodplain (Kupsch, 1957). The Cretaceous-aged rocks of western Canada were not deeply buried or heated (Walls et al., 1979), which implies good potential for preservation of the plant wax *n*-alkanes applied in this study.

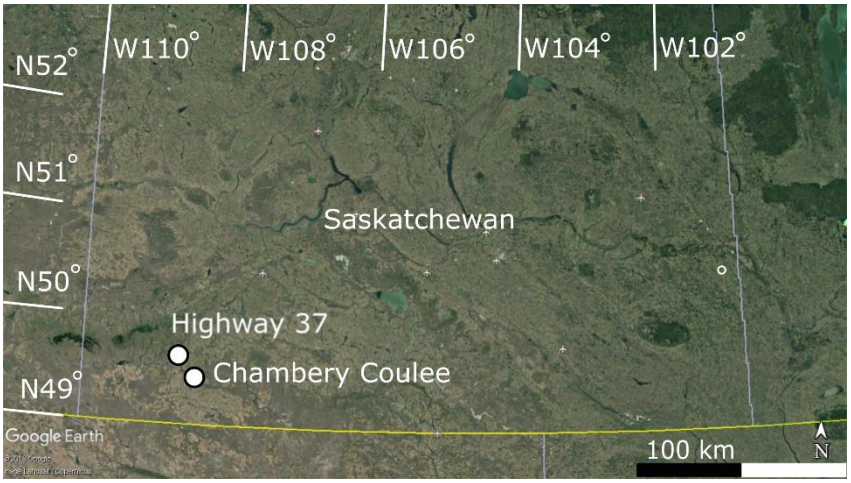

Figure 1. Map of southern Saskatchewan with the field sites for HW37 and CC marked. Photo taken from Google Earth Pro.

The site at CC (Figure 2-b) is a relatively small exposure on private property, with the exposure extending down a slope leading into the Frenchman River Valley near a dirt road. The site has over 30 meters of exposed strata with around 6 meters of the lowermost Ravenscrag overlying the Frenchman Formation, which can be up to 35 meters thick in some areas. The site of HW37 (Figure 2-a) is a recently exposed outcrop that was uncovered during the construction of the highway for which it is named, about 20 km south of Shawnovan, SK (McIver, 2002). The K-Pg section at this site has undergone little weathering due to the recently exposed nature of the site. The section is 18 m thick with around 9 meters of strata from each of the formations exposed, with the top of the section capped by Quaternary glacial till. The two sites are separated by 28.5 km, providing a comparison of geographically proximal strata.

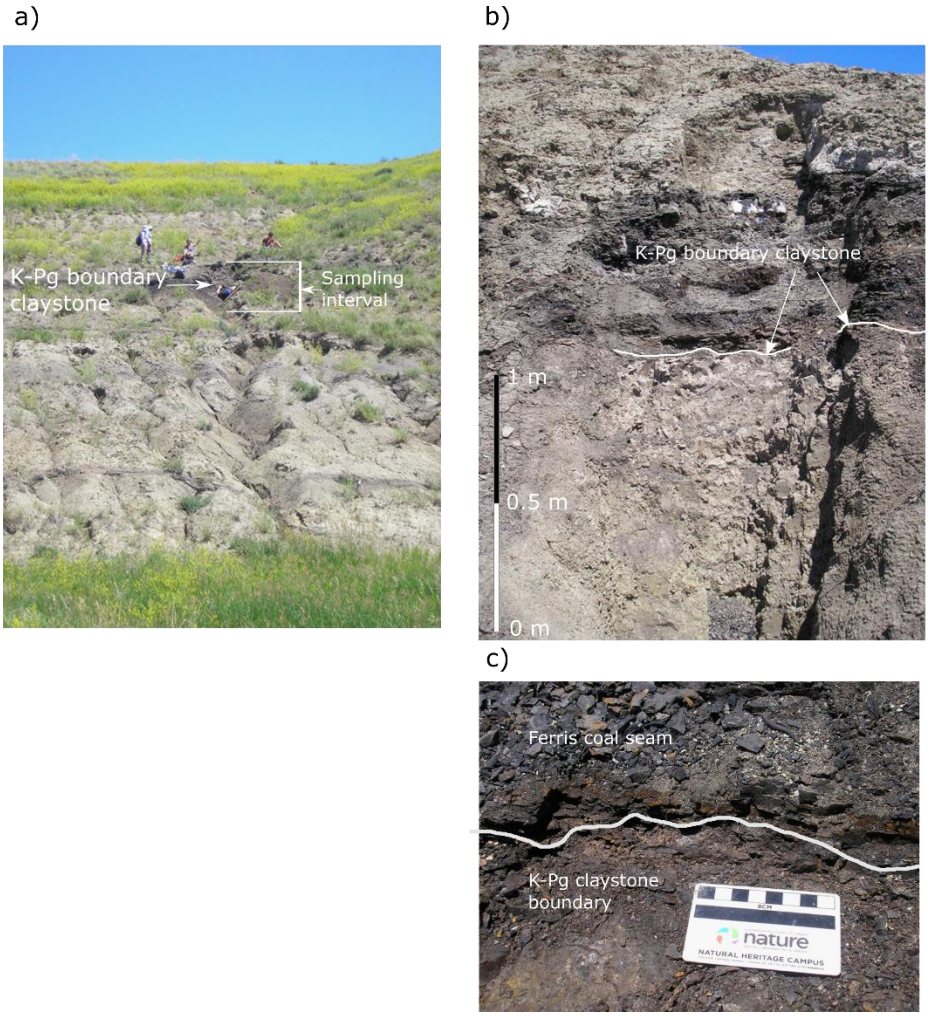

Figure 2: Photos of the field sites visited for sample collection. (A) The roadside of HW37, with the two-meter boundary section located next to seated field assistants. (B) Photo of the section at CC, with the 2-meter section exposed in the frame. The dark layer centered in the image is the Ferris coal seam with the boundary sandwiched between the coal layer and the larger bed of siltstone below it. (B) Close up of the K-Pg boundary from CC, indicated by a faintly pink-brown layer of clay found underneath the dark shelf of coal above, with the scale bar level with the boundary.

2.2 Sample collection

Sampling was focused within a 1 m window above and below the K-Pg boundary. Two types of samples were collected: 1) larger samples with an average weight of 400 g collected for the leaf wax isotopic analysis at a resolution of 10 cm; and 2) smaller samples of at least 5 mg

collected for bulk organic carbon $\delta^{13}C$ analyses at a resolution of 2 cm. In total, 22 compound specific isotope samples from CC and 25 samples from HW37 were analyzed, and 68 bulk OC isotope samples from CC and 68 samples from HW37 were analyzed.

2.3 Bulk $\delta^{13}C$ analyses

Around 5 mg of sediment per sample was ground to a fine powder with a mortar and pestle. Bulk organic carbon content (%OC) and $\delta^{13}C$ values were analyzed at the Geotop Light Stable Isotope Laboratory at the University of Quebec at Montreal. The samples were acid fumigated in silver capsules prior to analysis to remove inorganic carbon (Harris et al., 2001). The silver capsules were then closed and placed within tin capsules to be analyzed, with the samples being processed on an Isoprime 100 MicroCube mass spectrometer coupled to an Elemental Vario MicroCube elemental analyzer in Continuous Flow mode. A first analysis measured the weight percent organic carbon (%OC), and a second analysis measured the $\delta^{13}C$ value of organic carbon. Laboratory $\delta^{13}C$ standards with values of -42.5‰ and -17.0‰ (VPDB) were used for correcting raw data with a calibration line. These laboratory reference materials were normalized on the NBS19-LSVEC scale for $\delta^{13}C$. A third internal reference with a $\delta^{13}C$ value of -28.7‰ was used to ensure accuracy of the calibration. The analytical error of the bulk $\delta^{13}C$ analyses was ±0.3‰.

2.4 Lipid extraction and analysis

Sediments for compound specific isotope analysis were first freeze dried, ground into a fine powder, and weighed. The amount of sediment extracted varied depending on organic carbon content, with carbon-rich samples typically requiring 40 g of sediment while carbon-poor samples required up to 200 g of sediment to yield sufficient *n*-alkanes for isotopic analysis. The

sediments were put into CEM MARS 6 solvent extraction tubes, along with a 9:1 ratio of dichloromethane (DCM) to methanol solution, with the volume of solvent scaled to the volume of sediment (approximately 1:1 sediment/solvent by volume), followed by extraction using a MARS6 microwave at a temperature of 80° C for 15 minutes. Samples were then transferred into vials to be centrifuged to separate residual sediment from solvent, before pippeting the solvent and transferring it to evaporation tubes. The sediment was then further rinsed with solvent and centrifuged three times. Once all the samples were extracted, the solvent extracts were placed in a Rapidvap to be evaporated under N_2 gas. A silica gel column was then prepared for lipid purification, with a Pasteur pipette filled with 1 g of silica gel and 0.5 g of sodium sulphate on top of glass wool. Each vial had 15 ml of hexane added, which was then passed through the silica gel column to elute the hydrocarbon fraction. We then collected the polar fraction by eluting 15 ml of methanol, followed by 1 ml of dichloromethane. The polar fraction was reserved for future study.

The samples were analyzed for *n*-alkane relative abundance with a Thermo Trace 13-10 gas chromatograph (GC) with a flame ionization detector (FID), using a Thermo TR-5 GC column (60m x 0.25mmID, 0.25 µm film), at McGill University. *n*-Alkane hydrogen and carbon isotope measurements were made using a Thermo Delta V Plus Isotope Ratio Mass Spectrometer (IRMS) coupled to a Thermo GC-IsoLink at McGill University, which uses a Thermo TG5Ms column (60m × 0.25mm × 0.25µm film). Compound-specific isotope values were calibrated to the V-SMOW and V-PDB scales using a set of *n*-alkane standards (Mix A6) that were measured offline in references to international standards at Indiana University (arndt.schimmelmann.us/compounds.ht). The Mix A6 standards were used to calibrate both hydrogen and carbon isotope measurements for *n*-alkanes and were analyzed at least twice daily.

The Mix A6 δ^2H and $\delta^{13}C$ standard values can be found in supplementary table 1. Laboratory standards were also analyzed to monitor for instrumental drift and assess measurement reproducibility. The laboratory standards were derived from extracts of maple (*Acer* sp.) leaves that were collected on the McGill campus, with synthetic alkanes (SigmaAldrich) added to enhance the C_{22} and C_{30} *n*-alkane concentrations. The maple standard measurements were analyzed for, with δ^2H values of -173.5‰ for C_{22}, -194.3‰ for C_{27}, -175.5‰ for C_{29}, -51. 5‰ for C_{30}, and -167.7‰ for C_{31}. The $\delta^{13}C$ values are -28.9‰ for C_{20}, -30.9‰ for C_{27}, -35.3‰ for C_{29}, -33.0‰ for C_{30}, and -37.0‰ for C_{31}. Laboratory standards were run after every 3 samples to check for instrumental drift. The long-term standard deviations of the laboratory standard *n*-alkane $\delta^{13}C$ measurements over the course of the study was 0.3‰, while the standard deviation of the laboratory standard δ^2H measurements was 4‰.

To estimate the uncertainty of compound-specific isotope measurements we followed the recommendations of Polissar and D'Andrea (2014). Specifically, we calculated the pooled standard deviation for the C_{25}, C_{27}, and C_{29} *n*-alkane $\delta^{13}C$ and δ^2H values, including all samples with replicate measurements from both sites, using the formula:

$$SD_{pooled} = \sqrt{\frac{(n_1-1)s_1{}^2+(n_2-1)s_2{}^2+\cdots+(n_k-1)s_k{}^2}{n_1+n_2+\cdots+n_k-k}} \quad \textbf{(1)}$$

Where n is the number of replicates per sample, s is the sample standard deviation, and k is the total number of samples measured per chain length.

We then calculated the standard error for each sample, including samples with only one measurement (Polissar and D'Andrea 2014; Niedemeyer et al., 2010), as follows.

$$SE = \frac{SD_{pooled}}{\sqrt{n}} \quad \textbf{(2)}$$

The resulting standard error is considered to be the most accurate estimate of measurement uncertainty for individual samples (Polissar and D'Andrea, 2014).

2.5 n-Alkane chain length analyses

We calculated two indices of the relative abundance of different *n*-alkanes within each sample. The average chain length (ACL) is based on the following equation.

$$ACL = \frac{(A23*23)+(A24*24)+(A25*25)+(A26*26)+(A27*27)+(A28*28)+(A29*29)+(A30*30)+(A31*31)}{A23+A24+A25+A26+A27+A28+A29+A30+A31} \quad \textbf{(3)}$$

Where Ax is the area of the GC-FID trace for a specific *n*-alkane chain length (x).

The Paq' index (Liu et al., 2019), which is applied to determine if *n*-alkanes are predominately derived from aquatic or terrestrial plants, was calculated using the same measurements. Paq' values are intended to be used in the context of ancient, sediment-derived *n*-alkanes rather than from extant ecosystems (Liu et al., 2019). The calculation is as follows.

$$Paq' = \frac{A21+A23+A25}{A21+A23+A25+A27+A29+A31} \quad \textbf{(4)}$$

Paq' is derived from the previously developed Paq index (Ficken et al., 2000), which is focused on extant ecosystems:

$$Paq = \frac{A23+A25}{A23+A25+A29+A31} \quad \textbf{(5)}$$

Paq' was used for the purpose of this study as it was developed and optimized for analyzing plant wax alkanes from sedimentary rocks. The only notable difference between the two indices is the addition of A21, A27, A31, and A33, and in the calculations for Paq'. However, we did not include A33 in the calculations of this index as the C_{33} *n*-alkane was undetectable in many of our samples.

2.6 Modeled values of bulk $\delta^{13}C$

In order to constrain how changing plant sources of sedimentary organic carbon and plant $\delta^{13}C$ values potentially affected bulk $\delta^{13}C$ values, we calculated a predicted bulk organic $\delta^{13}C$ value based on plant-wax distributions and $\delta^{13}C$ values. This calculation was performed to assess how plant $\delta^{13}C$ values as determined using compound-specific isotope measurements compare with the bulk $\delta^{13}C$ measurements, which would help to examine whether changes in bulk organic $\delta^{13}C$ measurements primarily reflect changes in plant $\delta^{13}C$ and the relative abundance of plant types.

We used C_{25} and C_{29} $\delta^{13}C$ values (after correcting for appropriate fractionation factors) as being representative of aquatic and terrestrial plants, respectively (see Discussion section 4.2 for a detailed rationale). Paq' values were used to estimate the relative abundance of aquatic and terrestrial plant matter contributing to the bulk sedimentary organic carbon.

To perform these calculations we first estimated the fraction of organic matter derived from terrestrial and aquatic plants, using the following equation.

$$Paq' = \left(f_{aq} x Em_{aq}\right) x \left(f_t x Em_t\right) \quad \textbf{(6)}$$

Where Paq' is from the observed measurements, "f" is the fraction of the plant group we are solving for (aq – aquatic, t – terrestrial), and Em is the end-member value of Paq' for terrestrial and submerged aquatic plants. We applied values of $Em_{aq} = 0.80$ and $Em_t = 0.07$ (the minimum and maximum Paq' values observed in our dataset) such hat f_{aq} and f_t were consistently between 0 and 1. To solve for f_{aq} and f_t, we combined equation 4 with the following equation:

$$1 = f_{aq} + f_t \quad \textbf{(7)}$$

Next the bulk $\delta^{13}C$ of aquatic and terrestrial plants were calculated using the following equations:

$$\delta^{13}C_{aquatic} = \frac{(\delta^{13}C_{25}+1000)}{(\frac{\varepsilon_{aq}}{1000}+1)} - 1000 \quad (8)$$

$$\delta^{13}C_{terrestrial} = \frac{(\delta^{13}C_{29}+1000)}{(\frac{\varepsilon_{t}}{1000}+1)} - 1000 \quad (9)$$

Where ε is the carbon isotopic fractionation between bulk plant tissue and the specific *n*-alkane referred to (C_{25} or C_{29}), and $\delta^{13}C_{25}$ and $\delta^{13}C_{29}$ refer to the measured $\delta^{13}C$ value from those specific *n*-alkanes. ε_t (i.e. fractionation between C_{29} and bulk terrestrial plants; -3.1±2.0‰) was derived from Chikaraishi and Naraoka, using measurements of all terrestrial plants in that study (2003). $\varepsilon_{aquatic}$ (i.e. fractionation between C_{25} and bulk aquatic plants -7.4±2.9‰) was derived from measurements of freshwater aquatic plants from Chikaraishi and Naraoka, (2003) and Aichner et al., (2010).

Once the $\delta^{13}C$ of bulk aquatic and terrestrial plants were calculated, the total bulk $\delta^{13}C$ ($\delta^{13}C_{bulk}$) was estimated using the following equation.

$$\delta^{13}C_{bulk} = \left(f_{aq} x \delta^{13}C_{aquatic}\right) + \left(f_t x \delta^{13}C_{terrestrial}\right) \quad (10)$$

These modeled values of bulk $\delta^{13}C$ assumes that the bulk organic matter present in sediments is directly linked to the $\delta^{13}C$ of sedimentary plant-derived OM. This is an oversimplification, as it ignores other sources of carbon, such as algal, microbial, and heterotrophic biomass, and any isotopic effects of sedimentary OM decomposition. However, this analysis provides a first-order indication of how changes in plant inputs and changing plant $\delta^{13}C$ values could interact to influence the bulk $\delta^{13}C$ record.

3. Results

3.1 Percent organic carbon

There is a steady increase in weight percent organic carbon (%OC) leading up to the boundary at both sites, with values rising from below 0.3% to ~3%. Within the boundary clay layer, HW37 (Figure 3-a) has %OC of 10.1% whereas CC (Figure 3-d) had a lower value of 2.6%. Above the boundary, both sites contain very large amounts of organic carbon in the Ferris coal ranging from 28.5% to 70.1%. The coal layer is overlain by relatively carbon-poor strata (0.4% to 1.1%) followed by a second peak in values (12-24%) between 30-50 cm. Following this second peak %OC at CC stabilizes around 0.5%, while at HW37 it stabilizes around 3 to 5%.

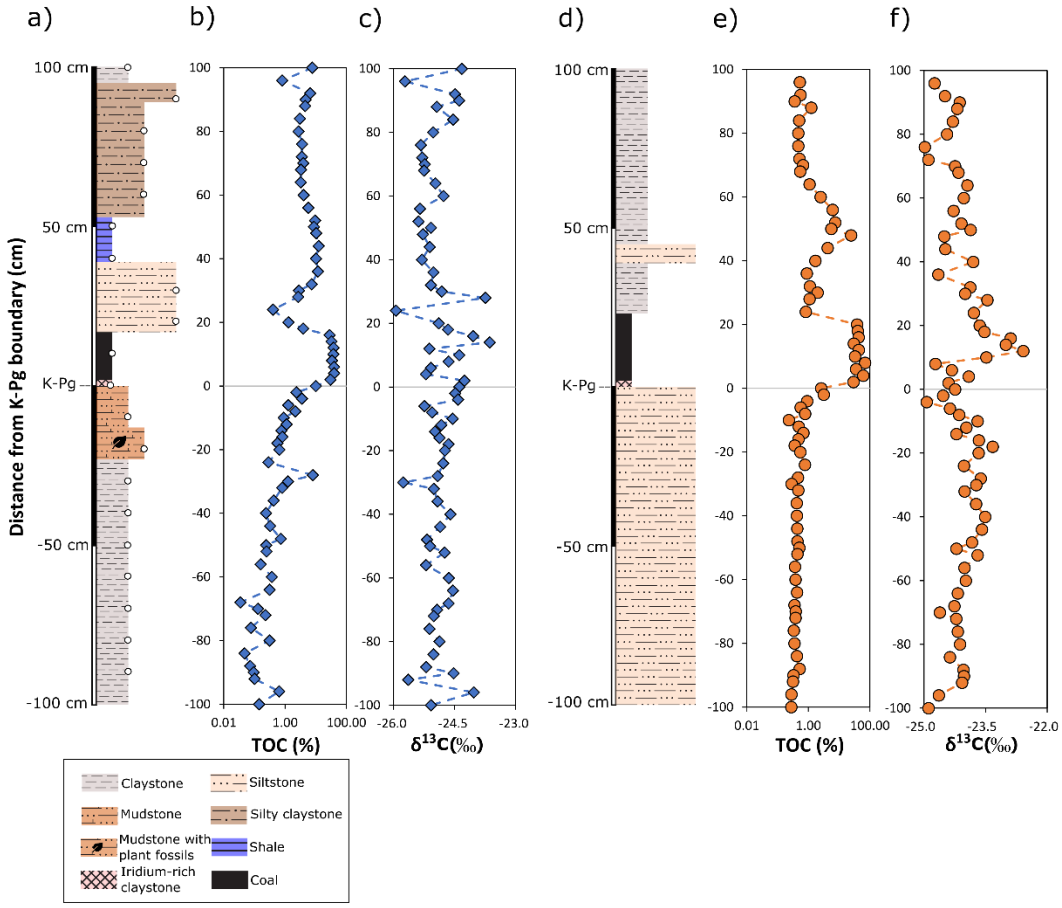

Figure 3: Measurements of percent organic carbon and $\delta^{13}C_{bulk}$ made from the HW37 (a-c) and CC (d-f) sections. TOC values plotted on a logarithmic scale in order to highlight variability below the boundary.

335

Distance from boundary (cm)	HW37 - bulk $\delta^{13}C$ (‰)	HW37 – Corg (%)	CC - bulk $\delta^{13}C$ (‰)	CC – Corg (%)
100	-24.3	7.7		
96	-25.7	0.8	-24.8	0.5
92	-24.5	6.6	-24.5	0.6
90	-24.4	4.7	-24.1	0.4
88	-25.0	4.5	-24.2	1.2
84	-24.5	3.0	-24.3	0.5
80	-25.0	2.8	-24.4	0.5
76	-25.3	3.6	-25.0	0.5
72	-25.3	3.5	-24.9	0.5
70	-25.2	3.9	-24.3	0.7
68	-25.3	3.3	-24.2	0.5
64	-25.0	3.2	-23.9	1.1
60	-24.8	4.1	-24.0	2.5
56	-25.4	5.7	-24.3	6.2
52	-25.4	9.6	-24.1	7.5
50	-25.1	8.7	-23.9	5.5
48	-25.3	10.4	-24.5	24.3
44	-25.1	12.5	-24.5	4.2
40	-25.3	10.1	-23.8	1.7
36	-25.0	11.8	-24.7	0.9
32	-25.1	7.5	-23.9	1.1
30	-24.8	2.8	-24.0	2.0
28	-23.7	2.7	-23.5	1.1
24	-25.9	0.4	-23.8	0.8
20	-24.9	1.3	-23.7	38.3
18	-24.7	3.9	-23.5	40.0
16	-24.0	28.5	-22.9	43.0
14	-23.6	32.6	-23.0	30.1
12	-25.1	38.2	-22.6	43.2
10	-24.4	37.6	-23.5	32.8
8	-24.7	33.8	-24.7	70.1
6	-25.1	39.7	-24.3	35.3
4	-25.2	39.8	-23.9	60.4
2	-24.3	30.2	-24.4	29.1
0	-24.4	10.1	-24.3	2.6
-2	-24.5	2.3	-24.5	3.2
-4	-24.4	3.6	-24.9	0.9
-6	-25.2	1.3	-24.4	0.6
-8	-25.1	2.2	-24.2	0.8
-10	-24.6	0.9	-23.7	0.2
-12	-24.8	1.1	-24.0	0.5
-14	-25.0	0.8	-24.2	0.7
-16	-24.9	0.8	-23.7	0.5
-18	-24.7	0.6	-23.3	0.4
-20	-24.7	0.7	-23.7	0.6
-24	-24.8	0.3	-24.0	0.8
-28	-24.9	8.2	-23.6	0.5
-30	-25.8	1.3	-23.7	0.3

-32	-25.0	0.8	-24.0	0.5
-36	-24.9	0.4	-23.7	0.4
-40	-24.6	0.2	-23.5	0.4
-44	-24.9	0.3	-23.6	0.4
-48	-25.2	0.7	-23.8	0.4
-50	-25.1	0.2	-24.2	0.5
-52	-24.8	0.3	-23.7	0.4
-56	-25.2	0.2	-24.0	0.4
-60	-24.6	0.4	-24.0	0.4
-64	-24.5	0.3	-24.2	0.4
-68	-24.7	0.0	-24.3	0.4
-70	-24.9	0.1	-24.6	0.4
-72	-25.0	0.2	-24.2	0.4
-76	-25.1	0.1	-24.2	0.3
-80	-24.9	0.3	-24.1	0.4
-84	-25.0	0.1	-24.4	0.4
-88	-25.2	0.1	-24.0	0.5
-90	-24.5	0.1	-24.0	0.3
-92	-25.6	0.1	-24.1	0.3
-96	-24.0	0.6	-24.6	0.3
-100	-25.1	0.1	-24.9	0.3

Table 1: $\delta^{13}C_{bulk}$ and organic carbon percentage.

3.2 Bulk organic carbon $\delta^{13}C$

Below the boundary at HW37 (Figure 3-b) bulk $\delta^{13}C$ exhibits fluctuations between -24.5 to -25.2‰, while at CC (Figure 3-e) there is a gradual rise in $\delta^{13}C$ from -24.9‰ to -23.5‰ over 60 cm, followed by a decline to -24.9‰ leading up to the boundary. The values at the boundary are similar at both sites, with HW37 having a value of -24.4‰ and CC having a value of -24.3‰. The samples above the boundary show high-amplitude and high-frequency variability with little correlation between the two sites. Furthermore, there is no clear indication of a negative CIE that is outside the range of background variability of the bulk $\delta^{13}C$ records directly above the K-Pg boundary. Beyond 30 cm above the boundary, the bulk $\delta^{13}C$ signals at the two sites begin to stabilize, with values similar to those observed before the boundary.

3.3 Average chain length

The ACL at HW37 (Figure 4-d) was relatively stable below the boundary with an average length between 26.5 and 27.5. By contrast, CC (Figure 5-d) exhibited lower ACL values below the boundary between 25.3 and 26.3. Both sites also show very similar ACL values at the K-Pg boundary of approximately 26.5. Above the boundary, both sites show higher and more variable ACL values.

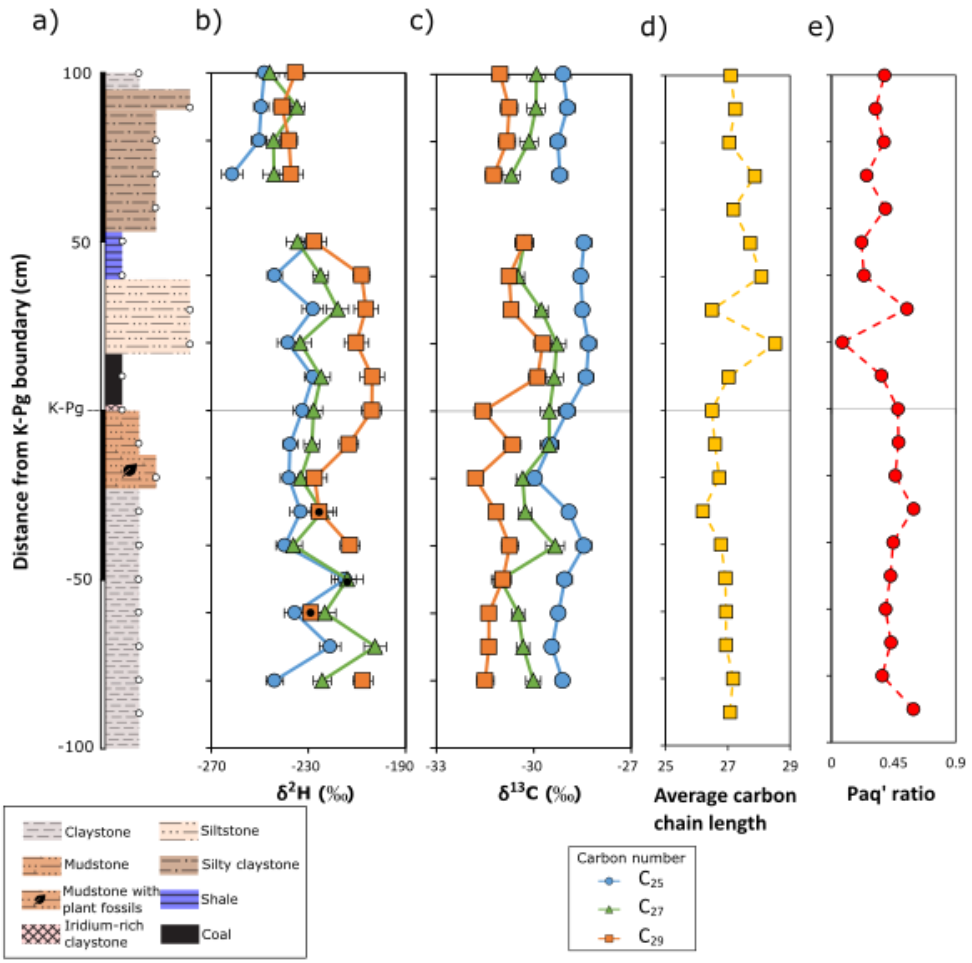

Figure 4: The measurements and calculations made from the HW37 section in relation to *n*-alkane isotopes. Pictured are the stratigraphic section (a), the δ^2H (b) and $\delta^{13}C$ (c) stable isotope measurements derived from plant wax lipids, with black points indicating samples with a single measurement. Average chain length (d) and the Paq' (e) values indicate changes in the abundance of *n*-alkanes derived from aquatic vs terrestrial plants.

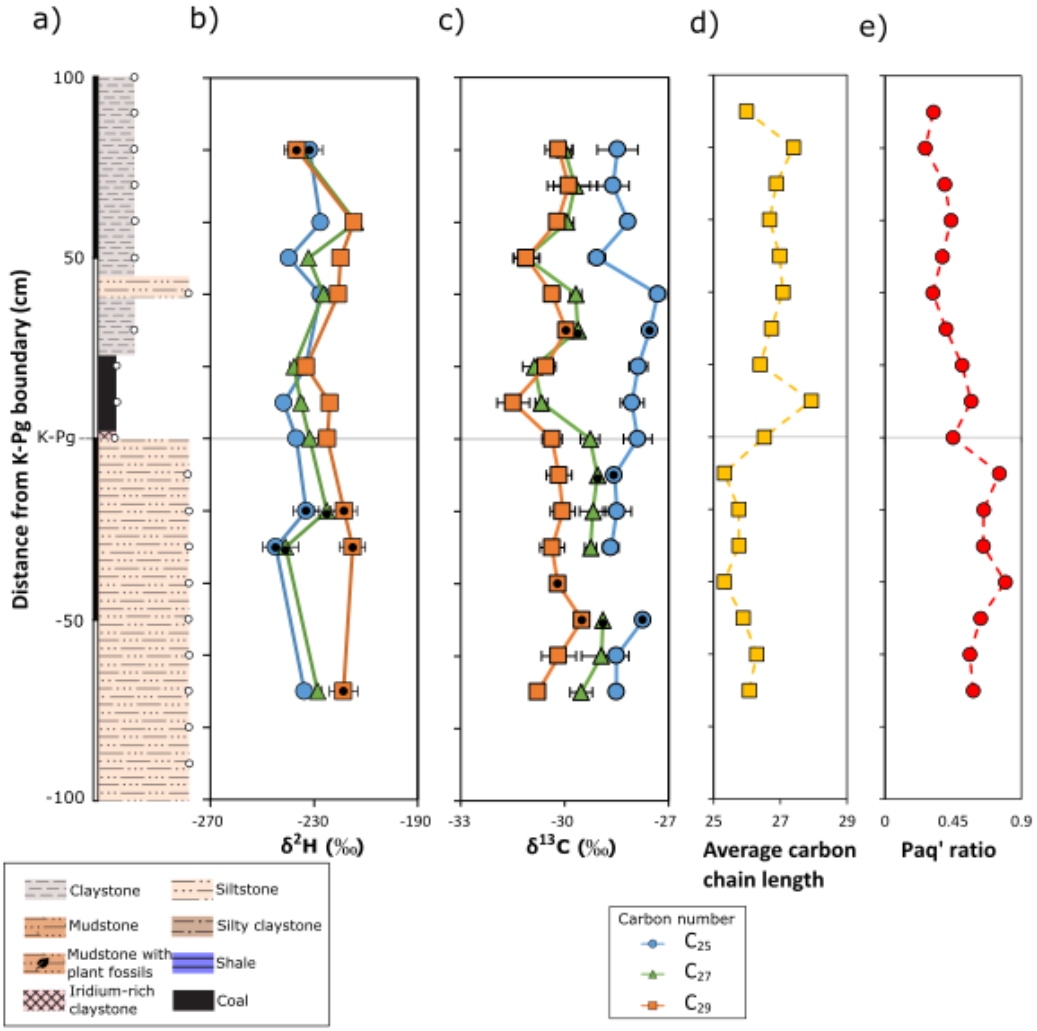

Figure 5: The measurements and calculations made from the CC section in relation to *n*-alkane isotopes. Pictured are the stratigraphic section (a), the δ^2H (b) and $\delta^{13}C$ (c) stable isotope measurements derived from plant wax lipids, with black points indicating samples with a single measurement. Average chain length (d) and the Paq' (e) values indicate changes in the abundance of *n*-alkanes derived from aquatic vs terrestrial plants.

3.4 Paq'

Paq' values (Figure 4-e, 5-e, Table 2) show relatively stable signals below the boundary with standard deviations of approximately 0.1 for both localities. The mean values at HW37 was 0.6 while the mean values at CC was 0.8. A major shift in Paq' occurs above the boundary at

both sites, with samples almost uniformly lower above the boundary than below it. Although the values remain higher at CC than at HW37, the shift to lower values that occurs across the extinction event is comparable in magnitude and is consistent between both sites. At HW37 there is especially high-amplitude variability in Paq' values in the first 40 cm above the boundary.

Distance from boundary (cm)	HW37 - Paq'	CC - Paq'	HW37 - ACL	CC - ACL
100	0.4		27.1	
90	0.3	0.3	27.2	26.0
80	0.4	0.3	27.0	27.4
70	0.3	0.4	27.9	26.9
60	0.4	0.4	27.2	26.7
50	0.2	0.4	27.7	27.0
40	0.2	0.3	28.1	27.1
30	0.5	0.4	26.5	26.7
20	0.1	0.5	28.5	26.4
10	0.4	0.6	27.0	27.9
0	0.5	0.4	26.5	26.5
-10	0.5	0.8	26.6	25.3
-20	0.5	0.7	26.7	25.8
-30	0.6	0.6	26.2	25.8
-40	0.4	0.8	26.8	25.3
-50	0.4	0.6	26.9	25.9
-60	0.4	0.6	26.9	26.3
-70	0.4	0.6	26.9	26.1
-80	0.4		27.2	
-90	0.6		27.1	

Table 2: Paq' and average chain length measurements.

3.5 δ^2H n-alkane isotope measurements

We report the δ^2H values for the C_{25}, C_{27}, and C_{29} *n*-alkanes. Other *n*-alkanes were typically too low in abundance for accurate isotope measurements. At HW37 (Figure 4-b, Table 4), the δ^2H values for each chain length were within the range of -203‰ to -261‰, with C_{25} on average having the most negative values at -236‰ and C_{29} having the highest values with an

384 average of -219‰. The CC (Figure 5-b, Table 3) samples range from -196.2‰ to -245‰, and
385 C_{29} also typically exhibits the most positive values with an average of -223‰ and C_{25} typically
386 has the most negative values with an average of -235‰. There are no clear trends in δ^2H
387 variability in the C_{25} and C_{27} n-alkanes across the studied sections. The C_{29} n-alkanes exhibit
388 greater δ^2H variability between -20 to 50 cm (relative to the boundary), with inconsistent
389 patterns at the two sites. During this interval C_{29} n-alkane δ^2H increases and then decreases by
390 about 25‰ at HW37. In contrast at CC C_{29} n-alkane δ^2H decreases and then increases by about
391 15‰.

392 Some samples for the *n*-alkane isotope measurements were only measured once due to
393 their relatively low concentration. Analysis of samples with a single measurement is at times
394 necessary in compound-specific isotope studies due to small sample sizes (e.g. Niedermeyer et
395 al., 2010), The error estimation technique used for the compound specific isotope analyses takes
396 into account the greater uncertainty associated with non-replicate measurements (Polissar and
397 D'Andrea, 2015; see Section 2.4). However, samples with single measurements are subject to
398 greater uncertainty than other sample analyses, and for this reason we specifically identify these
399 samples in figures 4 and 5. These samples should be interpreted with caution, but in general do
400 not strongly influence our overall interpretation of the data. We note that because of a lack of
401 replicate measurements is a larger degree of uncertainty in compound specific δ^2H values from
402 the CC section below the K-PG boundary.

403

Distance from boundary (cm)	CC - C_{25} δ^2H (‰)	SE - CC - C_{25} δ^2H (‰)	CC - C_{27} δ^2H (‰)	SE - CC - C_{27} δ^2H (‰)	CC - C_{29} δ^2H (‰)	SE - CC - C_{29} δ^2H (‰)
80	*-232*	6	*-235*	6	*-237*	7
60	-227	4	-214	5	-215	5

50	-240	4	-232	5	-220	5
40	-227	4	-226	5	-221	5
20	-233	4	-238	5	-233	5
10	-242	4	-235	5	-224	5
0	-237	4	-232	5	-225	5
-20	*-233*	6	*-225*	6	*-218*	7
-30	*-245*	6	*-241*	6	*-215*	7
-70	-234	4	-229	5	*-219*	7

Table 3: CC δ^2H measurements from plant wax lipids. Samples that were measured once are italicized.

Distance from boundary (cm)	HW37 - C_{25} δ^2H (‰)	SE - HW37 - C_{25} δ^2H (‰)	HW37 - C_{27} δ^2H (‰)	SE - HW37 - C_{27} δ^2H (‰)	HW37 - C_{29} δ^2H (‰)	SE - HW37 - C_{29} δ^2H (‰)
100	-248	4	-246	4	-235	4
90	-249	3	-235	3	-241	4
80	-250	3	-244	3	-238	4
70	-261	4	-244	5	-237	5
50	-229	4	-235	5	-228	5
40	-244	3	-225	3	-208	4
30	-228	4	-218	5	-206	5
20	-238	4	-233	5	-210	5
10	-228	4	-225	4	-204	5
0	-233	4	-228	4	-204	4
-10	-237	3	-229	3	-213	4
-20	-238	4	-233	4	-227	5
-30	-233	4	-224	5	*-226*	7
-40	-240	4	-236	4	-213	4
-50	-215	4	*-214*	6		
-60	-236	4	-223	5	*-229*	7
-70	-221	4	-203	5		
-80	-244	4	-224	4	-208	4

Table 4: HW37 δ^2H measurements from plant wax lipids. Blank entries indicate no measurement due to low concentration. Samples that were measured once are italicized.

3.6 $\delta^{13}C$ n-alkane isotope measurements

The $\delta^{13}C$ values from HW37 (Figure 4-c, Table 6) range from -28.3‰ to -31.8‰, with shorter hydrocarbon chains consistently expressing more positive values than those of longer

chain lengths, with C_{25} measurements averaging -29.0‰, while C_{29} averages -30.9‰. The CC (Figure 5-c, Table 5) samples range from -27.3‰ to -31.5‰, exhibiting the same pattern as HW37 with the shorter chain length hydrocarbons having more positive values. At CC the C_{25} values average -28.2‰ and C_{29} values average -30.3‰. At HW37 we observe an increase of 2 to 2.5‰ in the C_{25} and C_{29} n-alkanes respectively between -20 to +20 cm, which is not apparent in the other n-alkanes. At CC we observe a similar 2‰ enrichment in the C_{25} n-alkane between -20 to +40 cm, but not in the C_{29} n-alkane. At both HW37 and CC we observe short-term depletions (spanning 10 cm) in C_{29} $\delta^{13}C$ (at 0 and +10 cm respectively), of 1 to 1.5‰.

Distance from boundary (cm)	CC - C_{25} $\delta^{13}C$ (‰)	SE - CC - C_{25} $\delta^{13}C$ (‰)	CC - C_{27} $\delta^{13}C$ (‰)	SE - CC - C_{27} $\delta^{13}C$ (‰)	CC - C_{29} $\delta^{13}C$ (‰)	SE - CC - C_{29} $\delta^{13}C$ (‰)
80	-28.5	0.2	-30.0	0.3	-30.2	0.3
70	-28.6	0.2	-29.7	0.2	-29.9	0.2
60	-28.2	0.2	-29.9	0.3	-30.2	0.3
50	-29.1	0.2	-31.1	0.3	-31.1	0.3
40	-27.3	0.2	-29.7	0.3	-30.4	0.3
30	*-27.5*	0.3	*-29.6*	0.4	*-29.9*	0.4
20	-27.9	0.2	-30.9	0.3	-30.5	0.3
10	-28.1	0.2	-30.7	0.3	-31.5	0.3
0	-27.9	0.2	-29.3	0.3	-30.4	0.3
-10	*-28.6*	0.3	*-29.0*	0.4	-30.2	0.3
-20	-28.5	0.2	-29.2	0.2	-30.1	0.2
-30	-28.7	0.2	-29.3	0.2	-30.4	0.2
-40					*-30.2*	0.4
-50	*-27.7*	0.3	*-28.9*	0.4	*-29.5*	0.4
-60	-28.5	0.2	-28.9	0.3	-30.2	0.3
-70	-28.5	0.2	-29.5	0.3	-30.8	0.3

Table 5: CC $\delta^{13}C$ measurements from plant wax lipids. Blank entries indicate no measurement due to low concentration. Samples that were measured once are italicized.

Distance from boundary (cm)	HW37 - C_{25} $\delta^{13}C$ (‰)	SE - HW37 - C_{25} $\delta^{13}C$ (‰)	HW37 - C_{27} $\delta^{13}C$ (‰)	SE - HW37 - C_{27} $\delta^{13}C$ (‰)	HW37 - C_{29} $\delta^{13}C$ (‰)	SE - HW37 - C_{29} $\delta^{13}C$ (‰)
100	-29.1	0.2	-29.9	0.3	-31.0	0.3
90	-29.0	0.2	-29.9	0.3	-30.8	0.3
80	-29.3	0.2	-30.2	0.3	-30.8	0.3
70	-29.2	0.2	-30.7	0.3	-31.2	0.3
50	-28.4	0.2	-30.3	0.3	-30.3	0.3
40	-28.5	0.2	-30.5	0.2	-30.8	0.2
30	-28.5	0.2	-29.8	0.2	-30.7	0.2
20	-28.3	0.2	-29.3	0.3	-29.7	0.3
10	-28.4	0.2	-29.4	0.3	-29.9	0.3
0	-29.0	0.2	-29.5	0.3	-31.6	0.3
-10	-29.5	0.2	-29.5	0.3	-30.7	0.3
-20	-30.0	0.2	-30.3	0.2	-31.8	0.2
-30	-28.9	0.2	-30.3	0.2	-31.2	0.2
-40	-28.5	0.2	-29.3	0.3	-30.7	0.3
-50	-29.1	0.2	-31.0	0.3	-31.0	0.3
-60	-29.2	0.2	-30.5	0.2	-31.4	0.2
-70	-29.4	0.2	-30.3	0.2	-31.4	0.2
-80	-29.1	0.2	-30.0	0.2	-31.5	0.3

Table 6: HW37 $\delta^{13}C$ measurements from plant wax lipids. Samples that were measured once are italicized.

3.7 Modeled bulk $\delta^{13}C$

The modeled bulk $\delta^{13}C$ displays a temporal pattern similar to the Paq' measurements, with values that overlap with the bulk $\delta^{13}C$ measurements for some portions of the record but not others (Figure 6). The modeled values at CC range from -25.6‰ to -21.7‰ while the HW37 values range from -26.7‰ to -23.5‰. The overall variability of these modeled values are greater than the measured bulk $\delta^{13}C$. For example, the standard deviations of the measured bulk $\delta^{13}C$ is 0.5 and 0.4 for CC and HW37 respectively, while the standard deviation of the modeled $\delta^{13}C$ values are 1.2 and 0.9 for the respective sites. This is especially noticeable when comparing the modeled values for CC above the boundary, which range between –25.6 and -23.2, to those from

435 below the boundary, which range from -23.2 to -21.7. The HW37 results show widely ranging
436 values that overlap with the observed data. The model calculations result in high amplitude
437 variability in the 40 cm above the boundary, which is a pattern similar to the observed values.

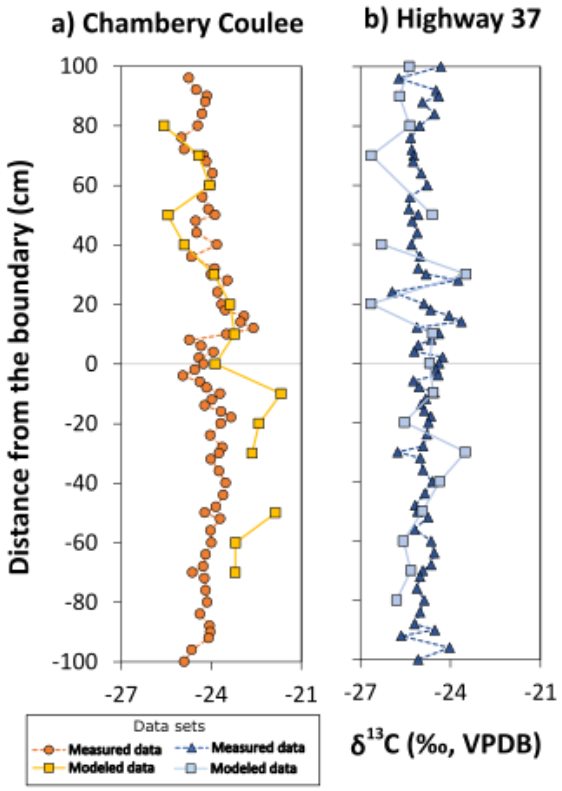

438

439 Figure 6: Modeled bulk $\delta^{13}C$ values derived from the *n*-alkane $\delta^{13}C$ and Paq' values plotted against the measured
440 $\delta^{13}C_{bulk}$ data.

441

442 ## 4. Discussion

443

444 *4.1 Geochronology and the timing of environmental change*

445 Currently there are limited constraints on the chronology of the Frenchman Formation,
446 which limits our ability to estimate the duration and rate of the observed geochemical signals.
447 However, we can make approximate estimates of the timespan for the stratigraphic interval based
448 on the timing of the CIE immediately above the boundary inferred from the C_{29} carbon *n*-alkane

449 measurements (Figure 7). These geochronological estimates are primarily relevant to the section
450 above the K-Pg Boundary. At CC we observe the CIE (i.e. the decrease and recovery of C_{29}
451 $\delta^{13}C$) occur within 20 cm above the boundary. At HW37 the CIE occurs within 10 cm above the
452 boundary. We argue that C_{29} $\delta^{13}C$ is the best indicator of the CIE given that it is a direct indicator
453 of the $\delta^{13}C$ of terrestrial plants. Bulk OC $\delta^{13}C$ can be influenced by variable source inputs, as
454 discussed in Section 4.5. Aquatic plant *n*-alkane $\delta^{13}C$ (i.e. C_{25}) may be influenced by variables
455 that would influence the $\delta^{13}C$ of dissolved inorganic carbon, such as weathering rates and aquatic
456 respiration, that could potentially obscure the expression of the CIE (see Section 4.2).
457 Using radiometric age constraints for the duration of the CIE from the Hell Creek
458 Formation (Renne et al., 2013), which was measured to be 5,000 ± 3,000 years after the iridium-
459 rich boundary, we estimate that these sites experienced sedimentation rates of 250-500 years/cm
460 in the earliest Paleogene. Assuming that this sedimentation rate was constant, the upward trend
461 in *n*-alkane $\delta^{13}C$ values spanning the K-Pg boundary observed at both sites (Figure 7; see in
462 section 4.4) would have lasted approximately 10,000 to 25,000 years. An assumption of constant
463 sedimentation rates is not well constrained, and this time estimate should be considered
464 preliminary. A coarsening upward trend above the boundary is indicated by the stratigraphic
465 column, suggesting an increased sedimentation rate through time (Nichols, 2013). This
466 coarsening trend implies that a constant rate of sedimentation is unlikely, and that the period of
467 increasing *n*-alkane $\delta^{13}C$ values may be shorter than we have.
468
469 *4.2 Evidence for changes in plant distribution and ecology*
470 A Paq' value above 0.4 is interpreted to indicate that *n*-alkanes are primarily derived
471 from submerged aquatic plants, whereas a Paq' of below 0.1 is interpreted as indicating that *n*-

alkanes are primarily derived from terrestrial plants (Liu et al., 2019). Below the boundary, Paq' values at both HW37 and CC are primarily above 0.4 suggesting dominant *n*-alkane input from aquatic plants at both sites. Paq' values at both sites shift to lower values above the boundary. This shift is consistent with a long-term increase in the relative abundance of terrestrial plants in the catchment of these sedimentary deposits. In the first 40 cm above the boundary, there is marked variability at HW37 (Figure 4-e), while the data from CC exhibit a continuous decline (Figure 5-e). Values at both sites stabilize around 40 cm above the boundary, at a lower value than observed below the boundary.

The ACL measurements also support a change in the source of *n*-alkanes across the boundary, with values increasing at both sites. This increase is also consistent with a greater relative abundance of terrestrial plants. As with the Paq' values, there is a period of greater variability above the boundary, up to 40-50 cm, after which the values are more stable. Furthermore, a change in *n*-alkane sources across the boundary is supported by the evolution of C_{27} $\delta^{13}C$ values, as discussed below (see Section 4.3). We do not think that other sources of n-alkanes such as ferns, algae, or fungi are likely to have influenced the Paq' and ACL data. The limited data available for *n*-alkane distributions in ferns indicate conflicting results with ferns producing either more short or longer chain *n*-alkanes (Bush and McInerney, 2013; Zhao et al., 2018). Zhao et al. (2018) also show that ferns produce relatively low concentrations of *n*-alkanes overall. Similarly, there is limited data on long-chaing n-alkane production by algae, with available data indicating that algae produce long chain n-alkanes in much lower abundance than aquatic or terrestrial plants (Liu and Liu, 2016). Similarly, available data on fungi indicate they primarily produce short-chain *n*-alkanes (C_{10} to C_{18}), (Markovetz et al., 1967; Elshafie et al., 2007).

Based on these observations we infer that there was a clear shift to an increased abundance of terrestrial plants relative to aquatic plants above the K-Pg boundary at these sites. This suggests that an ecological shift occurred during and after the end-Cretaceous extinction that affected the distribution of flora in the sedimentary basin of the Frenchman Formation. Increased dominance of angiosperms in terrestrial ecosystems could have potentially contributed to this shift as well, since angiosperms produce greater amounts of *n*-alkanes than gymnosperms, at least in extant North American taxa (Diefendorf et al., 2011). As gymnosperms produce fewer n-alkanes but have a similar distribution to angiosperms (Elshafie et al., 2007; Diefendorf et al., 2011), it is highly unlikely that changes in the relative abundance of gymnosperms would have been responsible for the changes in ACL or Paq' values. We also believe that this shift was indicative of a change with terrestrial plants as a whole as gymnosperms and angiosperms both produce more longer chain *n*-alkanes when compared to aquatic plants (Diefendorf et al., 2011). An intriguing possibility is that the extinction of the non-avian dinosaurs, and especially large herbivores, resulted in the complete loss of medium to large bodied vertebrate herbivores in terrestrial ecosystems, potentially allowing for an increase in terrestrial plant standing biomass.

The stratigraphy immediately above the boundary in both our localities does not indicate a trend toward a more terrestrial deposition. Instead, shales are present above the boundary at HW37 and lithologies in Chambery Coulee are similar to those below the boundary. Thus, the inferred shift toward a higher abundance in terrestrial plants based on Paq' values most likely do not reflect a geomorphological change in the fluvial environment, are more likely to be associated with upland or riparian ecological changes and support an inference of a greater abundance of terrestrial plants. The mid-latitude, subtropical forest environment of the Frenchman Formation precludes any extant analogue. However, future work could examine the

518 rates of which forests recovered with models predicting the presence and absence of large-bodied
519 herbivores.
520 Comparison of our results to regional pollen records (Braman and Sweet, 1999; Sweet et
521 al., 1999) offers some additional insights on changes in vegetation distribution. Unfortunately the
522 temporal coverage of these studies was very different from this work. Braman and Sweet (1999)
523 observe changes over nearly 60 meters of cores, with a four-meter difference between their
524 lowest sample in the Ravenscrag Formation and their uppermost sample in the Frenchman
525 Formation. Sweet et al. (1999) and Sweet and Braman (1992) provide a more high-resolution
526 analysis, but the comparability with this study remains limited as their sampling range was
527 limited to tens of cm above and below the boundary, with the samples above the boundary being
528 limited to the first coal layer. However, a key feature of these records is that the abundance of
529 algal pollen is diminished across the boundary. This suggests a decline in aquatic primary
530 productivity, which is consistent with the decrease in Paq' we observe across the boundary. In
531 addition, these pollen records indicate an increase in the relative abundance of angiosperms that
532 begins at the K-Pg boundary which is also consistent with the observed decrease in Paq' (Sweet
533 et al., 1999). Conspicuous abundance spikes in *Ulmoideipites* spp. and *Kurtzipites* spp. were
534 recorded for Alberta and Saskatchewan K-Pg boundaries (Sweet and Braman 1992; Sweet et al.
535 1999). Some of these localities recorded these two taxa comprising over 40% of all sampled
536 palynomorphs. *Kurtzipites* is most comparable to extant *Betlaceae*, *Carpinaceae* and *Corylaceae*
537 (birch trees) (Srivasta 1981). *Ulmoideipites* is tentatively considered an ulmaceous grain
538 comparable to extant *Ulmaceae* (elm and zelkova trees) (Varicchio et al. 2010). Blooms of these
539 angiosperms recorded in the post boundary palynology record may be responsible for the

reduced Paq' we recovered. Of note is that these trees are not herbivore dependent for their seed dispersal, perhaps allowing their rise to dominance in the absence of large herbivores.

It is important to note that there is a high degree of variability between regional pollen records (Braman and Sweet, 1999; Sweet et al., 1999). With the exception of the *Ulmoideipites* and *Kurtzipites* abundance spikes, pollen records are otherwise varied with differences in the relative abundance of different taxonomic groups, as well as in the observed rates of change. While there are some discernable broad trends as discussed above, by and large there is little uniformity between the different sites. This provides evidence for spatial heterogeneity in plant responses to the K-Pg impact and extinction, although the cause of this heterogeneity is uncertain. While we observe a relatively consistent pattern in the Paq' and ACL data between our two study sites, heterogeneity in plant distribution as indicated by pollen records could have led to important long-scale variability compound-specific isotope data, especially for the C_{29} *n*-alkane, as discussed in Sections 4.3, 4.4, and 4.5 below. An important caveat with interpreting palynological data is that taxonomic differences in pollen production can lead to biases in the perceived inferred plant community composition (Odgaard, 1999). *n*-Alkane production is relatively constant within angiosperms (Diefendorf et al., 2011), meaning that our *n*-alkane data could be complementary to pollen records in interpreting major changes in plant ecology.

Previous studies have found evidence for a reduction in plant species diversity across the K-Pg boundary (McElwain and Punyasena, 2007), however, there are no other studies indicating an increase in terrestrial plant abundance or a loss in aquatic plant biomass. The pattern we observe could be a primarily local or regional signal, and additional studies of *n*-alkane distributions, alongside palynological and macrofossil studies, will be valuable to ascertain

whether there was a broader shift towards increased terrestrial plant biomass following the K-Pg extinction.

The high-amplitude shifts in Paq' and ACL observed over the first 40 cm above the boundary suggests a period of ecosystem instability as the sources of the *n*-alkane lipids changed relatively rapidly before stabilizing. This is in line with the documented period of vegetation recovery for flora after the K-Pg extinction with a general trend from the dominance of ferns, followed by a shift to gymnosperms and then angiosperms (Braman and Sweet, 1999; Sweet et al., 1999; Vajda et al., 2001). As seen in the pollen record from Sweet et al. (1999), the recovery was not a single continuous trend as several fern spikes are visible in some of the pollen cores taken, along with an early spike in angiosperm pollen, which may add credibility to the idea that ecosystems did not recover at a continuous pace and that there may have been periods of rapid ecological change.

4.3 Isotopic differences between n-alkane carbon chain lengths

In freshwater depositional systems C_{25} *n*-alkanes are typically predominately produced by submerged aquatic plants while C_{29} *n*-alkanes are primarily derived from terrestrial plants (Ficken et al., 2000; Aichner et al., 2010). These different plant groups have different carbon sources and carbon fixation pathways that influence their carbon isotopic compositions. Aquatic plants tend to have more enriched isotopic compositions due to the effects of low diffusivity of dissolved CO_2 in benthic habitats, as well as the fixation of bicarbonate by some plants (Keeley and Sandquist, 1992; France 1995). This mechanism is consistent with the enrichment of the C_{25} *n*-alkane $\delta^{13}C$ values relative to C_{29}. In contrast, terrestrial plants are relatively depleted in ^{13}C because enhanced diffusion of CO_2 to and from leaf stomata entails stronger carbon isotope

fractionation (Farquhar et al., 1989). The isotopic difference between the C_{25} and C_{29} *n*-alkanes remains relatively constant through the record, suggesting that the plant sources of these molecules did not change significantly. In contrast, at both sites the C_{27} $\delta^{13}C$ values shift from being more similar to C_{25} values below the boundary to being more similar to C_{29} values above the boundary. We infer that this represents an overall shift to a greater input of C_{27} *n*-alkanes from terrestrial plants above the boundary, which is consistent with the Paq' data indicating a greater overall input of *n*-alkanes from terrestrial plants.

As the C_{25} *n*-alkane lipid values are derived primarily from aquatic plants, the hydrogen isotope measurements for these *n*-alkanes likely reflects the isotopic composition of freshwater bodies, in this case a floodplain river. By contrast, the C_{29} *n*-alkane measurements, which are primarily derived from terrestrial plants, reflect the isotopic composition of precipitation and soil water (Sachse et al., 2012). The C_{25} measurements are generally lower than the C_{29} values which is consistent with the inferred different water sources, as soil water would generally be subject to greater fractional evaporation, which would act to raise the $\delta^{2}H$ ratio (Douglas et al., 2012). It is important to note that standing bodies of water, such as lakes, can exhibit a strong evaporative influence of water isotope values (Rach et al., 2014). However, this is likely not the case for this locality as the Frenchman Formation was deposited in a well drained fluvial flood plain. Although the rate of sedimentation and type of fluvial system did fluctuate, there is no evidence that there was standing water in this system with the exception of a few isolated, iron rich units, largely located in the upper Frenchman (Bamforth, 2013; Bamforth et al., 2014), but absent from the sections measured here. Along with evaporation, seasonal differences in precipitation could influence the difference in $\delta^{2}H$ between precipitation and river water observed in C_{29} and C_{25} *n*-alkanes, as previous studies of the Frenchman Formation indicated seasonal variations in

608 temperature (Bamforth et al., 2014). The δ^2H of precipitation is typically lower during winter
609 months (Rozanski et al., 1993), which would cause aquatic plants to incorporate annually
610 averaged precipitation in the form of river water with the lower values of winter precipitation
611 causing the δ^2H for C_{25} to be lowered. In contrast, terrestrial plants would be likely to be biased
612 towards growing season (i.e. summer) precipitation as it is during this season where most of the
613 growth and wax production takes place, giving the δ^2H for C_{29} to be higher by comparison
614 (Sachse et al., 2012).
615
616 *4.4 Patterns of $\delta^{13}C$ variability recorded in n-alkanes*
617 *n*-Alkane carbon isotope measurements from both sites express fluctuations on the order
618 of 1-2‰. In analyzing these signals, we focus on the C_{25} and C_{29} alkanes, both because they
619 express the clearest signal, and because we infer they are the best representatives of signals from
620 aquatic and terrestrial plants, respectively (See Section 4.3). The HW37 section (Fig. 4-c) shows
621 the $\delta^{13}C$ of C_{25} and C_{29} varying in parallel through the section, and in particular increasing by
622 about 1.5 to 2‰ from -20 to 20 cm. A key exception is at the boundary, where the C_{29} value
623 exhibits a short-term decrease of 0.9‰, which we infer represents the K-Pg CIE identified at
624 other terrestrial sections (Arens and Jahren, 2000; Maruoka et al., 2007; Therrien, 2007). In
625 contrast, the CC section (Fig. 5-c) indicates different temporal patterns in C_{25} and C_{29} $\delta^{13}C$. CC's
626 C_{25} signal resembles the trajectory observed at HW37 (Fig. 7-a), with progressive enrichment of
627 1.5‰ spanning the boundary. The C_{29} values appear to vary with greater frequency, but without
628 the progressive enrichment observed in C_{25} or in C_{29} at HW37. At CC we also observe a putative
629 CIE of 1.1‰, with the minimum value at +10 cm.

We suggest that the increase in $\delta^{13}C$ of 1.5 to 2‰ values across the boundary observed in C_{25} and C_{29} at HW37 and in C_{25} at CC had a singular cause. The increase in C_{25} $\delta^{13}C$ values is consistent at both sites except for a slight stratigraphic offset (Figure 7-A), while the increase in C_{25} and C_{29} at HW37 are also temporally consistent. It is unclear why C_{29} $\delta^{13}C$ at CC does not express this enrichment. One possibility is that the C_{29} $\delta^{13}C$ signals were modulated by local hydrological or ecological effects on terrestrial plant carbon isotope fractionation. We note that C_{29} $\delta^{2}H$ at HW37 increased during this interval, suggesting increased evapotranspiration, while C_{29} $\delta^{2}H$ at CC decreased, suggesting decreased evapotranspiration (Figures 4 and 5). Drier conditions and increased evapotranspiration is associated with greater ^{13}C fractionation in plants (Farquhar et al., 1989). Therefore, evapotranspiration effects would have tended to enhance $\delta^{13}C$ enrichment at HW37, while dampening it at CC. Indeed, we note that the expression of $\delta^{13}C$ enrichment at HW37 is greater in C_{29} than C_{25}, which is consistent with the signal in C_{29} being amplified by hydrological change. It is also possible that differences in vegetation composition between these sites could have influenced the C_{29} carbon isotope signals. There is clear spatial variability in pollen records across the K-Pg boundary in Saskatchewan (Braman and Sweet, 1999; Sweet et al., 1999), implying spatial variability in terrestrial plant ecological dynamics following the K-Pg boundary. Given taxonomic differences in terrestrial plant carbon isotopic fractionation (Diefendorf and Freimuth, 2017), this spatial variability could have also influenced the differential trends in C_{29} $\delta^{13}C$ in these two sections.

Given that the $\delta^{13}C$ enrichment was observed in both the C_{25} and C_{29} *n*-alkanes at HW37, we infer that it was likely caused by a mechanism that affected both aquatic and terrestrial plants. Furthermore, the absence of a consistent and complimentary signal in the n-alkane $\delta^{2}H$, Paq', or ACL data between -20 to 20 cm suggests that this enrichment was not primarily caused by

hydrological change or by changes in plant ecology. A shift towards a greater relative abundance of terrestrial plants, as inferred from the Paq' and ACL data, would tend to lead to more depleted $\delta^{13}C$ values, not more enriched values, as discussed in section 4.3. It is possible that this signal reflects a global increase in the $\delta^{13}C$ of atmospheric CO_2, but more study is needed to examine possible local or regional causes.

We note that the carbon isotope variability observed in the *n*-alkane $\delta^{13}C$ record is not consistent with volcanic inputs of atmospheric CO_2, despite the possible occurrence of Deccan Trap flood basalt volcanism during this time (Schoene et al., 2019; Sprain et al., 2019). Volcanic CO_2 input would generally be very similar isotopically to background atmospheric CO_2 (6±2‰) (Gales et al., 2020; Mason et al., 2017). This implies that unrealistically large amounts of CO_2 would be needed to produce the 2‰ enrichment observed in the *n*-alkanes. Furthermore, a recent study estimated that $\delta^{13}C$ shift caused by volcanic emissions would have been quite small (-0.2 to -0.3‰) and that the bulk of the outgassing would have occurred long before the impact (Hull et al., 2020).We cannot rule out that Earth system feedbacks related to flood basalt eruptions could have driven this shift, although we are unaware of a feedback mechanism through which volcanic eruptions would lead to a substantial increase in the $\delta^{13}C$ of atmospheric CO_2.

Using our approximation for the rate of sedimentation (section 4.1), the observed enrichment in *n*-alkane $\delta^{13}C$ values spanning the K-Pg boundary was approximately 10,000 to 25,000 years in duration. However, we note that this time estimate is uncertain, especially since time constraints are highly uncertain below the K-Pg boundary. Despite the uncertainty in its cause, geographic extent, and duration, this pronounced enrichment in n-alkane $\delta^{13}C$ spanning the K-Pg boundary is intriguing and merits further investigation.

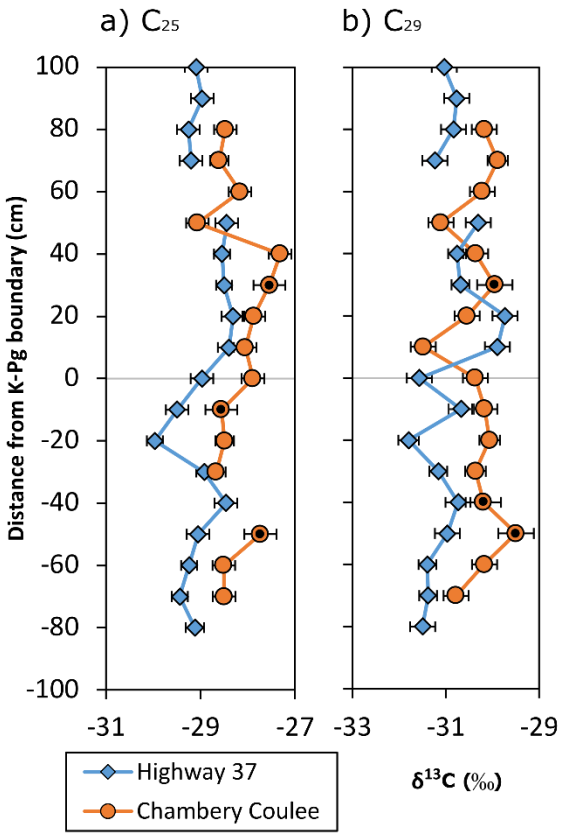

Figure 7: $\delta^{13}C$ measurements of C_{25} (a) and C_{29} (b) compared between the two sites demonstrating similarities and differences in the overall trends observed through the stratigraphic sections, with black points indicating samples with a single measurement.

4.5 Inferences on the isotopic composition of precipitation

We applied the δ^2H values of *n*-alkanes to estimate the δ^2H of regional precipitation. For our analysis we assumed a net fractionation factor between water and *n*-alkanes ($\varepsilon_{water\text{-}n\text{-}alkane}$) of -121‰ for C_{29} (McFarlin et al., 2019). We focussed on C_{29} measurements because the fractionation factor of McFarlin et al. (2019) was specifically developed for C_{29} *n*-alkanes, and because terrestrial plant *n*-alkanes are typically a better indicator of precipitation δ^2H. This fractionation factor is consistent with previous inferred values for C_3 conifers and angiosperms

(Sachse et al., 2012), which were the dominant woody plants in this region. Using this value for $\varepsilon_{water\text{-}n\text{-}alkane}$, estimated δ^2H of precipitation based on the C_{29} alkane ranges between -95‰ and -160‰, with an average δ^2H of -111±17‰ HW and -116±8‰ for CC. These values are within uncertainty of the δ^2H values from annual precipitation water in present day western Canada of -121‰ (values taken from wateriso.utah.edu, Bowen, 2019; Bowen and Revenaugh, 2003; IAEA/WMO, 2015). We do not observe clear evidence for environmental changes that would have altered the isotopic fractionation between plant water and the C_{29} *n*-alkane, although we do infer possible changes in evapotranspiration that could have influenced the δ^2H value of plant water relative to precipitation. While changes in temperature could have had an influence on the isotopic composition of regional precipitation (Rozanski et al., 1993), temperature is not considered to be an important factor influencing hydrogen isotope fractionation between n-alkanes and precipitation in higher plants, other than through its influence on evapotranspiration (Sachse et al., 2012). Furthermore, while we infer an overall shift towards a greater abundance of aquatic plants, we think this change would not have strongly influenced hydrogen isotope fractionation between water and the C_{29} *n*-alkane. As discussed above (Section 4.3), the relatively constant isotopic differences between the C_{29} and C_{25} *n*-alkanes, both in terms of $\delta^{13}C$ and δ^2H, suggests that terrestrial plants remained the dominant source for the C_{29} *n*-alkane. However, we cannot rule out that local-scale changes in plant sources or evapotranspiration rates could have influenced the inferred precipitation δ^2H values, as discussed below. Therefore, we have focused our interpretation on the mean inferred precipitation δ^2H values, as opposed to variability through the record. We note that compound-specific δ^2H measurements at CC below the K-Pg boundary are especially uncertain due to the lack of replicate measurements (See Section 3.5).

712 We estimated the δ^2H of water in the northern WIS, based on the estimate of water $\delta^{18}O$
713 published by Petersen et al., 2016-b (-20‰), and assuming that these waters would plot on the
714 global meteoric water line (GWML). Using the GWML equation $\delta^2H = (8.0 * \delta^{18}O) + 10‰$
715 (Craig, 1961), a δ^2H value of -150‰ was calculated for the waters of the northern WIS. Petersen
716 et al., (2016-b) suggested that the depleted isotopic value inferred from their study was the result
717 of isotopically depleted runoff flowing into the northern WIS. Our inferred precipitation values,
718 though not as depleted as the values observed in the northern WIS, support the conjecture that
719 runoff into the northern WIS would have been isotopically depleted, especially given that C_{29}
720 δ^2H values may be biased towards summer precipitation (see section 4.3). The cause of this
721 isotopically depleted precipitation is not well constrained as there are few proxy data for the
722 isotopic composition of precipitation from this time period. We suggest it might be the result of
723 orographic precipitation in the Rocky Mountains to the west of our study site. Isotopically
724 enabled climate model studies for this time period would be useful to test this hypothesis.
725 Although there are a few estimates of precipitation isotopes from the Late Cretaceous in
726 North America and globally, overlapping values (-123‰ to 82‰) have been recorded in plant
727 wax *n*-alkanes from Late Santonian to Late Campanian sediments of the Canadian Arctic (Super
728 et al., 2018), which was located at around 71°30′N during the Late Cretaceous, about 20° north
729 of our field sites. The similar estimated δ^2H of precipitation between Saskatchewan and the
730 Canadian high Arctic could imply reduced latitudinal δ^2H gradients during the Late Cretaceous
731 relative to modern conditions, although these samples are also separated by about 17 million
732 years, limiting direct comparisons.
733 There is minimal variability in the *n*-alkane δ^2H measurements across the study interval
734 of both sites. In particular the C_{25} *n*-alkane values exhibit little variability across the K-Pg

735 boundary, with variation on the order of 10-15‰ across the boundary (Figure 4-b, 5-b). Given
736 that the samples below the boundary at CC were not large enough for replicate measurements,
737 more data is needed to confirm our observation of limited change in δ^2H across the K-Pg
738 boundary. The C_{29} δ^2H values express greater variability across the boundary on the order of 20-
739 30‰, but this change is not consistent between sites, with decreasing values at CC and
740 increasing values at HW37 (Figure 7). For comparison, changes in δ^2H of plant waxes across the
741 latest Pleistocene deglaciation are frequently much larger, on the order of 50-100‰ (eg. Fornace
742 et al., 2014; Tierney and deMenocal, 2013). The differential direction of change in the C_{29}
743 alkanes δ^2H at these two proximal sites suggests that the forcing mechanism driving these
744 changes was local and was not related to large-scale changes in the isotopic composition of
745 precipitation. Possible local forcing mechanisms could include vegetation change or differential
746 changes in isotopic fractionation related to soil evaporation and transpiration (Sacshe et al.,
747 2013).

748 We also observe a long-term decreasing trend of 20 to 30‰ in the C_{25}, C_{27}, and C_{29} δ^2H
749 values across the record at HW37 (Figure 4-b), although a similar pattern is not evident at CC,
750 further highlighting possible site-specific variations (Figure 5-b). The absence of any major
751 shifts in *n*-alkane δ^2H after the K-Pg boundary suggest that, if the impact did have a major effect
752 on global water cycling that influenced the distribution of precipitation isotopes, its effect most
753 likely only lasted a few thousand years. However, we cannot rule out the possibility that large-
754 scale changes in precipitation δ^2H were obscured by co-occurring changes in evapotranspiration,
755 plant ecology, or plant physiology. For example Baczynski et al. (2017-a), found that *n*-alkane
756 δ^2H records at the Paleocene-Eocene boundary did not record the full magnitude of precipitation
757 isotopic change, most likely because the *n*-alkane δ^2H data were also influenced by changes in

seasonal rainfall isotopic composition and a shift in the season of *n*-alkane production. Additional data either using alternative proxies for precipitation isotopic composition or data from a wider geographic range of study sites will be needed to compare with our results to develop a stronger understanding of how the Chicxulub impact affected the global water cycle.

4.6 Bulk organic carbon isotope data

It is notable that the bulk organic $\delta^{13}C$ record from both HW37 and CC do not exhibit a clear CIE directly above the K-Pg boundary, in contrast to other sections from western North America (Arens and Jahren, 2000; Maruoka et al., 2007; Therrien, 2007). This excursion is found in nearby sites, where it reaches values as low as -2‰ at 2 to 3 cm above the boundary (Jerrett et al., 2015). Other excursions of similar magnitude can be found above the boundary in coeval outcrops in southern Alberta's Scollard Formation, Canada (Therrien et al., 2007). In contrast our sites show an overall rise in $\delta^{13}C$ in the first 20 cm above the boundary. However, the magnitude and duration of the excursion has been found to be highly variable in other sections in North America (Maruoka et al., 2007; Therrien, 2007; Yamamoto et al., 2010).

The absence of a CIE in the bulk OC $\delta^{13}C$ may be due to bulk carbon being a complex mixture of many carbon sources. We show that the $\delta^{13}C$ values of different *n*-alkane behave differently in that the CIE appears to be reflected in the terrestrial plant signal but not the aquatic plants (Figures 7, 8, 10; section 4.1).

Along with the lack of a distinct CIE, both sites show a high degree of variability in bulk $\delta^{13}C$ in the 30 cm above the boundary. Despite the lack of an obvious signal for the CIE, this variability likely indicates ecological or biogeochemical changes. The variation in the bulk $\delta^{13}C$ was most likely not caused by changes in the carbon isotope composition of plant organic matter,

781 as such a change is not apparent in the *n*-alkane $\delta^{13}C$ data. This variation also suggest that the
782 two sites responded differently in the wake of the K-Pg extinction despite their proximity, which
783 could imply different plant communities, as shown by the highly variably pollen records of the
784 region (Braman and Sweet, 1999; Sweet et al., 1999), as well as the differences in the C29 n-
785 alkane isotopic data (Sections 4.4 and 4.5).

786 The modeled $\delta^{13}C$ values potentially provide some insights into possible causes of the
787 variability in the bulk $\delta^{13}C$ values. We note that the modeled values have a range of 3-4‰ while
788 the measured data has a range of 2‰ across both sites. This larger range of variability in the
789 model suggests that other sources of carbon, such as algae or microbial biomass, were important
790 sources of organic matter to sediments and likely dampened $\delta^{13}C$ variability in bulk sedimentary
791 OC. This finding is similar to that reached by Baczynski et al. (2017-b), who applied a similar
792 approach to understand factors controlling the bulk $\delta^{13}C$ record across the Paleocene-Eocene
793 thermal maximum in the Bighorn Basin. That study found a similarly muted bulk $\delta^{13}C$ reading
794 and suggested that microbial degradation of soil organic matter played a key role in the
795 dampened signal in bulk OC $\delta^{13}C$ measurements.

796 However, there are similarities in the temporal patterns of the modeled and observed $\delta^{13}C$
797 values, particularly in the 40 cm above the boundary. For example, at CC the ~2‰ rise and fall
798 of the observed data during this interval is reflected in the modeled values. Similarly, at HW37
799 the marked variability in the observed data in this interval is reflected in the modeled values.
800 Based on these patterns we infer that while terrestrial and aquatic plants were not the only
801 sources of sedimentary OM, the interaction of changes in plant $\delta^{13}C$ and changing relative
802 abundances of these two plant groups could have had a strong effect on sedimentary bulk $\delta^{13}C$
803 values. Furthermore, the modeled data do not express a clear CIE, despite the presence of a CIE

804 in the C_{29} $\delta^{13}C$ record. This implies that the lack of a clear CIE in our bulk data may be the result
805 of the absence of a CIE in aquatic plants and changes in the relative abundance of terrestrial and
806 aquatic plants that effectively masked this signal.

807 Overall, this comparison of modeled and observed bulk $\delta^{13}C$ values highlight the
808 importance of constraining specific carbon sources when interpreting bulk organic $\delta^{13}C$ records,
809 which could help to explain spatial variation in the expression of the terrestrial CIE in K-Pg
810 sediments. This is important as many, though not all, previous studies have only considered the
811 measurements of bulk organic $\delta^{13}C$ in their analysis of the CIE and did not isolate or identify the
812 primary contributors to bulk sedimentary organic carbon. More work will need to be done to
813 better constrain the magnitude, timing, and consistency of the terrestrial CIE going forward,
814 including additional $\delta^{13}C$ analyses of *n*-alkanes and other source-specific carbon fractions.
815
816 *4.7 Relation to the K-Pg extinction*

817 Our results suggest that the K-Pg impact did not have a long-lasting effect on regional
818 carbon and water cycle processing in western Canada. The *n*-alkane $\delta^{13}C$ data imply that ^{13}C
819 enrichment in aquatic and terrestrial plants that began before the boundary continued afterward,
820 with only a brief interruption evident in the C_{29} *n*-alkane $\delta^{13}C$ values. This suggests that the
821 short-term carbon cycle disruptions provoked by the impact did not significantly disrupt longer-
822 term carbon cycle variations, although the mechanism driving the observed enrichment remains
823 unclear. Furthermore, the hydrogen isotope data also suggest that there were no large-scale
824 regional hydrological changes at the boundary, at least on timescales longer than 5000 years. We
825 do note that there were local changes evident in the C_{29} $\delta^{2}H$ data, but they did not have a
826 consistent expression between our two sites.

These results suggests that the terrestrial carbon cycle and potentially the hydrological cycle essentially recovered within roughly 10,000 years, which is consistent with other studies that have suggested similar or even faster recovery times for terrestrial ecosystems (Fastovsky et al., 2016; Lomax et al., 2001; Maruoka et al., 2007; Renne et al., 2013). We note that the role of local and global-scale variability in the carbon- and water-cycles remain incompletely resolved in our dataset, and more research is needed to test for global-scale changes. Our *n*-alkane distribution data do clearly indicate a long-term regional ecological shift towards a greater proportion of terrestrial plants relative to aquatic plants. This ecological change may have been related to broader ecological changes associated with the K-Pg mass extinction, including decreased herbivory as a consequence of the extinction of megafauna, including the extinction of large terrestrial herbivores (see Section 4.2).

5. Conclusions

Our analyses of *n*-alkane and bulk sedimentary isotope ratios across the K-Pg boundary in southern Saskatchewan helped to constrain a number of aspects of environmental change across this key interval of Earth history. We found a notable shift in the dominant plant groups producing sedimentary n-alkanes. Aquatic plants dominated below the boundary whereas terrestrial plants dominated above the boundary, suggesting that plant communities experienced a long-term shift following the extinction event. We speculate this shift may have been driven by the sudden extinction of large terrestrial dinosaur herbivores, which in turn, may have facilitated rapid terrestrial plant recovery and increased terrestrial plant biomass. Presence of high abundances of birches and elms lend support toward a successional forest recovery unlimited by herbivory. Precipitation in the region appears to have had depleted δ^2H values between -86 to -

160‰, values that are broadly consistent with inferences of a depleted isotopic composition for the northern WIS in the late Cretaceous. *n*-Alkane $\delta^{13}C$ measurements indicate a long-term increase of approximately 2‰ spanning the K-Pg boundary that we tentatively estimate as occurring over a time span of approximately 10,000 to 25,000 years. The lack of an obvious long-term disturbance to *n*-alkane carbon, and less conclusively the hydrogen, isotope values following the boundary suggests both the terrestrial water and carbon cycles recovered within 5,000 to 10,000 years after the impact, although the role of local-scale processes influencing n-alkane isotopic fractionation needs to be further resolved. Additionally, the large variability in the bulk organic carbon $\delta^{13}C$ record after the impact suggests a period of instability in sedimentary organic carbon sources which we interpret as being partly related to short-term variability in carbon inputs from terrestrial and aquatic primary production. The modeling exercise illustrated that changes in the plant sources of sedimentary organic matter have a noticeable affect on the bulk organic $\delta^{13}C$. This presents a cautionary example of how relying on bulk OM $\delta^{13}C$ measurements can lead to misleading inferences regarding the magnitude of carbon isotope excursions. In addition, the differences in bulk and compound-specific isotopic signals between the two sites, despite their proximity, is noteworthy, and is consistent with variability in palynological and bulk carbon isotope studies in other studies from this region. These data suggest a high degree of heterogeneity in terrestrial K-Pg boundary sections and emphasize the importance of caution in interpreting data from a small set of study sites.

Acknowledgements

The authors would like to thank Emily Bamforth for her assistance and guidance with field sampling. Thanks to Agnieszka Adamowiscz-Walczak and Jean-Francois Helie for their aid

with analyses at the Geotop Stable Isotope Lab at UQAM, to Benjamin Keenan for assistance with sample preparation, and to Thi Hao Bui for assistance with compound GC-FID and GC-IRMS analyses at McGill University. We also would like to thank the Allemand family for sample collection on their property. This work was supported by the NSERC Discovery Grant to Peter Douglas (2017-03902), as well as funding from the Delise Alison Award which was provided through the Redpath Museum, and the Eric Mountjoy Fellowship and the Graduate Research Ehnancement and Travel award that were provided through the Earth and Planetary Science department at McGill University to Robert Bourque.

References:

Aichner B., Herzschuh U., & Wilkes H. (2010). Influence of aquatic macrophytes on the stable carbon isotope signatures of sedimentary organic matter in lakes on the Tibetan Plateau. *Organic Chemistry*, 41, 706-718.

Alegret L. & Thomas E. (2009). Food supply to the seafloor in the Pacific Ocean after the Cretaceous/Paleogene boundary event. *Marine Micropaleontology*, 73, 105-116.

Alvarez L. W., Alvarez W., Asaro F., & Michel H. V. (1980). Extraterrestrial Cause for the Cretaceous-Tertiary Extinction. *Science*, 208, 1095-1108.

Arens N. C. & Jahren A. J. (2000). Carbon isotope excursion in Atmospheric CO_2 at the Cretaceous-Tertiary boundary: evidence from terrestrial sediments. *PALAIOS*, 15, 312-322.

Baczynski A. A., McInerney F. A., Wing S. L., Kraus M. J., Bloch J. I., & Secord R. (2017). Constraining paleohydrologic change during the Paleocene-Eocene Thermal Maximum in the continental interior of North America. *Palaeogeography, Palaeoclimatology, Palaeoecology,* 465, 237-246.-a

Baczynski A. A., McInerney F. A., Wing S. L., Kraus M. J., Morse P. E., Bloch J. I., Chung A. H., & Freeman K. H. (2017). Distortion of carbon isotope excursion in bulk soil organic matter during the Paleocene-Eocene thermal maximum. *Geological Society of America Bulletin*, 128, 1352-1366.-b

Bamforth, E.L. (2013). Paleoecology and paleoenvironmental trends immediately prior to the End-Cretaceous extinction in the latest Maastrichtian (66Ma) Frenchman Formation, Saskatchewan, Canada (Ph.D.). McGill University, Montreal.

Bamforth E. L., Button C. L., & Larsson H. C. E. (2014). Paleoclimate estimates and fire ecology immediately prior to the end-Cretaceous mass extinction in the Frenchman Formation (66 Ma), Saskatchewan, Canada. *Palaeogeography, Palaeoclimatology, Palaeoecology*, 401, 96-110.

Barnet J. S. K., Littler K., Kroon D., Leng M. J., Westerhold T., Röhl U., & Zachos J. C. (2018). A new high-resolution chronology for the late Maastrichtian warming event: Establishing robust temporal links with the onset of Deccan volcanism. *Geology*, 46, 147-150.

Berry K. (2017). New paleontological constraints on the paleogeography of the Western Interior Seaway near the end of the Cretaceous (late Campanian-Maastrichtian) with a special emphasis on the paleogeography of southern Colorado, U.S.A. *Rocky Mountain Geology*, 52, 1-16.

Bowen G. J. and Revenaugh J. (2003). Interpolating the isotopic composition of modern meteoric precipitation. *Water Resources Research* **39**(10), 1299, doi:10.129/2003WR002086.

Bowen, G. J. (2019). The Online Isotopes in Precipitation Calculator, version 3.0. http://www.waterisotopes.org.

Braman D. R. & Sweet A. R. (1999). Terrestrial palynomorph biostratigraphy of the Cypress Hills, Wood Mountain, and Turtle Mountain areas (Upper Cretaceous – Paleocene) of Western Canada. *Canadian Journal of Earth Sciences*, 36, 725-741.

Bush R. T. & McInerney F. A. (2013). Leaf wax *n*-alkane distributions in and across modern plants: Implications for paleoecology and chemotaxonomy. *Geochimicha et Cosmochimica Acta*, 117, 161-179.

Chikaraishi Y. & Naraoka H. (2003). Compound-specific δD & δ^{13}C analyses of *n*-alkanes extracted from terrestrial and aquatic plants. *Phytochemistry*, 63, 361-371.

Craig H. (1961). Isotopic variations in meteoric waters. *Science*, 133, 1702-1703.

D'Hondt S., Donaghay P., Zachos J. C., Luttenberg D., & Lindinger M. (1998). Organic carbon fluxes and ecological recovery from the Cretaceous-Tertiary mass extinction. *SCIENCE*, 282, 276-279.

Diefendorf A. F., Freeman K. H., Wing S. L., & Graham H. V. (2011). Production of *n*-alkyl in living plants and implications for geologic past. *Geochimica et Cosmochimica Acta*, 75, 7472-7485.

Diefendorf A. F. & Freimuth E. J. (2017). Extracting the most from terrestrial plant-derived *n*-alkyl lipids and their carbon isotopes from the sedimentary record: A review. *Organic Geochemistry*, 103, 1-21.

Douglas P. M. J., Pagani M., Brenner M., Hodell D. A., & Curtis J. H. (2012). Aridity and vegetation composition are important determinants of leaf-wax δD values in southeastern Mexico and Central America. *Geochimica et Cosmochimica Acta*, 97, 24-45.

Elshafie A., AlKindi A. Y., Al-Busaidi S., Bakheit C., & Albahry S. N. (2007). Biodegradation of crude oil and n-alkanes by fungi isolated from Oman. *Marine Pollution Bulletin*, 54, 1692-1696.

Farquhar G. D., Ehleringer J. R., & Hubick K. T. (1989). Carbon isotope discrimination and photosynthesis. *Annual review of plant biology*, 40, 503-537.

964 Fastovsky D. E. & Bercovici A. (2016). The Hell Creek Formation and its contribution to the
965 Cretaceous-Paleogene extinction: A short primer. *Cretaceous Research*, 57, 368-390.
966
967 Ficken K. J., Li B., Swain D. L., & Eglinton G. (2000). An *n*-alkane proxy for the sedimentary
968 input of submerged/floating freshwater aquatic macrophytes. *Organic Geochemistry*, 31, 745-
969 749.
970
971 Fornace K. L., Hughen K. A., Shanahan K. A., Fritz S. C., & Baker P. A. (2014). A 60,000-year
972 record of hydrologic variability in central Andes from the hydrogen isotopic composition of leaf
973 waxes in Lake Titicaca sediments. *Earth and Planetary Science Letters*, 408, 263-271
974
975 France R. L. (1995). Differentiation between littoral and pelagic food webs in lakes using stable
976 carbon isotopes. *Limnology and Oceanography*, 40 (7), 1310-1313.
977
978 Gales E., Black B., & Elkins-Tanton L. T. (2020). Carbonatites as a record of the carbon isotope
979 composition of large igneous province outgassing. *Earth and Planetary Science Letters*, 535,
980 116076.
981
982 Harris D., Horwath W. R., & Kessel C. V. (2001). Acid fumigation of soils to remove carbonates
983 prior to total organic carbon or carbon-13 isotopic analysis. *Soil Science Society of America*
984 *Journal*, 65, 1853-1856.
985

Hildebrand A. R., Penfield G. T., Kring D. A., Pilkington M., Camargo A. Z., Jacobsen S. B., & Boynton W. V. (1991). Chicxulub Crater: A possible Cretaceous/Tertiary boundary impact crater on the Yucatán Peninsula, Mexico. *Geology*, 19, 867-871.

Hull P. M., Bornemann A., Penman D. E., Henehan M. J., Norris R. D., Wilson P. A., Blum P., Alegret L., Batenburg S. J., Bown P. R., Bralower T. J., Cournede C., Deutsch A., Donner B., Friedrich O., Jehle S., Kim H., Kroon D., Lippert P. C., Loroch D., Moebius I., Moriya K., Peppe D. J., Ravizza G. E., Röhl U., Schueth J. D., Sepúlveda J., Sexton P. F., Sibert E. C., Sliwinska K. K., Summons R. E., Thomas E., Westerhold T., Whiteside J. H., Yamaguchi T., and Zachos J. C. (2020). On impact and volcanism across the Cretaceous-Paleogene boundary. *Science*, 367, 266-272.

IAEA/WMO (2015). Global Network of Isotopes in Precipitation. The GNIP Database.

Jerrett R. M., Price G. D., Grimes S. T., & Dawson A. T. (2015). A paleoclimate and paleoatmospheric record from peatlands accumulating during the Cretaceous-Paleogene boundary event, Western Interior Basin, Canada. *GSA Bulletin*, 127, 1564-1582.

Keeley J. E. & Sandquist D. R. (1992). Carbon: freshwater plants. *Plant, Cell, and Environment*, 15, 1021-1035.

Kupsch W. O. (1957). Frenchman Formation of Eastern Cypress Hills, Saskatchewan, Canada. *Bulletin of the Geological Society of America*, 68, 413-420.

Labandeira C. C., Johnson K. R., & Lang P. (2002). Preliminary assessment of insect herbivory across the Cretaceous-Tertiary boundary: Major extinction and minimal rebound. *Geological Society of America Special Paper*, 361, 297-327.

Liu H. & Liu W. (2016). *n*-Alkane distributions and concentrations in algae, submerged plants and terrestrial plants from the Qinghai-Tibetan Plateau. *Organic Geochemistry*, 99, 10-22.

Liu H., Liu Z., Zhao C., & Liu W. (2019). *n*-Alkyl lipid concentrations and distributions in aquatic plants and their individual δD variations. *Science China Earth Science*, 62, https://doi.org/10.1007/s11430-019-9370-8

Lomax B., Beerling D. Upchurch G Jr, & Otto-Bliesner B. (2001). Rapid (10-yr) recovery of terrestrial productivity in a simulation study of the terminal Cretaceous impact event. *Earth and Planetary Science Letters*, 192, 137-144.

Macleod K. G., Quinton P. C., Sepúlveda J., & Negra M. H. (2018). Postimpact earliest Paleogene warming shown by fish debris oxygen isotopes (El Kef, Tunisia). *Science*, 360, 1467-1469.

Markovetz A. J., Cazin J. Jr., & Allen J. E. (1968). Assimilation of alkanes and alkenes by fungi. *Applied Microbiology*, 16, 487-489.

Maruoka T., Koerberl C., & Bohor B. F. (2007). Carbon isotopic compositions of organic matter across continental Cretaceous–Tertiary (K-T) boundary sections: Implications for paleovenvironment after the K-T extinction event. *Earth and Planetary Science Letters*, 253, 226-238.

Mason E., Edmonds M., & Turchyn A. V. (2017). Remobilization of crustal carbon may dominate volcanic arc emissions. *Science*, 357, 290-294.

McIver E. E. (1989). Fossil Flora of the Paleocene Ravenscrag Formation, Southwestern Saskatchewan, Canada. *University of Saskatchewan*.

McIver E. E. (1999). Paleobotanical evidence for ecosystem disruption at the Cretaceous-Tertiary boundary from Wood Mountain, Saskatchewan, Canada. *Canadian Journal of Earth Sciences*, 36, 775-789.

McIver E. E. (2002). The paleoenvironment of *Tyrannosaurus rex* from southwestern Saskatchewan, Canada. *Canadian Journal of Earth Sciences*, 39, 207-221.

McElwain J. C. & Punyasena S. W. (2007). Mass extinction events and the plant fossil record. *TRENDS in Ecology and Evolution*, 22, 548-557.

McFarlin J. M., Axford Y., Masterson A. L., & Osburn M. R. (2019). Calibration of modern sedimentary $\delta^{2}H$ plant wax-water relationships in Greenland lakes. *Quaternary Science Reviews*, 225, [105978]. https://doi.org/10.1016/j.quascirev.2019.105978.

Moore N., Arima E., Walker R., & Silva R. R. (2007). Uncertainty and the changing hydroclimatology of the Amazon. *Geophysical Research Letters*, 34, doi:10.1029/2007GL030157.

Nichols, G. (2013). Sedimentology and Stratigraphy. Somerset: Wiley.

Niedermeyer E. M., Schefuß E., Sessions A. L., Mulitza S., Mollenhauer G., Schulz M., & Wefer G. (2010). Orbital- and millennial-scale changes in the hydrologic cycle and vegetation in the western African Sahel: insights from individual plant wax δD and $\delta^{13}C$. *Quaternary Science Reviews*, 29, 2996-3005.

Norris R. D., Huber B. T., & Self-Trail J. (1999). Synchroneity of the K-T oceanic mass extinction and the meteorite impact: Blake Nose, western North Atlantic. *Geology*, 27, 419-422.

Odgaard B. V. (1999). Fossil pollen as a record of past biodiversity. *Journal of Biogeography*, 26, 7-17.

1074 Petersen S. V., Dutton A., & Lohmann K. C. (2016). End-Cretaceous extinction in Antarctica
1075 linked to both Deccan volcanisms and meteorite impact via climate change. *Nature*
1076 *Communications*, DOI: 10.1038/ncomms12079.-a
1077
1078 Petersen S. V., Tabor C. R., Lohmann K. C., Poulsen C. J., Meyer K. W., & Carpenter S. J.
1079 (2016). Temperature and salinity of the Late Cretaceous Western Interior Seaway. *Geology*, 44,
1080 903-906.-b
1081
1082 Polissar P. J. & D'Andrea W. J. (2014). Uncertainty in paleohydrologic reconstructions from
1083 molecular δD values. *Geochimica et Cosmochimica Acta*, 129, 146-156.
1084
1085 Pope K. O., Baines K. H., Ocampo A. C., & Ivanov B. A. (1994). Impact winter and the
1086 Cretaceous/Tertiary extinctions: Results of a Chicxulub asteroid impact model. *Earth and*
1087 *Planetary Science Letters*, 128, 719-725.
1088
1089 Rach O., Brauer A., Wilkes H., & Sachse D. (2014). Delayed hydrological response to
1090 Greenland cooling at the onset of the Younger Dryas in western Europe. *Nature Geoscience*, 7,
1091 109-112.
1092
1093 Redman C. M., Gardner J. D., Scott C. S., & Braman D. R. (2015). Geological setting of
1094 vertebrate microfossil localities across the Cretaceous-Paleogene boundary in southwestern
1095 Saskatchewan, Canada. *Canadian Journal of Earth Sciences*, 52, 846-862.
1096

1097 Renne P. R., Deino A. L., Hilgen F. J., Kuiper K. F., Mark D. F., Mitchel III W. S., Morgan L.
1098 E., Mundil R., & Smit J. (2013). Time scales of critical events around the Cretaceous-Paleogene
1099 boundary. *SCIENCE*, 339, 684-687.
1100
1101 Rozanski K., Araguás- Araguás L., Gonfiantini R. (1993). Isotopic Patterns in Modern Global
1102 Precipitation. *Climate change in continental isotopic records*, 78, 1-36.
1103
1104 Sachse D., Billault I., Bowen G. J., Chikaraishi Y., Dawson T. E., Feakins S. J., Freeman K. H.,
1105 Magill C. R., McInerney F. A., van der Meer M. T. J., Polissar P., Robins R. J., Sachs J. P.,
1106 Shmidt H. L., Sessions A. L., White J. W. C., West J. B., & Kahmen A. (2012). Molecular
1107 Paleohydrology: Interpreting the Hydrogen-Isotopic Composition of Lipid Biomarkers from
1108 Photosynthesizing Organisms. *Annual Review of Earth and Planetary Sciences*, 40, 221-249.
1109
1110 Schoene B., Eddy M. P., Samperton K. M., Keller C. B., Keller G., Adatte T., & Khadri S. F. R.
1111 (2019). U-Pb constraints on pulsed eruption of the Deccan Traps across the End-Cretaceous mass
1112 extinction. *Science*, 363, 862-866.
1113
1114 Sepúlveda J., Alegret L., Thomas E., Haddad E., Cao C., & Summons R. E. (2019). Stable
1115 isotope constraints on marine productivity across the Cretaceous-Paleogene mass extinction.
1116 *Paleoceanography and Paleoclimatology*, 34, 1195-1217.
1117

Setegn S. G., Rayner D., Melesse A. M., Dargahi B., & Srinivasan R. (2011). Impact of climate change on the hydroclimatology of Lake Tana Basin, Ethiopia. *Water Resources Research*, 74, doi:10.1029/2010WR009248.

Smit J. & Hertogen J. (1980). An extraterrestrial event at the Cretaceous-Tertiary boundary. *Nature*, 285, 198-200.

Sprain C. J., Renne P. R., Vanderkluysen L., Pande K., Self S., & Mittal T. (2019). The eruptive tempo of Deccan volcanism in relation to the Cretaceous-Paleogene boundary. *Science*, 363, 866-870.

Srivasta S. K. (1981). Fossil pollen genus Kurtzipites Anderson. *Journal of Palaeontology*, 55, 868-879.

Super J. R., Chin K., Pagani M., Li H., Tabor C., Harwood D. M., & Hull P. M. (2018). Late Cretaceous climate in the Canadian Arctic: Multi-proxy constraints from Devon Island. *Palaeoceanography, Palaeoclimatology, Palaeoecology*, 504, 1-22.

Sweet A. R., & Braman D. R. (1992). The K-T boundary and contiguous strata in western Canada: interactions between paleoenvironments and palynological assemblages. *Cretaceous Research*, 13, 31-79.

Sweet A. R., Braman D. R., & Lerbekmo J. F. (1999). Sequential palynological changes across the composite Cretaceous-Tertiary (K-T) boundary claystone and contiguous strata, western Canada and Montana, U.S.A. *Canadian Journal of Earth Sciences*, 36, 743-768.

Therrien F., Eberth D. A., Braman D. R., & Zelenitsky (2007). High-resolution organic carbon isotope record across the Cretaceous-Tertiary boundary in south-central Alberta: implications for the post-impact recovery rate of terrestrial systems and use of $\delta^{13}C$ as a boundary marker. *Canadian Journal of Earth Sciences*, 44, 529-542.

Tierney J. E. & deMenocal P. B. (2013). Abrupt shifts in Horn of Africa hydroclimate since the last glacial maximum. *Science 342.6160*, 843-846.

Vajda V., Raine J. I., & Hollis C. J. (2001). Indication of global deforestation at the Cretaceous-Tertiary boundary be New Zealand fern spike. *Science*, 294, 1700-1702.

Vajda V. & Raine J. I. (2003). Pollen and spores in marine Cretaceous/Tertiary boundary sediments at mid-Waipara River, North Cantebury, New Zealand. *New Zealand Journal of Geology & Geophysics*, 46, 255-273.

Vajda V. & McLoughlin S. (2007). Extinction and recovery patterns of the vegetation across the Cretaceous-Paleogene boundary – a tool for unraveling the causes of the end-Permian mass-extinction. *Review of Paleobotany and Palynology*, 144, 99-112.

1163 Varricchio, D. J., C. Koeberl, R. F. Raven, W. S. Wolbach, W. C. Elsik, and D. P. Miggins.
1164 (2010). Tracing the Manson impact event across the Western Interior Cretaceous Seaway. P. in
1165 Large Meteorite Impacts and Planetary Evolution IV. *Geological Society of America Special*
1166 *Paper*, 465, 269-299.
1167
1168 Vellekoop J., Sluijs A., Smit J., Schouten S., Weijers J. W. H., Sinninghe Damsté J. S., &
1169 Brinkhuis H. (2014). Rapid short-term cooling following the Chicxulub impact at the
1170 Cretaceous-Paleogene boundary. *PNAS*, 111, 7537-7541.
1171
1172 Vellekoop J., Esmeray-Senlet S., Miller K. G., Browning J. V., Sluijs A., van der Schootbrugge
1173 B., Sinninghe Damasté J. S., & Brinkhuis H. (2016). Evidence for Cretaceous-Paleogene
1174 boundary bolide "impact winter" conditions from New Jersey, USA. *Geology*, 44, 619-622.
1175
1176 Vellekoop J., Woelders L., van Helmond N. A. G. M., Galeotti S., Smit J., Slomp C. P.,
1177 Brinkhuis H., Claeys P., & Speijer R. P. (2018). Shelf hypoxia in response to global warming
1178 after the Cretaceous-Paleogene boundary impact. *Geology*, 46, 683-686.
1179
1180 Walls R. A., Mountjoy E. W., & Fritz P. (1979). Isotopic composition and diagenetic history of
1181 carbonate cements in Devonian Golden Spike reef, Alberta, Canada. *Geological Society of*
1182 *America Bulletin*, 90, 963-982.
1183

Wilf P., Johnson K. R., & Huber B. T. (2003). Correlated terrestrial and marine evidence for global climate changes before mass extinction at the Cretaceous-Paleogene boundary. *PNAS*, 100, 599-604.

Wolfe J. A. & Upchurch Jr. G. R. (1986). Vegetation, climactic, and floral changes at the Cretaceous-Tertiary boundary. *Nature*, 324, 148-152.

Yamamoto S., Hasegawa T., Tada R., Goto K., Rojas-Consuegra R., Díaz-Otero C., García-Delgado D. E., Yamamoto S., Sakuma H., & Matsui T. (2010). Environmental and vegetational changes recorded in sedimentary leaf wax *n*-alkanes across the Cretaceous-Paleogene boundary at Loma Capiro, Central Cuba. *Palaeogeography, Palaeoclimatology, Palaeoecology*, 295, 31-41.

Zhao B., Zhang Y., Huang X., Qiu R., Zhang Z., & Meyers P. A. (2018). Comparison of *n*-alkane molecular, carbon and hydrogen isotope compositions of different types of plants in the Dajiuhu peatland, central China. *Organic Geochemistry*, 124, 1-11.

Reviewer #1: The authors did a good job in the revision and the manuscript was improved quite a lot. An ecological shift from aquatic plants to terrestrial plants is documented to occur across the K-Pg boundary by Paq, ACL as well as the compound-specific carbon isotope composition of n-alkanes. The authors present robust and clear evidence for this ecological shift from both sites, and this is of significance to the ecological understanding associated with the bolide-induced mass extinction.

What still surprises me is the unchanged record of the deuterium content of n-alkanes at both sites. In particular, some deuterium data were shown and included without any duplicate analysis; this is abnormal in organic geochemistry and I do not believe the authors' statement that analysis of samples with a single measurement is often necessary in compound-specific isotope studies due to small sample sizes (Line 392-393). In fact, caution should be particularly taken when discussion is based on some data with single measurement in compound-specific hydrogen isotope composition. Theoretically, an ecological shift infers the changes in both the vegetation and environmental conditions, both of which would cause the shift in the hydrogen isotope composition of n-alkanes. The authors should leave some rooms for the additional discussion of the unchanged trends which might be biased by the single measurement, or influenced by the balance of different environmental factors, before
any full discussion on the regional precipitation.

- We have emphasized that the *n*-alkane δ^2H data should be interpreted with caution, with a larger emphasis put on the uncertainty of the data, especially for samples without replicate analyses (lines 399-403; lines 710-712; lines 736-739). We note that for the most part the non-replicated samples do not strongly influence the interpretations in the paper, with the exception of the data below the K-Pg boundary at the Chambre Coulee section. We also add additional discussion of the possibility that co-occurring changes in vegetation and climate could obscure changes in the isotopic composition of precipitation (lines 754-762). With this in mind we cite Baczynski et al. (2017-a), who note a similar lack of change in δ^2H across the Paleocene-Eocene boundary, while other sources did indicate a change in isotopic composition. We highlight the need for additional studies to further constrain changes in precipitation isotopic composition across the K-Pg boundary.

Minors
Line 571, 'In contrast, a both sites…..', 'a' should be 'at'.
Line 627, 'Given that the observed delta13C enrichment was observed in both the C25 and C29 n-alkanes', one of the two 'observed' could be deleted.

- These two minor points have been addressed.

Reviewer #3: Thanks for the replies to the comments and edit on the original version of the manuscript done by the authors. However, agree with the reviewers in the second round, I am also curious about the inconsistencies between the two sections, and among the different proxies in the same section. For example, there is ca. 1 per mil offset between the bulk carbon isotope compositions of bulk organic matter between the two sections. Across the K/Pg boundary, the bulk carbon isotope only shows minor changes in the HW37 section, while that of the CC section is obvious. Besides, in the same HW37 section, the Paq', d13C and d2H

sequences of n-alkanes show quite different variations. Though the authors argued that ratios Paq' and ACL reflect vegetation signals, while the compound-specific carbon and hydrogen isotope compositions correlate closely with environmental conditions or plant physiology, it is not easy to understand that the plant changes unfold with the environmental changes at the time with huge mass extinction across the K/Pg boundary. As a summary, local variations may have a very important effect on the data in this study, and the current broad conclusion is not completely supported by the dataset.

- The inconsistencies between the two sites is a key aspect of this dataset, and we have revised the manuscript in a number of places to emphasize this local-scale variability (line 29; lines 643-649; lines 782-786; lines 831-833; lines 857-858; lines 865-869). Local scale variability is also a key feature of previously palynological and paleoecological studies, and we have drawn clearer linkages between this feature in our dataset and previous studies. We have also emphasized that local heterogeneity was an important feature of environmental change at the K-Pg boundary in our conclusions.

- However, despite the evident differences between these sites there are also key aspects of that data that are consistent between them, which we continue to emphasize. In particular the shift that occurs in Paq' and ACL across the boundary at both sites supports the inference of a widespread regional change in plant ecology. In addition, the similar $\delta^{2}H$ values recorded at both sites supports our inference of generally isotopically depleted regional precipitation, even though the temporal variability may have been influenced by local factors. Finally, the consistent enrichment of $\delta^{13}C$ in the C_{25} n-alkane spanning the K-Pg in particular suggests a causal mechanism operating on a relatively large spatial scale, though more research is clearly needed to understand this phenomenon.

- In addition to these changes, we made additional edits to clarify our findings on the inferred vegetation change spanning the K-Pg boundary, including more detailed linkages to regional palynological records (lines 21-24; lines 534-546; lines 843-850). We also added a citation to a study that applied a similar approach to modeling bulk OC $\delta^{13}C$ values using compound-specific data (Baczynski et al, 2017-b), which validates the application of this approach in our study and supports our conclusions (lines 792-796).

Highlights:

- Plant wax records of Cretaceous-Paleogene (K-Pg) boundary environmental change
- A shift to more terrestrial sources of plant waxes after the K-Pg extinction event
- The mixing of different carbon sources masked the carbon isotope excursion signal
- Carbon and water cycles recovered in less than 10,000 years after extinction event
- Steady increase in n-alkane $\delta^{13}C$ values of 2‰ spanning the K-Pg boundary

Abstract

Changes in terrestrial environments across the Cretaceous-Paleogene boundary, including plant ecology and carbon and water-cycling, remain poorly defined. Fluvial sediments spanning the Cretaceous-Paleogene (K-Pg) boundary of southern Saskatchewan, Canada contain well preserved plant wax *n*-alkanes that provide a means of reconstructing changes to plant ecology and carbon and water cycling during this mass extinction event. We measured *n*-alkane carbon ($\delta^{13}C$) and hydrogen ($\delta^{2}H$) isotope ratios in two sedimentary sections and applied established fractionation factors to estimate the isotopic compositions of precipitation and bulk sedimentary organic matter sources. We also analyzed the distribution of *n*-alkanes as an indicator of the relative abundance of aquatic and terrestrial plants. We find a consistent shift towards a greater relative abundance of longer-chain *n*-alkanes across the boundary, implying a persistent increase in the relative abundance of terrestrial plants in the sedimentary basin. This is consistent with an increase in birch and elm palynomorphs immediately above the boundary. We hypothesize the extinction of all large herbivores at the boundary may have facilitated this transition to a terrestrial angiosperm dominated flora immediately after the boundary. We also find that the region was characterized by isotopically light precipitation, with $\delta^{2}H$ values between -95‰ to -160‰ but do not observe evidence for major millennial-scale changes in regional precipitation isotopic composition spanning the boundary. *n*-Alkanes derived from both aquatic and terrestrial plants at one site display an upward trend in $\delta^{13}C$ values of approximately 2‰ across the K-Pg boundary. This suggests millennial-scale local or global carbon-cycle variability altering either plant carbon isotope fractionation or the carbon isotope composition of dissolved inorganic carbon and atmospheric CO_2. Overall our results suggest that carbon and water cycle changes associated with the K-Pg impact in terrestrial environments in western Canada were short-lived, but ecological shifts in plant communities were longer-lasting.

Changes in terrestrial ecosystem across the Cretaceous-Paleogene boundary in western Canada inferred from plant wax lipid distributions and isotopic measurements

Robert D. Bourque[1], Peter M. J. Douglas[1], Hans C. E. Larsson[2]

[1] Department of Earth and Planetary Sciences, Geotop Research Centre, McGill University, 3450 University Street H3A 0E8, Montreal, Quebec, Canada.

[2] Redpath Museum, McGill University, 859 Sherbrooke Street West H3A 0C4, Montreal, Quebec, Canada.

Abstract

Changes in terrestrial environments across the Cretaceous-Paleogene boundary, including plant ecology and carbon and water-cycling, remain poorly defined. Fluvial sediments spanning the Cretaceous-Paleogene (K-Pg) boundary of southern Saskatchewan, Canada contain well preserved plant wax *n*-alkanes that provide a means of reconstructing changes to plant ecology and carbon and water cycling during this mass extinction event. We measured *n*-alkane carbon ($\delta^{13}C$) and hydrogen ($\delta^{2}H$) isotope ratios in two sedimentary sections and applied established fractionation factors to estimate the isotopic compositions of precipitation and bulk sedimentary organic matter sources. We also analyzed the distribution of *n*-alkanes as an indicator of the relative abundance of aquatic and terrestrial plants. We find a consistent shift towards a greater relative abundance of longer-chain *n*-alkanes across the boundary, implying a persistent increase in the relative abundance of terrestrial plants in the sedimentary basin. This is consistent with an increase in birch and elm palynomorphs immediately above the boundary. We hypothesize the extinction of all large herbivores at the boundary may have facilitated this transition to a terrestrial angiosperm dominated flora immediately after the boundary. We also find that the

region was characterized by isotopically light precipitation, with δ^2H values between -95‰ to -160‰ but do not observe evidence for major millennial-scale changes in regional precipitation isotopic composition spanning the boundary. *n*-Alkanes derived from both aquatic and terrestrial plants at one site display an upward trend in $\delta^{13}C$ values of approximately 2‰ across the K-Pg boundary. This suggests millennial-scale local or global carbon-cycle variability altering either plant carbon isotope fractionation or the carbon isotope composition of dissolved inorganic carbon and atmospheric CO_2. Overall our results suggest that carbon and water cycle changes associated with the K-Pg impact in terrestrial environments in western Canada were short-lived, but ecological shifts in plant communities were longer-lasting.

Keywords: plant wax lipids; carbon isotopes; hydrogen isotopes; mass extinction; compound specific isotope analysis; paleohydrology

1. Introduction

The Cretaceous-Paleogene (K-Pg) boundary is the most recent mass extinction event in Earth's history, with an estimated 75% of all plant and animal species on the planet having gone extinct at the time (Norris et al., 1999; Labandeira et al., 2002; Vajda et al., 2001; Wolfe and Upchurch, 1986). The primary driver of the extinction has been linked to an asteroid impact (Alvarez et al., 1980; Smit and Hertogen, 1980) that occurred near the present-day Yucatán Peninsula, Mexico (Hildebrand et al., 1991). However, identifying the cause of the extinction event is complicated by evidence of large shifts in global climate (Wilf et al., 2003; Petersen et al., 2016-a) and large-scale volcanism from the Deccan Traps of present day India occurring across the K-Pg boundary (Schoene et al., 2019; Sprain et al., 2019). A range of hypotheses has

been put forth on the effects such an impact would have caused to the Earth system, none mutually exclusive from each other, which have ranged from the release of a large enough volume of aerosols to create an extended period of darkness (Pope et al., 1994), short-term global cooling on the order of tens to hundreds of years (Vellekoop et al., 2014; Vellekoop et al., 2016), and warming that lasted for several millennia (MacLeod et al., 2018; Vellekoop et al., 2018). The K-Pg boundary is marked by an iridium-rich clay layer which has been mostly been associated with the fallout of an impact (Alvarez et al., 1980). In addition, a negative carbon isotope excursion (CIE) is one of the defining features of the extinction event (Arens and Jahren, 2000), and implies a global change in carbon cycling and a net input of ^{13}C depleted carbon to the atmosphere, although the duration, magnitude, and cause of this CIE remains subject to debate (Renne et al., 2013).

However, these data alone do not sufficiently resolve the large number of processes that could have altered the global carbon cycle. The isotopic signal of bulk sedimentary organic carbon, which is primarily used to infer the CIE in terrestrial sediments as well as some marine strata, is a complex mixture of multiple carbon-cycle processes as it represents a mixed signal of all sedimentary organic carbon sources, and does not account for differential carbon isotope fractionation by different primary producers, or the effects of subsequent decomposition and diagenesis (Sepúlveda et al., 2019). Most research on carbon cycle changes associated with the impact has come from marine records, where studies have shown a decoupling of the deep ocean and surface ocean carbon reservoirs and diminished transport of organic matter from the surface to the deep ocean. This shutdown of the biological pump has been estimated to last hundreds of thousands of years (D'Hondt et al., 1998, Alegret and Thomas, 2009). Despite this long-term reduction in transport of carbon to the deep ocean, surface ocean primary productivity is

estimated to have recovered within a period of 10,000 years (Alegret and Thomas, 2009), with some groups of planktonic organisms closer to shorelines and in the upper reaches of the deep ocean having shown evidence of also having recovered on even shorter time spans (Sepúlveda et al., 2019). A similarly rapid recovery is inferred to have occurred in terrestrial ecosystems (Vajda et al., 2001). In contrast with the relatively detailed studies of carbon-cycle changes, there are few data that constrain the effects the impact had on global or regional water cycling. This is important as changes in the water cycle strongly affect terrestrial ecosystem productivity and function, which could have potentially exacerbated ecological or carbon-cycle changes caused by the impact (Moore et al., 2007; Setegn et al., 2011).

The pre-impact climate was in the midst of cooling of approximately 5-8 °C that has been documented for the last 100,000 years of the Maastrichtian, following a period of warming of 2.5-5 °C over the preceding 150,000-300,000 years (Petersen et al., 2016-a). This warming event has been linked to eruption (Barnet et al., 2018) or degassing (Hull et al., 2020) associated with Deccan Traps volcanism that was occurring in the late Maastrichtian, and which is suggested to been an early driver of extinctions before the impact (Petersen et al., 2016-a). High-resolution reconstructions of global temperatures and carbonate $\delta^{13}C$ values indicate a cooling of approximately 2 °C over the 200,000 years preceding the K-Pg boundary and a dramatic drop in $\delta^{13}C$ at the boundary, with carbon isotope recovery in marine systems not occurring until nearly 1 Myr later (Hull et al. 2020). Combining the estimated temperatures and carbonate isotopes with modeling, Hull et al. (2020) suggested that Deccan Trap outgassing would not have been responsible for boundary CIE and suggested instead that biological processes were responsible. It is important to note that the CIE preserved in terrestrial sediments is estimated to have been much shorter in duration, lasting approximately 5,000 to 10,000 years (Renne et al., 2013).

Constraints on ecosystem recovery provided an important framework for understanding possible changes in the terrestrial carbon and water cycles. There is evidence that plant communities recovered in a fairly short amount of time, taking as little as 10 years to recover (Lomax et al., 2001; Maruoka et al., 2007). Along with changes to climate, changes to plant ecology across the extinction event have been inferred, with pollen studies indicating key trends in plant group abundance (Braman and Sweet, 1999; Sweet et al., 1999; Vajda et al., 2001). For example, studies from southwestern Canada show highly diverse angiosperm communities before the impact (McIver, 1999; McIver 2002). The impact was directly followed by several spikes in fern pollen, which is observed on a global level (Vajda et al., 2001), followed by the repopulation of angiosperms and gymnosperms, with angiosperm recovery slightly earlier and dominating the relative abundance of woody plant pollens (Sweet and Braman, 1992; Braman and Sweet, 1999; Sweet et al., 1999). It has also been demonstrated that while angiosperms and gymnosperms recovered relatively quickly over only a few thousand years (McIver, 1999; Vajda and Rained, 2003; Vajda and McLoughlin, 2007), biodiversity for these two groups of plants remained low for over one million years (McElwain and Punyasena, 2007).

The objective of this study was to perform measurements of plant wax *n*-alkane distributions and carbon and hydrogen isotopes, alongside measurements of bulk sediment organic matter (OC) carbon isotopes, across the K-Pg boundary to infer changes to the carbon and water cycles and to plant ecology before and after the impact. *n*-Alkane measurements can provide insights into the carbon isotope compositions of atmospheric CO_2 and the hydrogen isotope composition of precipitation, providing a unique means of examining changes to carbon and water cycling (Sachse et al., 2012; Diefendorf and Freimuth, 2017). Additionally, indices of the relative abundance of *n*-alkanes of different chain lengths can be used as an indicator of

changes in the sources of the plant waxes, and thus changes the relative abundance of different plant groups (Ficken et al., 2000; Liu et al., 2019).

2. Methodology

2.1 Study area and stratigraphic sections

The samples analyzed in this study were taken from a pair of sites in southern Saskatchewan, Canada. The two specific sampling locations were Chambery Coulee (CC) and Highway 37 (HW37, Figure 1), located at 49°N, 108°W and 49°35'28.03"N, 108°42'57.50"W respectively. Coordinates for CC are approximate in agreement with the wishes of the private landowners. These sites were chosen because of the exceptional preservation of the K-Pg boundary (McIver et al., 2002; Bamforth et al., 2014; Jerrett et al., 2015; Redman et al., 2015) as well as for the presence of sedimentary units of both the uppermost Frenchman and lowermost Ravenscrag formations.

The Frenchman Formation is a unit of latest Cretaceous aged strata that is contiguous with the Hell Creek Formation of Montana. Both the Hell Creek and Frenchman formations have similar fauna and are composed of latest Cretaceous sediments leading up to and including the K-Pg boundary. The Frenchman Formation is composed of sand and clay lithosome units (Kupsch, 1957) which can further be categorized into broader sandstone and mudstone units that cycle through fining upward sequences (Bamforth, 2013). Magnetostratigraphy of sections from Grasslands National Park, which are 100-150 km from the sites in this study, show that the upper Frenchman Formation spans approximately 300,000 to 500,000 years (Bamforth, 2013). Based on an average thickness of the upper Frenchman Formation of 35 meters, this implies an

approximate average sedimentation rate of 8,500 to 14,000 years per meter, although it is likely that sedimentation rates varied substantially within the formation and there may be unconformities. Magnetostratigraphic analyses of the Frenchman Formation have confirmed that the K-Pg boundary occurs at the top of the formation (Bamforth, 2013). The K-Pg boundary is marked by a thin layer of tonstein, a sedimentary rock primary composed of kaolinite clay, that has been found globally and is thought to be related to fallout from the Chicxulub impact (Alvarez et al., 1980; Smit and Hertogen, 1980).

The overlying Ravenscrag Formation is earliest Paleocene in age and is predominantly composed of silt. The lowest layers of the Ravenscrag Formation are composed of the Ferris coal seam, which overlies the iridium-rich boundary clay layer (McIver, 1989). A recent study estimated that the potential rate of peat accumulation that formed the Ferris Coal seam would have been 0.4 mm/yr with the total duration of the coal seam (~20 cm) lasting as long as 75,000 years (Jerrett et al., 2015). At the time of sediment deposition these sites were located at a paleolatitude similar to their current latitude, between 49° and 52° N (Bamforth, 2013). The sites were also within 1000 km of the Western Interior Seaway (WIS), a large seaway that flooded the interior basin of North America during the Late Cretaceous period (Berry, 2017), and the Frenchman Formation has been described as forming in a coastal floodplain (Kupsch, 1957). The Cretaceous-aged rocks of western Canada were not deeply buried or heated (Walls et al., 1979), which implies good potential for preservation of the plant wax *n*-alkanes applied in this study.

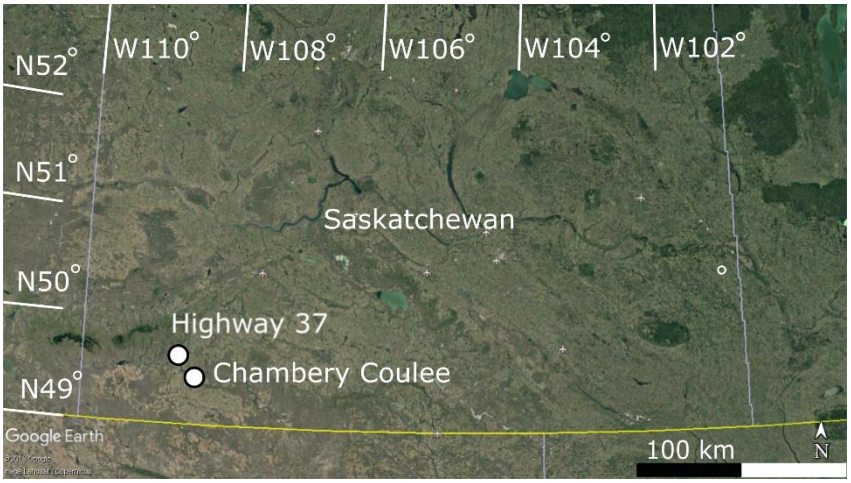

Figure 1. Map of southern Saskatchewan with the field sites for HW37 and CC marked. Photo taken from Google Earth Pro.

The site at CC (Figure 2-b) is a relatively small exposure on private property, with the exposure extending down a slope leading into the Frenchman River Valley near a dirt road. The site has over 30 meters of exposed strata with around 6 meters of the lowermost Ravenscrag overlying the Frenchman Formation, which can be up to 35 meters thick in some areas. The site of HW37 (Figure 2-a) is a recently exposed outcrop that was uncovered during the construction of the highway for which it is named, about 20 km south of Shawnovan, SK (McIver, 2002). The K-Pg section at this site has undergone little weathering due to the recently exposed nature of the site. The section is 18 m thick with around 9 meters of strata from each of the formations exposed, with the top of the section capped by Quaternary glacial till. The two sites are separated by 28.5 km, providing a comparison of geographically proximal strata.

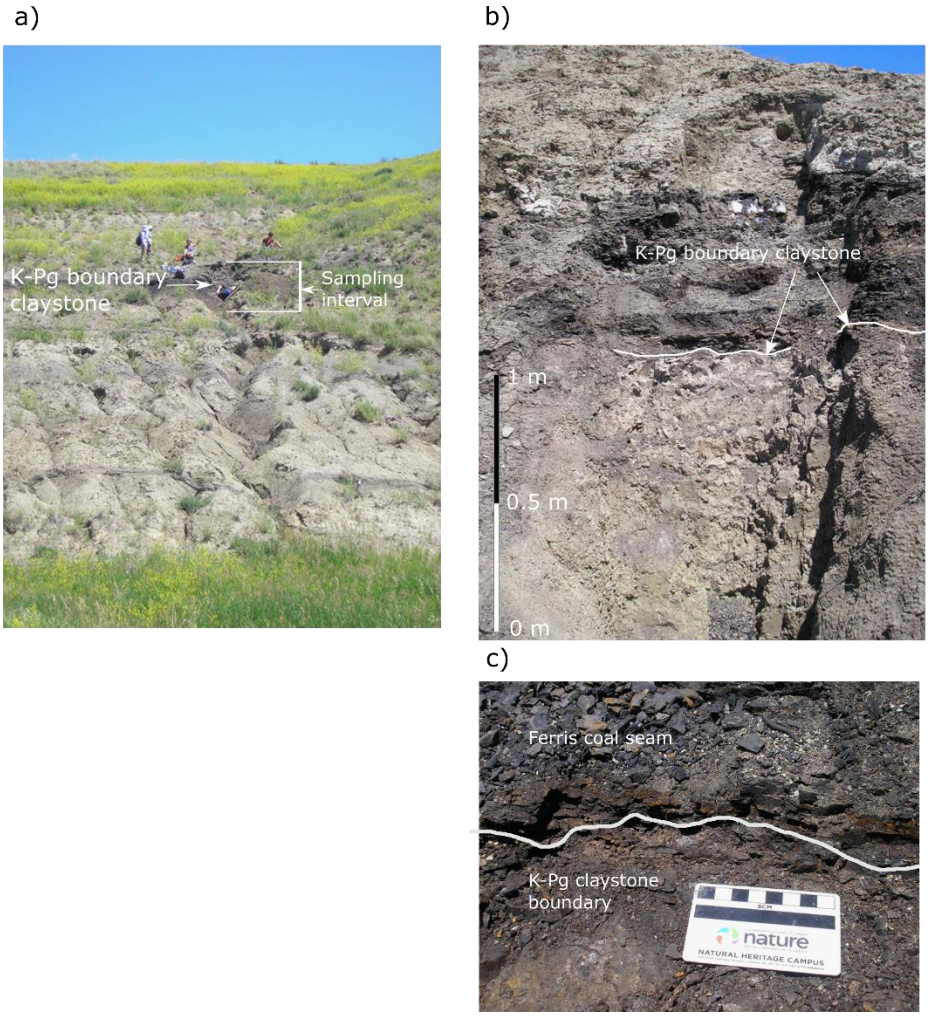

Figure 2: Photos of the field sites visited for sample collection. (A) The roadside of HW37, with the two-meter boundary section located next to seated field assistants. (B) Photo of the section at CC, with the 2-meter section exposed in the frame. The dark layer centered in the image is the Ferris coal seam with the boundary sandwiched between the coal layer and the larger bed of siltstone below it. (B) Close up of the K-Pg boundary from CC, indicated by a faintly pink-brown layer of clay found underneath the dark shelf of coal above, with the scale bar level with the boundary.

2.2 Sample collection

Sampling was focused within a 1 m window above and below the K-Pg boundary. Two types of samples were collected: 1) larger samples with an average weight of 400 g collected for the leaf wax isotopic analysis at a resolution of 10 cm; and 2) smaller samples of at least 5 mg

collected for bulk organic carbon $\delta^{13}C$ analyses at a resolution of 2 cm. In total, 22 compound specific isotope samples from CC and 25 samples from HW37 were analyzed, and 68 bulk OC isotope samples from CC and 68 samples from HW37 were analyzed.

2.3 Bulk $\delta^{13}C$ analyses

Around 5 mg of sediment per sample was ground to a fine powder with a mortar and pestle. Bulk organic carbon content (%OC) and $\delta^{13}C$ values were analyzed at the Geotop Light Stable Isotope Laboratory at the University of Quebec at Montreal. The samples were acid fumigated in silver capsules prior to analysis to remove inorganic carbon (Harris et al., 2001). The silver capsules were then closed and placed within tin capsules to be analyzed, with the samples being processed on an Isoprime 100 MicroCube mass spectrometer coupled to an Elemental Vario MicroCube elemental analyzer in Continuous Flow mode. A first analysis measured the weight percent organic carbon (%OC), and a second analysis measured the $\delta^{13}C$ value of organic carbon. Laboratory $\delta^{13}C$ standards with values of -42.5‰ and -17.0‰ (VPDB) were used for correcting raw data with a calibration line. These laboratory reference materials were normalized on the NBS19-LSVEC scale for $\delta^{13}C$. A third internal reference with a $\delta^{13}C$ value of -28.7‰ was used to ensure accuracy of the calibration. The analytical error of the bulk $\delta^{13}C$ analyses was ±0.3‰.

2.4 Lipid extraction and analysis

Sediments for compound specific isotope analysis were first freeze dried, ground into a fine powder, and weighed. The amount of sediment extracted varied depending on organic carbon content, with carbon-rich samples typically requiring 40 g of sediment while carbon-poor samples required up to 200 g of sediment to yield sufficient *n*-alkanes for isotopic analysis. The

sediments were put into CEM MARS 6 solvent extraction tubes, along with a 9:1 ratio of dichloromethane (DCM) to methanol solution, with the volume of solvent scaled to the volume of sediment (approximately 1:1 sediment/solvent by volume), followed by extraction using a MARS6 microwave at a temperature of 80° C for 15 minutes. Samples were then transferred into vials to be centrifuged to separate residual sediment from solvent, before pippeting the solvent and transferring it to evaporation tubes. The sediment was then further rinsed with solvent and centrifuged three times. Once all the samples were extracted, the solvent extracts were placed in a Rapidvap to be evaporated under N_2 gas. A silica gel column was then prepared for lipid purification, with a Pasteur pipette filled with 1 g of silica gel and 0.5 g of sodium sulphate on top of glass wool. Each vial had 15 ml of hexane added, which was then passed through the silica gel column to elute the hydrocarbon fraction. We then collected the polar fraction by eluting 15 ml of methanol, followed by 1 ml of dichloromethane. The polar fraction was reserved for future study.

The samples were analyzed for *n*-alkane relative abundance with a Thermo Trace 13-10 gas chromatograph (GC) with a flame ionization detector (FID), using a Thermo TR-5 GC column (60m x 0.25mmID, 0.25 µm film), at McGill University. *n*-Alkane hydrogen and carbon isotope measurements were made using a Thermo Delta V Plus Isotope Ratio Mass Spectrometer (IRMS) coupled to a Thermo GC-IsoLink at McGill University, which uses a Thermo TG5Ms column (60m × 0.25mm × 0.25µm film). Compound-specific isotope values were calibrated to the V-SMOW and V-PDB scales using a set of *n*-alkane standards (Mix A6) that were measured offline in references to international standards at Indiana University (arndt.schimmelmann.us/compounds.ht). The Mix A6 standards were used to calibrate both hydrogen and carbon isotope measurements for *n*-alkanes and were analyzed at least twice daily.

The Mix A6 δ^2H and $\delta^{13}C$ standard values can be found in supplementary table 1. Laboratory standards were also analyzed to monitor for instrumental drift and assess measurement reproducibility. The laboratory standards were derived from extracts of maple (*Acer* sp.) leaves that were collected on the McGill campus, with synthetic alkanes (SigmaAldrich) added to enhance the C_{22} and C_{30} *n*-alkane concentrations. The maple standard measurements were analyzed for, with δ^2H values of -173.5‰ for C_{22}, -194.3‰ for C_{27}, -175.5‰ for C_{29}, -51. 5‰ for C_{30}, and -167.7‰ for C_{31}. The $\delta^{13}C$ values are -28.9‰ for C_{20}, -30.9‰ for C_{27}, -35.3‰ for C_{29}, -33.0‰ for C_{30}, and -37.0‰ for C_{31}. Laboratory standards were run after every 3 samples to check for instrumental drift. The long-term standard deviations of the laboratory standard *n*-alkane $\delta^{13}C$ measurements over the course of the study was 0.3‰, while the standard deviation of the laboratory standard δ^2H measurements was 4‰.

To estimate the uncertainty of compound-specific isotope measurements we followed the recommendations of Polissar and D'Andrea (2014). Specifically, we calculated the pooled standard deviation for the C_{25}, C_{27}, and C_{29} *n*-alkane $\delta^{13}C$ and δ^2H values, including all samples with replicate measurements from both sites, using the formula:

$$SD_{pooled} = \sqrt{\frac{(n_1-1)s_1{}^2+(n_2-1)s_2{}^2+\cdots+(n_k-1)s_k{}^2}{n_1+n_2+\cdots+n_k-k}} \quad \textbf{(1)}$$

Where n is the number of replicates per sample, s is the sample standard deviation, and k is the total number of samples measured per chain length.

We then calculated the standard error for each sample, including samples with only one measurement (Polissar and D'Andrea 2014; Niedemeyer et al., 2010), as follows.

$$SE = \frac{SD_{pooled}}{\sqrt{n}} \quad \textbf{(2)}$$

The resulting standard error is considered to be the most accurate estimate of measurement uncertainty for individual samples (Polissar and D'Andrea, 2014).

2.5 n-Alkane chain length analyses

We calculated two indices of the relative abundance of different *n*-alkanes within each sample. The average chain length (ACL) is based on the following equation.

$$ACL = \frac{(A23*23)+(A24*24)+(A25*25)+(A26*26)+(A27*27)+(A28*28)+(A29*29)+(A30*30)+(A31*31)}{A23+A24+A25+A26+A27+A28+A29+A30+A31} \quad \textbf{(3)}$$

Where Ax is the area of the GC-FID trace for a specific *n*-alkane chain length (x).

The Paq' index (Liu et al., 2019), which is applied to determine if *n*-alkanes are predominately derived from aquatic or terrestrial plants, was calculated using the same measurements. Paq' values are intended to be used in the context of ancient, sediment-derived *n*-alkanes rather than from extant ecosystems (Liu et al., 2019). The calculation is as follows.

$$Paq' = \frac{A21+A23+A25}{A21+A23+A25+A27+A29+A31} \quad \textbf{(4)}$$

Paq' is derived from the previously developed Paq index (Ficken et al., 2000), which is focused on extant ecosystems:

$$Paq = \frac{A23+A25}{A23+A25+A29+A31} \quad \textbf{(5)}$$

Paq' was used for the purpose of this study as it was developed and optimized for analyzing plant wax alkanes from sedimentary rocks. The only notable difference between the two indices is the addition of A21, A27, A31, and A33, and in the calculations for Paq'. However, we did not include A33 in the calculations of this index as the C_{33} *n*-alkane was undetectable in many of our samples.

2.6 Modeled values of bulk $\delta^{13}C$

In order to constrain how changing plant sources of sedimentary organic carbon and plant $\delta^{13}C$ values potentially affected bulk $\delta^{13}C$ values, we calculated a predicted bulk organic $\delta^{13}C$ value based on plant-wax distributions and $\delta^{13}C$ values. This calculation was performed to assess how plant $\delta^{13}C$ values as determined using compound-specific isotope measurements compare with the bulk $\delta^{13}C$ measurements, which would help to examine whether changes in bulk organic $\delta^{13}C$ measurements primarily reflect changes in plant $\delta^{13}C$ and the relative abundance of plant types.

We used C_{25} and C_{29} $\delta^{13}C$ values (after correcting for appropriate fractionation factors) as being representative of aquatic and terrestrial plants, respectively (see Discussion section 4.2 for a detailed rationale). Paq' values were used to estimate the relative abundance of aquatic and terrestrial plant matter contributing to the bulk sedimentary organic carbon.

To perform these calculations we first estimated the fraction of organic matter derived from terrestrial and aquatic plants, using the following equation.

$$Paq' = \left(f_{aq} x Em_{aq}\right) x \left(f_t x Em_t\right) \quad \textbf{(6)}$$

Where Paq' is from the observed measurements, "f" is the fraction of the plant group we are solving for (aq – aquatic, t – terrestrial), and Em is the end-member value of Paq' for terrestrial and submerged aquatic plants. We applied values of $Em_{aq} = 0.80$ and $Em_t = 0.07$ (the minimum and maximum Paq' values observed in our dataset) such hat f_{aq} and f_t were consistently between 0 and 1. To solve for f_{aq} and f_t, we combined equation 4 with the following equation:

$$1 = f_{aq} + f_t \quad \textbf{(7)}$$

Next the bulk $\delta^{13}C$ of aquatic and terrestrial plants were calculated using the following equations:

$$\delta^{13}C_{aquatic} = \frac{(\delta^{13}C_{25}+1000)}{(\frac{\varepsilon_{aq}}{1000}+1)} - 1000 \quad (8)$$

$$\delta^{13}C_{terrestrial} = \frac{(\delta^{13}C_{29}+1000)}{(\frac{\varepsilon_{t}}{1000}+1)} - 1000 \quad (9)$$

Where ε is the carbon isotopic fractionation between bulk plant tissue and the specific *n*-alkane referred to (C_{25} or C_{29}), and $\delta^{13}C_{25}$ and $\delta^{13}C_{29}$ refer to the measured $\delta^{13}C$ value from those specific *n*-alkanes. ε_t (i.e. fractionation between C_{29} and bulk terrestrial plants; -3.1±2.0‰) was derived from Chikaraishi and Naraoka, using measurements of all terrestrial plants in that study (2003). $\varepsilon_{aquatic}$ (i.e. fractionation between C_{25} and bulk aquatic plants -7.4±2.9‰) was derived from measurements of freshwater aquatic plants from Chikaraishi and Naraoka, (2003) and Aichner et al., (2010).

Once the $\delta^{13}C$ of bulk aquatic and terrestrial plants were calculated, the total bulk $\delta^{13}C$ ($\delta^{13}C_{bulk}$) was estimated using the following equation.

$$\delta^{13}C_{bulk} = \left(f_{aq} x \delta^{13}C_{aquatic}\right) + \left(f_t x \delta^{13}C_{terrestrial}\right) \quad (10)$$

These modeled values of bulk $\delta^{13}C$ assumes that the bulk organic matter present in sediments is directly linked to the $\delta^{13}C$ of sedimentary plant-derived OM. This is an oversimplification, as it ignores other sources of carbon, such as algal, microbial, and heterotrophic biomass, and any isotopic effects of sedimentary OM decomposition. However, this analysis provides a first-order indication of how changes in plant inputs and changing plant $\delta^{13}C$ values could interact to influence the bulk $\delta^{13}C$ record.

3. Results

3.1 Percent organic carbon

There is a steady increase in weight percent organic carbon (%OC) leading up to the boundary at both sites, with values rising from below 0.3% to ~3%. Within the boundary clay layer, HW37 (Figure 3-a) has %OC of 10.1% whereas CC (Figure 3-d) had a lower value of 2.6%. Above the boundary, both sites contain very large amounts of organic carbon in the Ferris coal ranging from 28.5% to 70.1%. The coal layer is overlain by relatively carbon-poor strata (0.4% to 1.1%) followed by a second peak in values (12-24%) between 30-50 cm. Following this second peak %OC at CC stabilizes around 0.5%, while at HW37 it stabilizes around 3 to 5%.

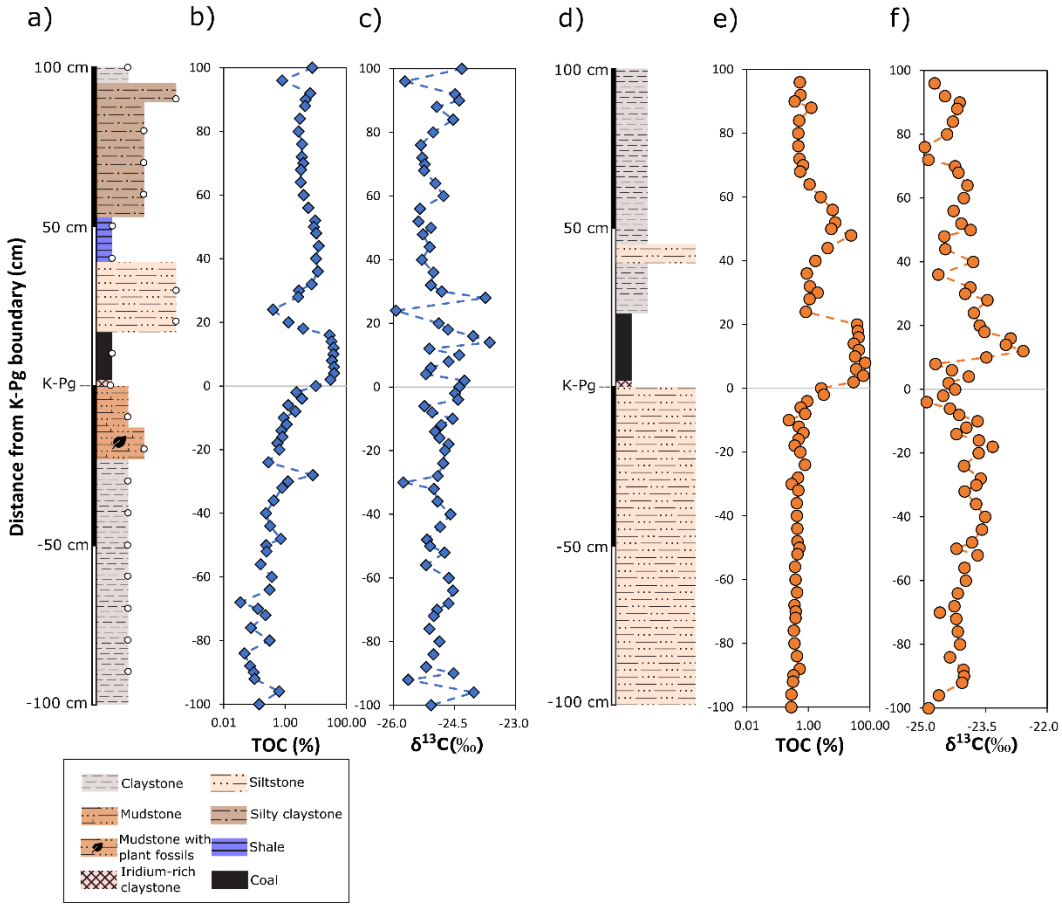

Figure 3: Measurements of percent organic carbon and $\delta^{13}C_{bulk}$ made from the HW37 (a-c) and CC (d-f) sections. TOC values plotted on a logarithmic scale in order to highlight variability below the boundary.

335

Distance from boundary (cm)	HW37 - bulk $\delta^{13}C$ (‰)	HW37 – Corg (%)	CC - bulk $\delta^{13}C$ (‰)	CC – Corg (%)
100	-24.3	7.7		
96	-25.7	0.8	-24.8	0.5
92	-24.5	6.6	-24.5	0.6
90	-24.4	4.7	-24.1	0.4
88	-25.0	4.5	-24.2	1.2
84	-24.5	3.0	-24.3	0.5
80	-25.0	2.8	-24.4	0.5
76	-25.3	3.6	-25.0	0.5
72	-25.3	3.5	-24.9	0.5
70	-25.2	3.9	-24.3	0.7
68	-25.3	3.3	-24.2	0.5
64	-25.0	3.2	-23.9	1.1
60	-24.8	4.1	-24.0	2.5
56	-25.4	5.7	-24.3	6.2
52	-25.4	9.6	-24.1	7.5
50	-25.1	8.7	-23.9	5.5
48	-25.3	10.4	-24.5	24.3
44	-25.1	12.5	-24.5	4.2
40	-25.3	10.1	-23.8	1.7
36	-25.0	11.8	-24.7	0.9
32	-25.1	7.5	-23.9	1.1
30	-24.8	2.8	-24.0	2.0
28	-23.7	2.7	-23.5	1.1
24	-25.9	0.4	-23.8	0.8
20	-24.9	1.3	-23.7	38.3
18	-24.7	3.9	-23.5	40.0
16	-24.0	28.5	-22.9	43.0
14	-23.6	32.6	-23.0	30.1
12	-25.1	38.2	-22.6	43.2
10	-24.4	37.6	-23.5	32.8
8	-24.7	33.8	-24.7	70.1
6	-25.1	39.7	-24.3	35.3
4	-25.2	39.8	-23.9	60.4
2	-24.3	30.2	-24.4	29.1
0	-24.4	10.1	-24.3	2.6
-2	-24.5	2.3	-24.5	3.2
-4	-24.4	3.6	-24.9	0.9
-6	-25.2	1.3	-24.4	0.6
-8	-25.1	2.2	-24.2	0.8
-10	-24.6	0.9	-23.7	0.2
-12	-24.8	1.1	-24.0	0.5
-14	-25.0	0.8	-24.2	0.7
-16	-24.9	0.8	-23.7	0.5
-18	-24.7	0.6	-23.3	0.4
-20	-24.7	0.7	-23.7	0.6
-24	-24.8	0.3	-24.0	0.8
-28	-24.9	8.2	-23.6	0.5
-30	-25.8	1.3	-23.7	0.3

-32	-25.0	0.8	-24.0	0.5
-36	-24.9	0.4	-23.7	0.4
-40	-24.6	0.2	-23.5	0.4
-44	-24.9	0.3	-23.6	0.4
-48	-25.2	0.7	-23.8	0.4
-50	-25.1	0.2	-24.2	0.5
-52	-24.8	0.3	-23.7	0.4
-56	-25.2	0.2	-24.0	0.4
-60	-24.6	0.4	-24.0	0.4
-64	-24.5	0.3	-24.2	0.4
-68	-24.7	0.0	-24.3	0.4
-70	-24.9	0.1	-24.6	0.4
-72	-25.0	0.2	-24.2	0.4
-76	-25.1	0.1	-24.2	0.3
-80	-24.9	0.3	-24.1	0.4
-84	-25.0	0.1	-24.4	0.4
-88	-25.2	0.1	-24.0	0.5
-90	-24.5	0.1	-24.0	0.3
-92	-25.6	0.1	-24.1	0.3
-96	-24.0	0.6	-24.6	0.3
-100	-25.1	0.1	-24.9	0.3

Table 1: $\delta^{13}C_{bulk}$ and organic carbon percentage.

3.2 Bulk organic carbon $\delta^{13}C$

Below the boundary at HW37 (Figure 3-b) bulk $\delta^{13}C$ exhibits fluctuations between -24.5 to -25.2‰, while at CC (Figure 3-e) there is a gradual rise in $\delta^{13}C$ from -24.9‰ to -23.5‰ over 60 cm, followed by a decline to -24.9‰ leading up to the boundary. The values at the boundary are similar at both sites, with HW37 having a value of -24.4‰ and CC having a value of -24.3‰. The samples above the boundary show high-amplitude and high-frequency variability with little correlation between the two sites. Furthermore, there is no clear indication of a negative CIE that is outside the range of background variability of the bulk $\delta^{13}C$ records directly above the K-Pg boundary. Beyond 30 cm above the boundary, the bulk $\delta^{13}C$ signals at the two sites begin to stabilize, with values similar to those observed before the boundary.

3.3 Average chain length

The ACL at HW37 (Figure 4-d) was relatively stable below the boundary with an average length between 26.5 and 27.5. By contrast, CC (Figure 5-d) exhibited lower ACL values below the boundary between 25.3 and 26.3. Both sites also show very similar ACL values at the K-Pg boundary of approximately 26.5. Above the boundary, both sites show higher and more variable ACL values.

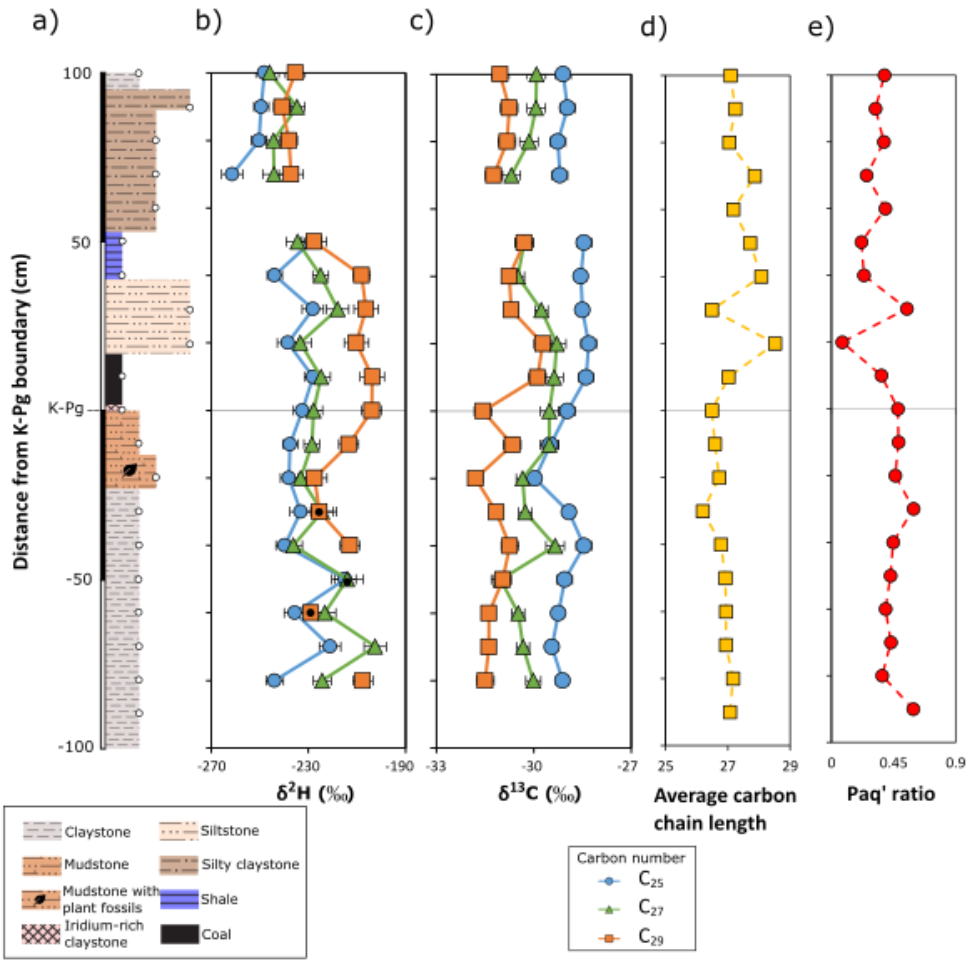

Figure 4: The measurements and calculations made from the HW37 section in relation to *n*-alkane isotopes. Pictured are the stratigraphic section (a), the δ^2H (b) and $\delta^{13}C$ (c) stable isotope measurements derived from plant wax lipids, with black points indicating samples with a single measurement. Average chain length (d) and the Paq' (e) values indicate changes in the abundance of *n*-alkanes derived from aquatic vs terrestrial plants.

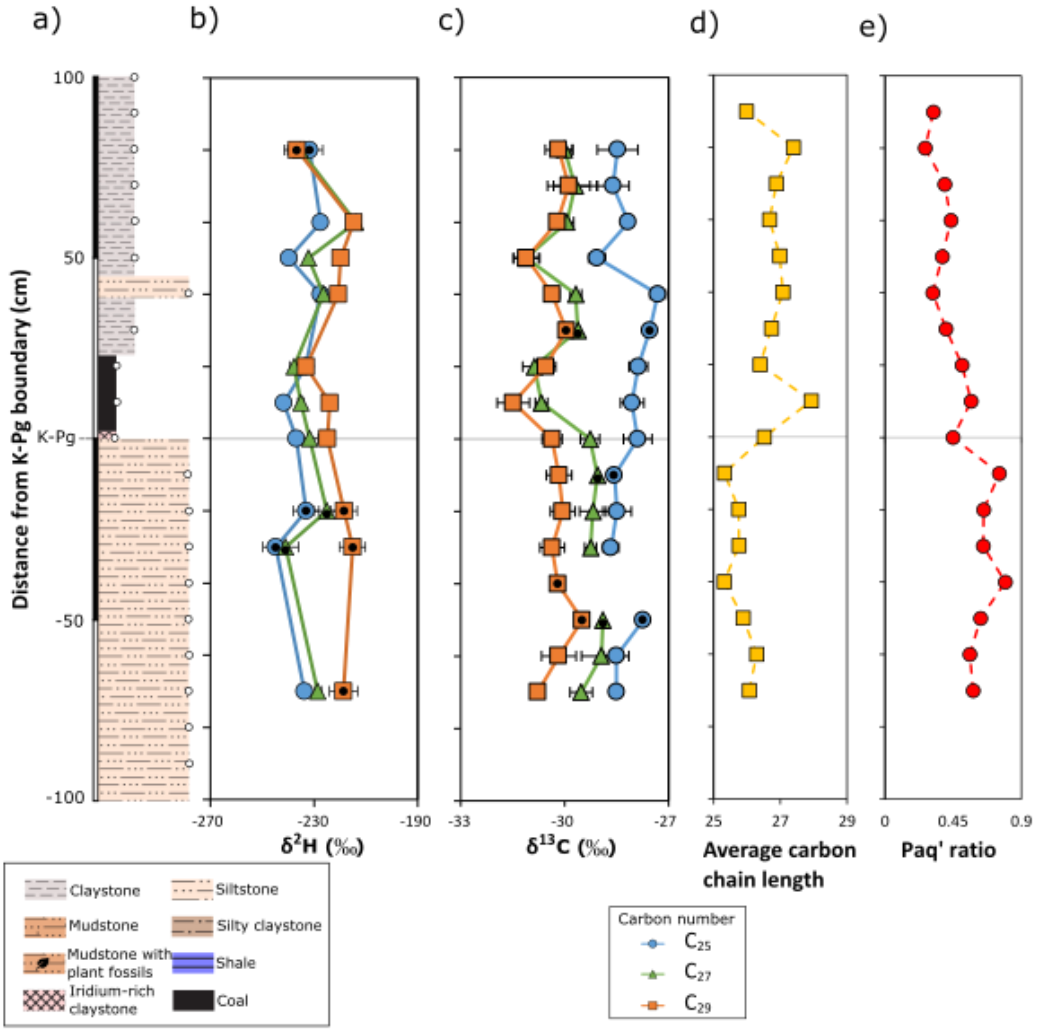

Figure 5: The measurements and calculations made from the CC section in relation to *n*-alkane isotopes. Pictured are the stratigraphic section (a), the δ^2H (b) and $\delta^{13}C$ (c) stable isotope measurements derived from plant wax lipids, with black points indicating samples with a single measurement. Average chain length (d) and the Paq' (e) values indicate changes in the abundance of *n*-alkanes derived from aquatic vs terrestrial plants.

3.4 Paq'

Paq' values (Figure 4-e, 5-e, Table 2) show relatively stable signals below the boundary with standard deviations of approximately 0.1 for both localities. The mean values at HW37 was 0.6 while the mean values at CC was 0.8. A major shift in Paq' occurs above the boundary at

both sites, with samples almost uniformly lower above the boundary than below it. Although the values remain higher at CC than at HW37, the shift to lower values that occurs across the extinction event is comparable in magnitude and is consistent between both sites. At HW37 there is especially high-amplitude variability in Paq' values in the first 40 cm above the boundary.

Distance from boundary (cm)	HW37 - Paq'	CC - Paq'	HW37 - ACL	CC - ACL
100	0.4		27.1	
90	0.3	0.3	27.2	26.0
80	0.4	0.3	27.0	27.4
70	0.3	0.4	27.9	26.9
60	0.4	0.4	27.2	26.7
50	0.2	0.4	27.7	27.0
40	0.2	0.3	28.1	27.1
30	0.5	0.4	26.5	26.7
20	0.1	0.5	28.5	26.4
10	0.4	0.6	27.0	27.9
0	0.5	0.4	26.5	26.5
-10	0.5	0.8	26.6	25.3
-20	0.5	0.7	26.7	25.8
-30	0.6	0.6	26.2	25.8
-40	0.4	0.8	26.8	25.3
-50	0.4	0.6	26.9	25.9
-60	0.4	0.6	26.9	26.3
-70	0.4	0.6	26.9	26.1
-80	0.4		27.2	
-90	0.6		27.1	

Table 2: Paq' and average chain length measurements.

3.5 δ^2H n-alkane isotope measurements

We report the δ^2H values for the C_{25}, C_{27}, and C_{29} *n*-alkanes. Other *n*-alkanes were typically too low in abundance for accurate isotope measurements. At HW37 (Figure 4-b, Table 4), the δ^2H values for each chain length were within the range of -203‰ to -261‰, with C_{25} on average having the most negative values at -236‰ and C_{29} having the highest values with an

384 average of -219‰. The CC (Figure 5-b, Table 3) samples range from -196.2‰ to -245‰, and
385 C_{29} also typically exhibits the most positive values with an average of -223‰ and C_{25} typically
386 has the most negative values with an average of -235‰. There are no clear trends in δ^2H
387 variability in the C_{25} and C_{27} n-alkanes across the studied sections. The C_{29} n-alkanes exhibit
388 greater δ^2H variability between -20 to 50 cm (relative to the boundary), with inconsistent
389 patterns at the two sites. During this interval C_{29} n-alkane δ^2H increases and then decreases by
390 about 25‰ at HW37. In contrast at CC C_{29} n-alkane δ^2H decreases and then increases by about
391 15‰.

392 Some samples for the *n*-alkane isotope measurements were only measured once due to
393 their relatively low concentration. Analysis of samples with a single measurement is at times
394 necessary in compound-specific isotope studies due to small sample sizes (e.g. Niedermeyer et
395 al., 2010), The error estimation technique used for the compound specific isotope analyses takes
396 into account the greater uncertainty associated with non-replicate measurements (Polissar and
397 D'Andrea, 2015; see Section 2.4). However, samples with single measurements are subject to
398 greater uncertainty than other sample analyses, and for this reason we specifically identify these
399 samples in figures 4 and 5. These samples should be interpreted with caution, but in general do
400 not strongly influence our overall interpretation of the data. We note that because of a lack of
401 replicate measurements is a larger degree of uncertainty in compound specific δ^2H values from
402 the CC section below the K-PG boundary.
403

Distance from boundary (cm)	CC - C_{25} δ^2H (‰)	SE - CC - C_{25} δ^2H (‰)	CC - C_{27} δ^2H (‰)	SE - CC - C_{27} δ^2H (‰)	CC - C_{29} δ^2H (‰)	SE - CC - C_{29} δ^2H (‰)
80	*-232*	6	*-235*	6	*-237*	7
60	-227	4	-214	5	-215	5

50	-240	4	-232	5	-220	5
40	-227	4	-226	5	-221	5
20	-233	4	-238	5	-233	5
10	-242	4	-235	5	-224	5
0	-237	4	-232	5	-225	5
-20	*-233*	6	*-225*	6	*-218*	7
-30	*-245*	6	*-241*	6	*-215*	7
-70	-234	4	-229	5	*-219*	7

Table 3: CC δ^2H measurements from plant wax lipids. Samples that were measured once are italicized.

Distance from boundary (cm)	HW37 - C_{25} δ^2H (‰)	SE - HW37 - C_{25} δ^2H (‰)	HW37 - C_{27} δ^2H (‰)	SE - HW37 - C_{27} δ^2H (‰)	HW37 - C_{29} δ^2H (‰)	SE - HW37 - C_{29} δ^2H (‰)
100	-248	4	-246	4	-235	4
90	-249	3	-235	3	-241	4
80	-250	3	-244	3	-238	4
70	-261	4	-244	5	-237	5
50	-229	4	-235	5	-228	5
40	-244	3	-225	3	-208	4
30	-228	4	-218	5	-206	5
20	-238	4	-233	5	-210	5
10	-228	4	-225	4	-204	5
0	-233	4	-228	4	-204	4
-10	-237	3	-229	3	-213	4
-20	-238	4	-233	4	-227	5
-30	-233	4	-224	5	*-226*	7
-40	-240	4	-236	4	-213	4
-50	-215	4	*-214*	6		
-60	-236	4	-223	5	*-229*	7
-70	-221	4	-203	5		
-80	-244	4	-224	4	-208	4

Table 4: HW37 δ^2H measurements from plant wax lipids. Blank entries indicate no measurement due to low concentration. Samples that were measured once are italicized.

3.6 $\delta^{13}C$ n-alkane isotope measurements

The $\delta^{13}C$ values from HW37 (Figure 4-c, Table 6) range from -28.3‰ to -31.8‰, with shorter hydrocarbon chains consistently expressing more positive values than those of longer

chain lengths, with C_{25} measurements averaging -29.0‰, while C_{29} averages -30.9‰. The CC (Figure 5-c, Table 5) samples range from -27.3‰ to -31.5‰, exhibiting the same pattern as HW37 with the shorter chain length hydrocarbons having more positive values. At CC the C_{25} values average -28.2‰ and C_{29} values average -30.3‰. At HW37 we observe an increase of 2 to 2.5‰ in the C_{25} and C_{29} n-alkanes respectively between -20 to +20 cm, which is not apparent in the other n-alkanes. At CC we observe a similar 2‰ enrichment in the C_{25} n-alkane between -20 to +40 cm, but not in the C_{29} n-alkane. At both HW37 and CC we observe short-term depletions (spanning 10 cm) in C_{29} $\delta^{13}C$ (at 0 and +10 cm respectively), of 1 to 1.5‰.

Distance from boundary (cm)	CC - C_{25} $\delta^{13}C$ (‰)	SE - CC - C_{25} $\delta^{13}C$ (‰)	CC - C_{27} $\delta^{13}C$ (‰)	SE - CC - C_{27} $\delta^{13}C$ (‰)	CC - C_{29} $\delta^{13}C$ (‰)	SE - CC - C_{29} $\delta^{13}C$ (‰)
80	-28.5	0.2	-30.0	0.3	-30.2	0.3
70	-28.6	0.2	-29.7	0.2	-29.9	0.2
60	-28.2	0.2	-29.9	0.3	-30.2	0.3
50	-29.1	0.2	-31.1	0.3	-31.1	0.3
40	-27.3	0.2	-29.7	0.3	-30.4	0.3
30	*-27.5*	0.3	*-29.6*	0.4	*-29.9*	0.4
20	-27.9	0.2	-30.9	0.3	-30.5	0.3
10	-28.1	0.2	-30.7	0.3	-31.5	0.3
0	-27.9	0.2	-29.3	0.3	-30.4	0.3
-10	*-28.6*	0.3	*-29.0*	0.4	-30.2	0.3
-20	-28.5	0.2	-29.2	0.2	-30.1	0.2
-30	-28.7	0.2	-29.3	0.2	-30.4	0.2
-40					*-30.2*	0.4
-50	*-27.7*	0.3	*-28.9*	0.4	*-29.5*	0.4
-60	-28.5	0.2	-28.9	0.3	-30.2	0.3
-70	-28.5	0.2	-29.5	0.3	-30.8	0.3

Table 5: CC $\delta^{13}C$ measurements from plant wax lipids. Blank entries indicate no measurement due to low concentration. Samples that were measured once are italicized.

Distance from boundary (cm)	HW37 - C_{25} $\delta^{13}C$ (‰)	SE - HW37 - C_{25} $\delta^{13}C$ (‰)	HW37 - C_{27} $\delta^{13}C$ (‰)	SE - HW37 - C_{27} $\delta^{13}C$ (‰)	HW37 - C_{29} $\delta^{13}C$ (‰)	SE - HW37 - C_{29} $\delta^{13}C$ (‰)
100	-29.1	0.2	-29.9	0.3	-31.0	0.3
90	-29.0	0.2	-29.9	0.3	-30.8	0.3
80	-29.3	0.2	-30.2	0.3	-30.8	0.3
70	-29.2	0.2	-30.7	0.3	-31.2	0.3
50	-28.4	0.2	-30.3	0.3	-30.3	0.3
40	-28.5	0.2	-30.5	0.2	-30.8	0.2
30	-28.5	0.2	-29.8	0.2	-30.7	0.2
20	-28.3	0.2	-29.3	0.3	-29.7	0.3
10	-28.4	0.2	-29.4	0.3	-29.9	0.3
0	-29.0	0.2	-29.5	0.3	-31.6	0.3
-10	-29.5	0.2	-29.5	0.3	-30.7	0.3
-20	-30.0	0.2	-30.3	0.2	-31.8	0.2
-30	-28.9	0.2	-30.3	0.2	-31.2	0.2
-40	-28.5	0.2	-29.3	0.3	-30.7	0.3
-50	-29.1	0.2	-31.0	0.3	-31.0	0.3
-60	-29.2	0.2	-30.5	0.2	-31.4	0.2
-70	-29.4	0.2	-30.3	0.2	-31.4	0.2
-80	-29.1	0.2	-30.0	0.2	-31.5	0.3

Table 6: HW37 $\delta^{13}C$ measurements from plant wax lipids. Samples that were measured once are italicized.

3.7 Modeled bulk $\delta^{13}C$

The modeled bulk $\delta^{13}C$ displays a temporal pattern similar to the Paq' measurements, with values that overlap with the bulk $\delta^{13}C$ measurements for some portions of the record but not others (Figure 6). The modeled values at CC range from -25.6‰ to -21.7‰ while the HW37 values range from -26.7‰ to -23.5‰. The overall variability of these modeled values are greater than the measured bulk $\delta^{13}C$. For example, the standard deviations of the measured bulk $\delta^{13}C$ is 0.5 and 0.4 for CC and HW37 respectively, while the standard deviation of the modeled $\delta^{13}C$ values are 1.2 and 0.9 for the respective sites. This is especially noticeable when comparing the modeled values for CC above the boundary, which range between –25.6 and -23.2, to those from

435 below the boundary, which range from -23.2 to -21.7. The HW37 results show widely ranging
436 values that overlap with the observed data. The model calculations result in high amplitude
437 variability in the 40 cm above the boundary, which is a pattern similar to the observed values.

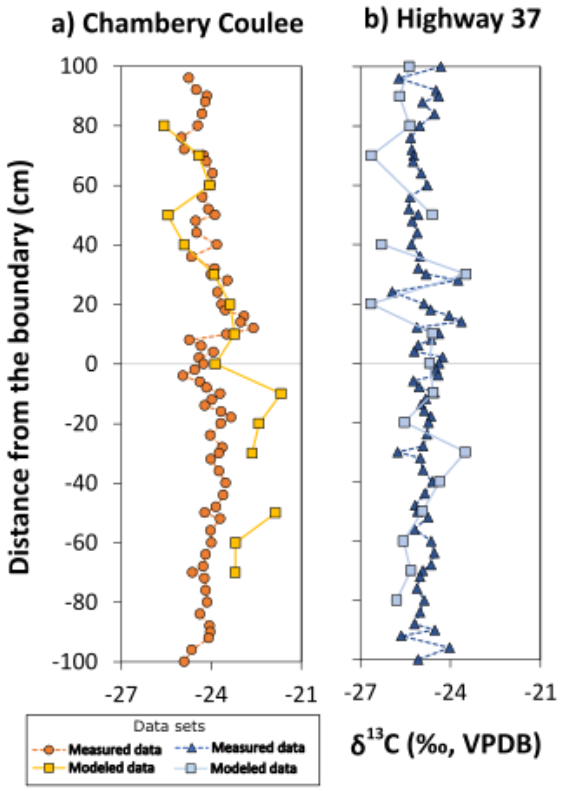

438

439 Figure 6: Modeled bulk $\delta^{13}C$ values derived from the *n*-alkane $\delta^{13}C$ and Paq' values plotted against the measured
440 $\delta^{13}C_{bulk}$ data.

441

442 ## 4. Discussion

443

444 *4.1 Geochronology and the timing of environmental change*

445 Currently there are limited constraints on the chronology of the Frenchman Formation,
446 which limits our ability to estimate the duration and rate of the observed geochemical signals.
447 However, we can make approximate estimates of the timespan for the stratigraphic interval based
448 on the timing of the CIE immediately above the boundary inferred from the C_{29} carbon *n*-alkane

449 measurements (Figure 7). These geochronological estimates are primarily relevant to the section
450 above the K-Pg Boundary. At CC we observe the CIE (i.e. the decrease and recovery of C_{29}
451 $\delta^{13}C$) occur within 20 cm above the boundary. At HW37 the CIE occurs within 10 cm above the
452 boundary. We argue that C_{29} $\delta^{13}C$ is the best indicator of the CIE given that it is a direct indicator
453 of the $\delta^{13}C$ of terrestrial plants. Bulk OC $\delta^{13}C$ can be influenced by variable source inputs, as
454 discussed in Section 4.5. Aquatic plant *n*-alkane $\delta^{13}C$ (i.e. C_{25}) may be influenced by variables
455 that would influence the $\delta^{13}C$ of dissolved inorganic carbon, such as weathering rates and aquatic
456 respiration, that could potentially obscure the expression of the CIE (see Section 4.2).
457 Using radiometric age constraints for the duration of the CIE from the Hell Creek
458 Formation (Renne et al., 2013), which was measured to be 5,000 ± 3,000 years after the iridium-
459 rich boundary, we estimate that these sites experienced sedimentation rates of 250-500 years/cm
460 in the earliest Paleogene. Assuming that this sedimentation rate was constant, the upward trend
461 in *n*-alkane $\delta^{13}C$ values spanning the K-Pg boundary observed at both sites (Figure 7; see in
462 section 4.4) would have lasted approximately 10,000 to 25,000 years. An assumption of constant
463 sedimentation rates is not well constrained, and this time estimate should be considered
464 preliminary. A coarsening upward trend above the boundary is indicated by the stratigraphic
465 column, suggesting an increased sedimentation rate through time (Nichols, 2013). This
466 coarsening trend implies that a constant rate of sedimentation is unlikely, and that the period of
467 increasing *n*-alkane $\delta^{13}C$ values may be shorter than we have.
468
469 *4.2 Evidence for changes in plant distribution and ecology*
470 A Paq' value above 0.4 is interpreted to indicate that *n*-alkanes are primarily derived
471 from submerged aquatic plants, whereas a Paq' of below 0.1 is interpreted as indicating that *n*-

alkanes are primarily derived from terrestrial plants (Liu et al., 2019). Below the boundary, Paq' values at both HW37 and CC are primarily above 0.4 suggesting dominant *n*-alkane input from aquatic plants at both sites. Paq' values at both sites shift to lower values above the boundary. This shift is consistent with a long-term increase in the relative abundance of terrestrial plants in the catchment of these sedimentary deposits. In the first 40 cm above the boundary, there is marked variability at HW37 (Figure 4-e), while the data from CC exhibit a continuous decline (Figure 5-e). Values at both sites stabilize around 40 cm above the boundary, at a lower value than observed below the boundary.

The ACL measurements also support a change in the source of *n*-alkanes across the boundary, with values increasing at both sites. This increase is also consistent with a greater relative abundance of terrestrial plants. As with the Paq' values, there is a period of greater variability above the boundary, up to 40-50 cm, after which the values are more stable. Furthermore, a change in *n*-alkane sources across the boundary is supported by the evolution of C_{27} $\delta^{13}C$ values, as discussed below (see Section 4.3). We do not think that other sources of n-alkanes such as ferns, algae, or fungi are likely to have influenced the Paq' and ACL data. The limited data available for *n*-alkane distributions in ferns indicate conflicting results with ferns producing either more short or longer chain *n*-alkanes (Bush and McInerney, 2013; Zhao et al., 2018). Zhao et al. (2018) also show that ferns produce relatively low concentrations of *n*-alkanes overall. Similarly, there is limited data on long-chaing n-alkane production by algae, with available data indicating that algae produce long chain n-alkanes in much lower abundance than aquatic or terrestrial plants (Liu and Liu, 2016). Similarly, available data on fungi indicate they primarily produce short-chain *n*-alkanes (C_{10} to C_{18}), (Markovetz et al., 1967; Elshafie et al., 2007).

Based on these observations we infer that there was a clear shift to an increased abundance of terrestrial plants relative to aquatic plants above the K-Pg boundary at these sites. This suggests that an ecological shift occurred during and after the end-Cretaceous extinction that affected the distribution of flora in the sedimentary basin of the Frenchman Formation. Increased dominance of angiosperms in terrestrial ecosystems could have potentially contributed to this shift as well, since angiosperms produce greater amounts of *n*-alkanes than gymnosperms, at least in extant North American taxa (Diefendorf et al., 2011). As gymnosperms produce fewer n-alkanes but have a similar distribution to angiosperms (Elshafie et al., 2007; Diefendorf et al., 2011), it is highly unlikely that changes in the relative abundance of gymnosperms would have been responsible for the changes in ACL or Paq' values. We also believe that this shift was indicative of a change with terrestrial plants as a whole as gymnosperms and angiosperms both produce more longer chain *n*-alkanes when compared to aquatic plants (Diefendorf et al., 2011). An intriguing possibility is that the extinction of the non-avian dinosaurs, and especially large herbivores, resulted in the complete loss of medium to large bodied vertebrate herbivores in terrestrial ecosystems, potentially allowing for an increase in terrestrial plant standing biomass.

The stratigraphy immediately above the boundary in both our localities does not indicate a trend toward a more terrestrial deposition. Instead, shales are present above the boundary at HW37 and lithologies in Chambery Coulee are similar to those below the boundary. Thus, the inferred shift toward a higher abundance in terrestrial plants based on Paq' values most likely do not reflect a geomorphological change in the fluvial environment, are more likely to be associated with upland or riparian ecological changes and support an inference of a greater abundance of terrestrial plants. The mid-latitude, subtropical forest environment of the Frenchman Formation precludes any extant analogue. However, future work could examine the

rates of which forests recovered with models predicting the presence and absence of large-bodied herbivores.

Comparison of our results to regional pollen records (Braman and Sweet, 1999; Sweet et al., 1999) offers some additional insights on changes in vegetation distribution. Unfortunately the temporal coverage of these studies was very different from this work. Braman and Sweet (1999) observe changes over nearly 60 meters of cores, with a four-meter difference between their lowest sample in the Ravenscrag Formation and their uppermost sample in the Frenchman Formation. Sweet et al. (1999) and Sweet and Braman (1992) provide a more high-resolution analysis, but the comparability with this study remains limited as their sampling range was limited to tens of cm above and below the boundary, with the samples above the boundary being limited to the first coal layer. However, a key feature of these records is that the abundance of algal pollen is diminished across the boundary. This suggests a decline in aquatic primary productivity, which is consistent with the decrease in Paq' we observe across the boundary. In addition, these pollen records indicate an increase in the relative abundance of angiosperms that begins at the K-Pg boundary which is also consistent with the observed decrease in Paq' (Sweet et al., 1999). Conspicuous abundance spikes in *Ulmoideipites* spp. and *Kurtzipites* spp. were recorded for Alberta and Saskatchewan K-Pg boundaries (Sweet and Braman 1992; Sweet et al. 1999). Some of these localities recorded these two taxa comprising over 40% of all sampled palynomorphs. *Kurtzipites* is most comparable to extant *Betlaceae*, *Carpinaceae* and *Corylaceae* (birch trees) (Srivasta 1981). *Ulmoideipites* is tentatively considered an ulmaceous grain comparable to extant *Ulmaceae* (elm and zelkova trees) (Varicchio et al. 2010). Blooms of these angiosperms recorded in the post boundary palynology record may be responsible for the

reduced Paq' we recovered. Of note is that these trees are not herbivore dependent for their seed dispersal, perhaps allowing their rise to dominance in the absence of large herbivores.

It is important to note that there is a high degree of variability between regional pollen records (Braman and Sweet, 1999; Sweet et al., 1999). With the exception of the *Ulmoideipites* and *Kurtzipites* abundance spikes, pollen records are otherwise varied with differences in the relative abundance of different taxonomic groups, as well as in the observed rates of change. While there are some discernable broad trends as discussed above, by and large there is little uniformity between the different sites. This provides evidence for spatial heterogeneity in plant responses to the K-Pg impact and extinction, although the cause of this heterogeneity is uncertain. While we observe a relatively consistent pattern in the Paq' and ACL data between our two study sites, heterogeneity in plant distribution as indicated by pollen records could have led to important long-scale variability compound-specific isotope data, especially for the C_{29} *n*-alkane, as discussed in Sections 4.3, 4.4, and 4.5 below. An important caveat with interpreting palynological data is that taxonomic differences in pollen production can lead to biases in the perceived inferred plant community composition (Odgaard, 1999). *n*-Alkane production is relatively constant within angiosperms (Diefendorf et al., 2011), meaning that our *n*-alkane data could be complementary to pollen records in interpreting major changes in plant ecology.

Previous studies have found evidence for a reduction in plant species diversity across the K-Pg boundary (McElwain and Punyasena, 2007), however, there are no other studies indicating an increase in terrestrial plant abundance or a loss in aquatic plant biomass. The pattern we observe could be a primarily local or regional signal, and additional studies of *n*-alkane distributions, alongside palynological and macrofossil studies, will be valuable to ascertain

whether there was a broader shift towards increased terrestrial plant biomass following the K-Pg extinction.

The high-amplitude shifts in Paq' and ACL observed over the first 40 cm above the boundary suggests a period of ecosystem instability as the sources of the *n*-alkane lipids changed relatively rapidly before stabilizing. This is in line with the documented period of vegetation recovery for flora after the K-Pg extinction with a general trend from the dominance of ferns, followed by a shift to gymnosperms and then angiosperms (Braman and Sweet, 1999; Sweet et al., 1999; Vajda et al., 2001). As seen in the pollen record from Sweet et al. (1999), the recovery was not a single continuous trend as several fern spikes are visible in some of the pollen cores taken, along with an early spike in angiosperm pollen, which may add credibility to the idea that ecosystems did not recover at a continuous pace and that there may have been periods of rapid ecological change.

4.3 Isotopic differences between n-alkane carbon chain lengths

In freshwater depositional systems C_{25} *n*-alkanes are typically predominately produced by submerged aquatic plants while C_{29} *n*-alkanes are primarily derived from terrestrial plants (Ficken et al., 2000; Aichner et al., 2010). These different plant groups have different carbon sources and carbon fixation pathways that influence their carbon isotopic compositions. Aquatic plants tend to have more enriched isotopic compositions due to the effects of low diffusivity of dissolved CO_2 in benthic habitats, as well as the fixation of bicarbonate by some plants (Keeley and Sandquist, 1992; France 1995). This mechanism is consistent with the enrichment of the C_{25} *n*-alkane $\delta^{13}C$ values relative to C_{29}. In contrast, terrestrial plants are relatively depleted in ^{13}C because enhanced diffusion of CO_2 to and from leaf stomata entails stronger carbon isotope

fractionation (Farquhar et al., 1989). The isotopic difference between the C_{25} and C_{29} *n*-alkanes remains relatively constant through the record, suggesting that the plant sources of these molecules did not change significantly. In contrast, at both sites the C_{27} $\delta^{13}C$ values shift from being more similar to C_{25} values below the boundary to being more similar to C_{29} values above the boundary. We infer that this represents an overall shift to a greater input of C_{27} *n*-alkanes from terrestrial plants above the boundary, which is consistent with the Paq' data indicating a greater overall input of *n*-alkanes from terrestrial plants.

As the C_{25} *n*-alkane lipid values are derived primarily from aquatic plants, the hydrogen isotope measurements for these *n*-alkanes likely reflects the isotopic composition of freshwater bodies, in this case a floodplain river. By contrast, the C_{29} *n*-alkane measurements, which are primarily derived from terrestrial plants, reflect the isotopic composition of precipitation and soil water (Sachse et al., 2012). The C_{25} measurements are generally lower than the C_{29} values which is consistent with the inferred different water sources, as soil water would generally be subject to greater fractional evaporation, which would act to raise the $\delta^{2}H$ ratio (Douglas et al., 2012). It is important to note that standing bodies of water, such as lakes, can exhibit a strong evaporative influence of water isotope values (Rach et al., 2014). However, this is likely not the case for this locality as the Frenchman Formation was deposited in a well drained fluvial flood plain. Although the rate of sedimentation and type of fluvial system did fluctuate, there is no evidence that there was standing water in this system with the exception of a few isolated, iron rich units, largely located in the upper Frenchman (Bamforth, 2013; Bamforth et al., 2014), but absent from the sections measured here. Along with evaporation, seasonal differences in precipitation could influence the difference in $\delta^{2}H$ between precipitation and river water observed in C_{29} and C_{25} *n*-alkanes, as previous studies of the Frenchman Formation indicated seasonal variations in

608 temperature (Bamforth et al., 2014). The δ^2H of precipitation is typically lower during winter
609 months (Rozanski et al., 1993), which would cause aquatic plants to incorporate annually
610 averaged precipitation in the form of river water with the lower values of winter precipitation
611 causing the δ^2H for C_{25} to be lowered. In contrast, terrestrial plants would be likely to be biased
612 towards growing season (i.e. summer) precipitation as it is during this season where most of the
613 growth and wax production takes place, giving the δ^2H for C_{29} to be higher by comparison
614 (Sachse et al., 2012).
615
616 *4.4 Patterns of $\delta^{13}C$ variability recorded in n-alkanes*
617 *n*-Alkane carbon isotope measurements from both sites express fluctuations on the order
618 of 1-2‰. In analyzing these signals, we focus on the C_{25} and C_{29} alkanes, both because they
619 express the clearest signal, and because we infer they are the best representatives of signals from
620 aquatic and terrestrial plants, respectively (See Section 4.3). The HW37 section (Fig. 4-c) shows
621 the $\delta^{13}C$ of C_{25} and C_{29} varying in parallel through the section, and in particular increasing by
622 about 1.5 to 2‰ from -20 to 20 cm. A key exception is at the boundary, where the C_{29} value
623 exhibits a short-term decrease of 0.9‰, which we infer represents the K-Pg CIE identified at
624 other terrestrial sections (Arens and Jahren, 2000; Maruoka et al., 2007; Therrien, 2007). In
625 contrast, the CC section (Fig. 5-c) indicates different temporal patterns in C_{25} and C_{29} $\delta^{13}C$. CC's
626 C_{25} signal resembles the trajectory observed at HW37 (Fig. 7-a), with progressive enrichment of
627 1.5‰ spanning the boundary. The C_{29} values appear to vary with greater frequency, but without
628 the progressive enrichment observed in C_{25} or in C_{29} at HW37. At CC we also observe a putative
629 CIE of 1.1‰, with the minimum value at +10 cm.

We suggest that the increase in $\delta^{13}C$ of 1.5 to 2‰ values across the boundary observed in C_{25} and C_{29} at HW37 and in C_{25} at CC had a singular cause. The increase in C_{25} $\delta^{13}C$ values is consistent at both sites except for a slight stratigraphic offset (Figure 7-A), while the increase in C_{25} and C_{29} at HW37 are also temporally consistent. It is unclear why C_{29} $\delta^{13}C$ at CC does not express this enrichment. One possibility is that the C_{29} $\delta^{13}C$ signals were modulated by local hydrological or ecological effects on terrestrial plant carbon isotope fractionation. We note that C_{29} $\delta^{2}H$ at HW37 increased during this interval, suggesting increased evapotranspiration, while C_{29} $\delta^{2}H$ at CC decreased, suggesting decreased evapotranspiration (Figures 4 and 5). Drier conditions and increased evapotranspiration is associated with greater ^{13}C fractionation in plants (Farquhar et al., 1989). Therefore, evapotranspiration effects would have tended to enhance $\delta^{13}C$ enrichment at HW37, while dampening it at CC. Indeed, we note that the expression of $\delta^{13}C$ enrichment at HW37 is greater in C_{29} than C_{25}, which is consistent with the signal in C_{29} being amplified by hydrological change. It is also possible that differences in vegetation composition between these sites could have influenced the C_{29} carbon isotope signals. There is clear spatial variability in pollen records across the K-Pg boundary in Saskatchewan (Braman and Sweet, 1999; Sweet et al., 1999), implying spatial variability in terrestrial plant ecological dynamics following the K-Pg boundary. Given taxonomic differences in terrestrial plant carbon isotopic fractionation (Diefendorf and Freimuth, 2017), this spatial variability could have also influenced the differential trends in C_{29} $\delta^{13}C$ in these two sections.

Given that the $\delta^{13}C$ enrichment was observed in both the C_{25} and C_{29} *n*-alkanes at HW37, we infer that it was likely caused by a mechanism that affected both aquatic and terrestrial plants. Furthermore, the absence of a consistent and complimentary signal in the n-alkane $\delta^{2}H$, Paq', or ACL data between -20 to 20 cm suggests that this enrichment was not primarily caused by

hydrological change or by changes in plant ecology. A shift towards a greater relative abundance of terrestrial plants, as inferred from the Paq' and ACL data, would tend to lead to more depleted $\delta^{13}C$ values, not more enriched values, as discussed in section 4.3. It is possible that this signal reflects a global increase in the $\delta^{13}C$ of atmospheric CO_2, but more study is needed to examine possible local or regional causes.

We note that the carbon isotope variability observed in the *n*-alkane $\delta^{13}C$ record is not consistent with volcanic inputs of atmospheric CO_2, despite the possible occurrence of Deccan Trap flood basalt volcanism during this time (Schoene et al., 2019; Sprain et al., 2019). Volcanic CO_2 input would generally be very similar isotopically to background atmospheric CO_2 (6±2‰) (Gales et al., 2020; Mason et al., 2017). This implies that unrealistically large amounts of CO_2 would be needed to produce the 2‰ enrichment observed in the *n*-alkanes. Furthermore, a recent study estimated that $\delta^{13}C$ shift caused by volcanic emissions would have been quite small (-0.2 to -0.3‰) and that the bulk of the outgassing would have occurred long before the impact (Hull et al., 2020).We cannot rule out that Earth system feedbacks related to flood basalt eruptions could have driven this shift, although we are unaware of a feedback mechanism through which volcanic eruptions would lead to a substantial increase in the $\delta^{13}C$ of atmospheric CO_2.

Using our approximation for the rate of sedimentation (section 4.1), the observed enrichment in *n*-alkane $\delta^{13}C$ values spanning the K-Pg boundary was approximately 10,000 to 25,000 years in duration. However, we note that this time estimate is uncertain, especially since time constraints are highly uncertain below the K-Pg boundary. Despite the uncertainty in its cause, geographic extent, and duration, this pronounced enrichment in n-alkane $\delta^{13}C$ spanning the K-Pg boundary is intriguing and merits further investigation.

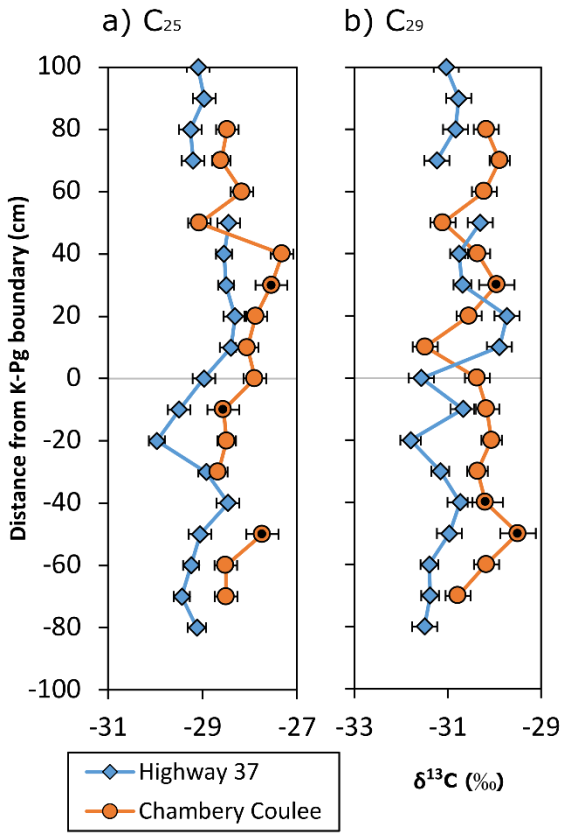

Figure 7: $\delta^{13}C$ measurements of C_{25} (a) and C_{29} (b) compared between the two sites demonstrating similarities and differences in the overall trends observed through the stratigraphic sections, with black points indicating samples with a single measurement.

4.5 Inferences on the isotopic composition of precipitation

We applied the δ^2H values of *n*-alkanes to estimate the δ^2H of regional precipitation. For our analysis we assumed a net fractionation factor between water and *n*-alkanes ($\varepsilon_{water\text{-}n\text{-}alkane}$) of -121‰ for C_{29} (McFarlin et al., 2019). We focussed on C_{29} measurements because the fractionation factor of McFarlin et al. (2019) was specifically developed for C_{29} *n*-alkanes, and because terrestrial plant *n*-alkanes are typically a better indicator of precipitation δ^2H. This fractionation factor is consistent with previous inferred values for C_3 conifers and angiosperms

(Sachse et al., 2012), which were the dominant woody plants in this region. Using this value for $\varepsilon_{water\text{-}n\text{-}alkane}$, estimated δ^2H of precipitation based on the C_{29} alkane ranges between -95‰ and -160‰, with an average δ^2H of -111±17‰ HW and -116±8‰ for CC. These values are within uncertainty of the δ^2H values from annual precipitation water in present day western Canada of -121‰ (values taken from wateriso.utah.edu, Bowen, 2019; Bowen and Revenaugh, 2003; IAEA/WMO, 2015). We do not observe clear evidence for environmental changes that would have altered the isotopic fractionation between plant water and the C_{29} *n*-alkane, although we do infer possible changes in evapotranspiration that could have influenced the δ^2H value of plant water relative to precipitation. While changes in temperature could have had an influence on the isotopic composition of regional precipitation (Rozanski et al., 1993), temperature is not considered to be an important factor influencing hydrogen isotope fractionation between n-alkanes and precipitation in higher plants, other than through its influence on evapotranspiration (Sachse et al., 2012). Furthermore, while we infer an overall shift towards a greater abundance of aquatic plants, we think this change would not have strongly influenced hydrogen isotope fractionation between water and the C_{29} *n*-alkane. As discussed above (Section 4.3), the relatively constant isotopic differences between the C_{29} and C_{25} *n*-alkanes, both in terms of $\delta^{13}C$ and δ^2H, suggests that terrestrial plants remained the dominant source for the C_{29} *n*-alkane. However, we cannot rule out that local-scale changes in plant sources or evapotranspiration rates could have influenced the inferred precipitation δ^2H values, as discussed below. Therefore, we have focused our interpretation on the mean inferred precipitation δ^2H values, as opposed to variability through the record. We note that compound-specific δ^2H measurements at CC below the K-Pg boundary are especially uncertain due to the lack of replicate measurements (See Section 3.5).

712 We estimated the δ^2H of water in the northern WIS, based on the estimate of water $\delta^{18}O$
713 published by Petersen et al., 2016-b (-20‰), and assuming that these waters would plot on the
714 global meteoric water line (GWML). Using the GWML equation $\delta^2H = (8.0 * \delta^{18}O) + 10‰$
715 (Craig, 1961), a δ^2H value of -150‰ was calculated for the waters of the northern WIS. Petersen
716 et al., (2016-b) suggested that the depleted isotopic value inferred from their study was the result
717 of isotopically depleted runoff flowing into the northern WIS. Our inferred precipitation values,
718 though not as depleted as the values observed in the northern WIS, support the conjecture that
719 runoff into the northern WIS would have been isotopically depleted, especially given that C_{29}
720 δ^2H values may be biased towards summer precipitation (see section 4.3). The cause of this
721 isotopically depleted precipitation is not well constrained as there are few proxy data for the
722 isotopic composition of precipitation from this time period. We suggest it might be the result of
723 orographic precipitation in the Rocky Mountains to the west of our study site. Isotopically
724 enabled climate model studies for this time period would be useful to test this hypothesis.
725 Although there are a few estimates of precipitation isotopes from the Late Cretaceous in
726 North America and globally, overlapping values (-123‰ to 82‰) have been recorded in plant
727 wax *n*-alkanes from Late Santonian to Late Campanian sediments of the Canadian Arctic (Super
728 et al., 2018), which was located at around 71°30′N during the Late Cretaceous, about 20° north
729 of our field sites. The similar estimated δ^2H of precipitation between Saskatchewan and the
730 Canadian high Arctic could imply reduced latitudinal δ^2H gradients during the Late Cretaceous
731 relative to modern conditions, although these samples are also separated by about 17 million
732 years, limiting direct comparisons.
733 There is minimal variability in the *n*-alkane δ^2H measurements across the study interval
734 of both sites. In particular the C_{25} *n*-alkane values exhibit little variability across the K-Pg

735 boundary, with variation on the order of 10-15‰ across the boundary (Figure 4-b, 5-b). Given
736 that the samples below the boundary at CC were not large enough for replicate measurements,
737 more data is needed to confirm our observation of limited change in δ^2H across the K-Pg
738 boundary. The C_{29} δ^2H values express greater variability across the boundary on the order of 20-
739 30‰, but this change is not consistent between sites, with decreasing values at CC and
740 increasing values at HW37 (Figure 7). For comparison, changes in δ^2H of plant waxes across the
741 latest Pleistocene deglaciation are frequently much larger, on the order of 50-100‰ (eg. Fornace
742 et al., 2014; Tierney and deMenocal, 2013). The differential direction of change in the C_{29}
743 alkanes δ^2H at these two proximal sites suggests that the forcing mechanism driving these
744 changes was local and was not related to large-scale changes in the isotopic composition of
745 precipitation. Possible local forcing mechanisms could include vegetation change or differential
746 changes in isotopic fractionation related to soil evaporation and transpiration (Sacshe et al.,
747 2013).

748 We also observe a long-term decreasing trend of 20 to 30‰ in the C_{25}, C_{27}, and C_{29} δ^2H
749 values across the record at HW37 (Figure 4-b), although a similar pattern is not evident at CC,
750 further highlighting possible site-specific variations (Figure 5-b). The absence of any major
751 shifts in *n*-alkane δ^2H after the K-Pg boundary suggest that, if the impact did have a major effect
752 on global water cycling that influenced the distribution of precipitation isotopes, its effect most
753 likely only lasted a few thousand years. However, we cannot rule out the possibility that large-
754 scale changes in precipitation δ^2H were obscured by co-occurring changes in evapotranspiration,
755 plant ecology, or plant physiology. For example Baczynski et al. (2017-a), found that *n*-alkane
756 δ^2H records at the Paleocene-Eocene boundary did not record the full magnitude of precipitation
757 isotopic change, most likely because the *n*-alkane δ^2H data were also influenced by changes in

seasonal rainfall isotopic composition and a shift in the season of *n*-alkane production. Additional data either using alternative proxies for precipitation isotopic composition or data from a wider geographic range of study sites will be needed to compare with our results to develop a stronger understanding of how the Chicxulub impact affected the global water cycle.

4.6 Bulk organic carbon isotope data

It is notable that the bulk organic $\delta^{13}C$ record from both HW37 and CC do not exhibit a clear CIE directly above the K-Pg boundary, in contrast to other sections from western North America (Arens and Jahren, 2000; Maruoka et al., 2007; Therrien, 2007). This excursion is found in nearby sites, where it reaches values as low as -2‰ at 2 to 3 cm above the boundary (Jerrett et al., 2015). Other excursions of similar magnitude can be found above the boundary in coeval outcrops in southern Alberta's Scollard Formation, Canada (Therrien et al., 2007). In contrast our sites show an overall rise in $\delta^{13}C$ in the first 20 cm above the boundary. However, the magnitude and duration of the excursion has been found to be highly variable in other sections in North America (Maruoka et al., 2007; Therrien, 2007; Yamamoto et al., 2010).

The absence of a CIE in the bulk OC $\delta^{13}C$ may be due to bulk carbon being a complex mixture of many carbon sources. We show that the $\delta^{13}C$ values of different *n*-alkane behave differently in that the CIE appears to be reflected in the terrestrial plant signal but not the aquatic plants (Figures 7, 8, 10; section 4.1).

Along with the lack of a distinct CIE, both sites show a high degree of variability in bulk $\delta^{13}C$ in the 30 cm above the boundary. Despite the lack of an obvious signal for the CIE, this variability likely indicates ecological or biogeochemical changes. The variation in the bulk $\delta^{13}C$ was most likely not caused by changes in the carbon isotope composition of plant organic matter,

781 as such a change is not apparent in the *n*-alkane $\delta^{13}C$ data. This variation also suggest that the
782 two sites responded differently in the wake of the K-Pg extinction despite their proximity, which
783 could imply different plant communities, as shown by the highly variably pollen records of the
784 region (Braman and Sweet, 1999; Sweet et al., 1999), as well as the differences in the C29 n-
785 alkane isotopic data (Sections 4.4 and 4.5).

786 The modeled $\delta^{13}C$ values potentially provide some insights into possible causes of the
787 variability in the bulk $\delta^{13}C$ values. We note that the modeled values have a range of 3-4‰ while
788 the measured data has a range of 2‰ across both sites. This larger range of variability in the
789 model suggests that other sources of carbon, such as algae or microbial biomass, were important
790 sources of organic matter to sediments and likely dampened $\delta^{13}C$ variability in bulk sedimentary
791 OC. This finding is similar to that reached by Baczynski et al. (2017-b), who applied a similar
792 approach to understand factors controlling the bulk $\delta^{13}C$ record across the Paleocene-Eocene
793 thermal maximum in the Bighorn Basin. That study found a similarly muted bulk $\delta^{13}C$ reading
794 and suggested that microbial degradation of soil organic matter played a key role in the
795 dampened signal in bulk OC $\delta^{13}C$ measurements.

796 However, there are similarities in the temporal patterns of the modeled and observed $\delta^{13}C$
797 values, particularly in the 40 cm above the boundary. For example, at CC the ~2‰ rise and fall
798 of the observed data during this interval is reflected in the modeled values. Similarly, at HW37
799 the marked variability in the observed data in this interval is reflected in the modeled values.
800 Based on these patterns we infer that while terrestrial and aquatic plants were not the only
801 sources of sedimentary OM, the interaction of changes in plant $\delta^{13}C$ and changing relative
802 abundances of these two plant groups could have had a strong effect on sedimentary bulk $\delta^{13}C$
803 values. Furthermore, the modeled data do not express a clear CIE, despite the presence of a CIE

804 in the C_{29} $\delta^{13}C$ record. This implies that the lack of a clear CIE in our bulk data may be the result
805 of the absence of a CIE in aquatic plants and changes in the relative abundance of terrestrial and
806 aquatic plants that effectively masked this signal.

807 Overall, this comparison of modeled and observed bulk $\delta^{13}C$ values highlight the
808 importance of constraining specific carbon sources when interpreting bulk organic $\delta^{13}C$ records,
809 which could help to explain spatial variation in the expression of the terrestrial CIE in K-Pg
810 sediments. This is important as many, though not all, previous studies have only considered the
811 measurements of bulk organic $\delta^{13}C$ in their analysis of the CIE and did not isolate or identify the
812 primary contributors to bulk sedimentary organic carbon. More work will need to be done to
813 better constrain the magnitude, timing, and consistency of the terrestrial CIE going forward,
814 including additional $\delta^{13}C$ analyses of *n*-alkanes and other source-specific carbon fractions.
815
816 *4.7 Relation to the K-Pg extinction*

817 Our results suggest that the K-Pg impact did not have a long-lasting effect on regional
818 carbon and water cycle processing in western Canada. The *n*-alkane $\delta^{13}C$ data imply that ^{13}C
819 enrichment in aquatic and terrestrial plants that began before the boundary continued afterward,
820 with only a brief interruption evident in the C_{29} *n*-alkane $\delta^{13}C$ values. This suggests that the
821 short-term carbon cycle disruptions provoked by the impact did not significantly disrupt longer-
822 term carbon cycle variations, although the mechanism driving the observed enrichment remains
823 unclear. Furthermore, the hydrogen isotope data also suggest that there were no large-scale
824 regional hydrological changes at the boundary, at least on timescales longer than 5000 years. We
825 do note that there were local changes evident in the C_{29} $\delta^{2}H$ data, but they did not have a
826 consistent expression between our two sites.

These results suggests that the terrestrial carbon cycle and potentially the hydrological cycle essentially recovered within roughly 10,000 years, which is consistent with other studies that have suggested similar or even faster recovery times for terrestrial ecosystems (Fastovsky et al., 2016; Lomax et al., 2001; Maruoka et al., 2007; Renne et al., 2013). We note that the role of local and global-scale variability in the carbon- and water-cycles remain incompletely resolved in our dataset, and more research is needed to test for global-scale changes. Our *n*-alkane distribution data do clearly indicate a long-term regional ecological shift towards a greater proportion of terrestrial plants relative to aquatic plants. This ecological change may have been related to broader ecological changes associated with the K-Pg mass extinction, including decreased herbivory as a consequence of the extinction of megafauna, including the extinction of large terrestrial herbivores (see Section 4.2).

5. Conclusions

Our analyses of *n*-alkane and bulk sedimentary isotope ratios across the K-Pg boundary in southern Saskatchewan helped to constrain a number of aspects of environmental change across this key interval of Earth history. We found a notable shift in the dominant plant groups producing sedimentary n-alkanes. Aquatic plants dominated below the boundary whereas terrestrial plants dominated above the boundary, suggesting that plant communities experienced a long-term shift following the extinction event. We speculate this shift may have been driven by the sudden extinction of large terrestrial dinosaur herbivores, which in turn, may have facilitated rapid terrestrial plant recovery and increased terrestrial plant biomass. Presence of high abundances of birches and elms lend support toward a successional forest recovery unlimited by herbivory. Precipitation in the region appears to have had depleted δ^2H values between -86 to -

160‰, values that are broadly consistent with inferences of a depleted isotopic composition for the northern WIS in the late Cretaceous. *n*-Alkane $\delta^{13}C$ measurements indicate a long-term increase of approximately 2‰ spanning the K-Pg boundary that we tentatively estimate as occurring over a time span of approximately 10,000 to 25,000 years. The lack of an obvious long-term disturbance to *n*-alkane carbon, and less conclusively the hydrogen, isotope values following the boundary suggests both the terrestrial water and carbon cycles recovered within 5,000 to 10,000 years after the impact, although the role of local-scale processes influencing n-alkane isotopic fractionation needs to be further resolved. Additionally, the large variability in the bulk organic carbon $\delta^{13}C$ record after the impact suggests a period of instability in sedimentary organic carbon sources which we interpret as being partly related to short-term variability in carbon inputs from terrestrial and aquatic primary production. The modeling exercise illustrated that changes in the plant sources of sedimentary organic matter have a noticeable affect on the bulk organic $\delta^{13}C$. This presents a cautionary example of how relying on bulk OM $\delta^{13}C$ measurements can lead to misleading inferences regarding the magnitude of carbon isotope excursions. In addition, the differences in bulk and compound-specific isotopic signals between the two sites, despite their proximity, is noteworthy, and is consistent with variability in palynological and bulk carbon isotope studies in other studies from this region. These data suggest a high degree of heterogeneity in terrestrial K-Pg boundary sections and emphasize the importance of caution in interpreting data from a small set of study sites.

Acknowledgements

The authors would like to thank Emily Bamforth for her assistance and guidance with field sampling. Thanks to Agnieszka Adamowiscz-Walczak and Jean-Francois Helie for their aid

with analyses at the Geotop Stable Isotope Lab at UQAM, to Benjamin Keenan for assistance with sample preparation, and to Thi Hao Bui for assistance with compound GC-FID and GC-IRMS analyses at McGill University. We also would like to thank the Allemand family for sample collection on their property. This work was supported by the NSERC Discovery Grant to Peter Douglas (2017-03902), as well as funding from the Delise Alison Award which was provided through the Redpath Museum, and the Eric Mountjoy Fellowship and the Graduate Research Ehnancement and Travel award that were provided through the Earth and Planetary Science department at McGill University to Robert Bourque.

References:

Aichner B., Herzschuh U., & Wilkes H. (2010). Influence of aquatic macrophytes on the stable carbon isotope signatures of sedimentary organic matter in lakes on the Tibetan Plateau. *Organic Chemistry*, 41, 706-718.

Alegret L. & Thomas E. (2009). Food supply to the seafloor in the Pacific Ocean after the Cretaceous/Paleogene boundary event. *Marine Micropaleontology*, 73, 105-116.

Alvarez L. W., Alvarez W., Asaro F., & Michel H. V. (1980). Extraterrestrial Cause for the Cretaceous-Tertiary Extinction. *Science*, 208, 1095-1108.

Arens N. C. & Jahren A. J. (2000). Carbon isotope excursion in Atmospheric CO_2 at the Cretaceous-Tertiary boundary: evidence from terrestrial sediments. *PALAIOS*, 15, 312-322.

Baczynski A. A., McInerney F. A., Wing S. L., Kraus M. J., Bloch J. I., & Secord R. (2017). Constraining paleohydrologic change during the Paleocene-Eocene Thermal Maximum in the continental interior of North America. *Palaeogeography, Palaeoclimatology, Palaeoecology,* 465, 237-246.-a

Baczynski A. A., McInerney F. A., Wing S. L., Kraus M. J., Morse P. E., Bloch J. I., Chung A. H., & Freeman K. H. (2017). Distortion of carbon isotope excursion in bulk soil organic matter during the Paleocene-Eocene thermal maximum. *Geological Society of America Bulletin*, 128, 1352-1366.-b

Bamforth, E.L. (2013). Paleoecology and paleoenvironmental trends immediately prior to the End-Cretaceous extinction in the latest Maastrichtian (66Ma) Frenchman Formation, Saskatchewan, Canada (Ph.D.). McGill University, Montreal.

Bamforth E. L., Button C. L., & Larsson H. C. E. (2014). Paleoclimate estimates and fire ecology immediately prior to the end-Cretaceous mass extinction in the Frenchman Formation (66 Ma), Saskatchewan, Canada. *Palaeogeography, Palaeoclimatology, Palaeoecology*, 401, 96-110.

Barnet J. S. K., Littler K., Kroon D., Leng M. J., Westerhold T., Röhl U., & Zachos J. C. (2018). A new high-resolution chronology for the late Maastrichtian warming event: Establishing robust temporal links with the onset of Deccan volcanism. *Geology*, 46, 147-150.

Berry K. (2017). New paleontological constraints on the paleogeography of the Western Interior Seaway near the end of the Cretaceous (late Campanian-Maastrichtian) with a special emphasis on the paleogeography of southern Colorado, U.S.A. *Rocky Mountain Geology*, 52, 1-16.

Bowen G. J. and Revenaugh J. (2003). Interpolating the isotopic composition of modern meteoric precipitation. *Water Resources Research* **39**(10), 1299, doi:10.129/2003WR002086.

Bowen, G. J. (2019). The Online Isotopes in Precipitation Calculator, version 3.0. http://www.waterisotopes.org.

Braman D. R. & Sweet A. R. (1999). Terrestrial palynomorph biostratigraphy of the Cypress Hills, Wood Mountain, and Turtle Mountain areas (Upper Cretaceous – Paleocene) of Western Canada. *Canadian Journal of Earth Sciences*, 36, 725-741.

Bush R. T. & McInerney F. A. (2013). Leaf wax *n*-alkane distributions in and across modern plants: Implications for paleoecology and chemotaxonomy. *Geochimicha et Cosmochimica Acta*, 117, 161-179.

Chikaraishi Y. & Naraoka H. (2003). Compound-specific δD & δ^{13}C analyses of *n*-alkanes extracted from terrestrial and aquatic plants. *Phytochemistry*, 63, 361-371.

Craig H. (1961). Isotopic variations in meteoric waters. *Science*, 133, 1702-1703.

D'Hondt S., Donaghay P., Zachos J. C., Luttenberg D., & Lindinger M. (1998). Organic carbon fluxes and ecological recovery from the Cretaceous-Tertiary mass extinction. *SCIENCE*, 282, 276-279.

Diefendorf A. F., Freeman K. H., Wing S. L., & Graham H. V. (2011). Production of *n*-alkyl in living plants and implications for geologic past. *Geochimica et Cosmochimica Acta*, 75, 7472-7485.

Diefendorf A. F. & Freimuth E. J. (2017). Extracting the most from terrestrial plant-derived *n*-alkyl lipids and their carbon isotopes from the sedimentary record: A review. *Organic Geochemistry*, 103, 1-21.

Douglas P. M. J., Pagani M., Brenner M., Hodell D. A., & Curtis J. H. (2012). Aridity and vegetation composition are important determinants of leaf-wax δD values in southeastern Mexico and Central America. *Geochimica et Cosmochimica Acta*, 97, 24-45.

Elshafie A., AlKindi A. Y., Al-Busaidi S., Bakheit C., & Albahry S. N. (2007). Biodegradation of crude oil and n-alkanes by fungi isolated from Oman. *Marine Pollution Bulletin*, 54, 1692-1696.

Farquhar G. D., Ehleringer J. R., & Hubick K. T. (1989). Carbon isotope discrimination and photosynthesis. *Annual review of plant biology*, 40, 503-537.

964 Fastovsky D. E. & Bercovici A. (2016). The Hell Creek Formation and its contribution to the
965 Cretaceous-Paleogene extinction: A short primer. *Cretaceous Research*, 57, 368-390.
966
967 Ficken K. J., Li B., Swain D. L., & Eglinton G. (2000). An *n*-alkane proxy for the sedimentary
968 input of submerged/floating freshwater aquatic macrophytes. *Organic Geochemistry*, 31, 745-
969 749.
970
971 Fornace K. L., Hughen K. A., Shanahan K. A., Fritz S. C., & Baker P. A. (2014). A 60,000-year
972 record of hydrologic variability in central Andes from the hydrogen isotopic composition of leaf
973 waxes in Lake Titicaca sediments. *Earth and Planetary Science Letters*, 408, 263-271
974
975 France R. L. (1995). Differentiation between littoral and pelagic food webs in lakes using stable
976 carbon isotopes. *Limnology and Oceanography*, 40 (7), 1310-1313.
977
978 Gales E., Black B., & Elkins-Tanton L. T. (2020). Carbonatites as a record of the carbon isotope
979 composition of large igneous province outgassing. *Earth and Planetary Science Letters*, 535,
980 116076.
981
982 Harris D., Horwath W. R., & Kessel C. V. (2001). Acid fumigation of soils to remove carbonates
983 prior to total organic carbon or carbon-13 isotopic analysis. *Soil Science Society of America*
984 *Journal*, 65, 1853-1856.
985

Hildebrand A. R., Penfield G. T., Kring D. A., Pilkington M., Camargo A. Z., Jacobsen S. B., & Boynton W. V. (1991). Chicxulub Crater: A possible Cretaceous/Tertiary boundary impact crater on the Yucatán Peninsula, Mexico. *Geology*, 19, 867-871.

Hull P. M., Bornemann A., Penman D. E., Henehan M. J., Norris R. D., Wilson P. A., Blum P., Alegret L., Batenburg S. J., Bown P. R., Bralower T. J., Cournede C., Deutsch A., Donner B., Friedrich O., Jehle S., Kim H., Kroon D., Lippert P. C., Loroch D., Moebius I., Moriya K., Peppe D. J., Ravizza G. E., Röhl U., Schueth J. D., Sepúlveda J., Sexton P. F., Sibert E. C., Sliwinska K. K., Summons R. E., Thomas E., Westerhold T., Whiteside J. H., Yamaguchi T., and Zachos J. C. (2020). On impact and volcanism across the Cretaceous-Paleogene boundary. *Science*, 367, 266-272.

IAEA/WMO (2015). Global Network of Isotopes in Precipitation. The GNIP Database.

Jerrett R. M., Price G. D., Grimes S. T., & Dawson A. T. (2015). A paleoclimate and paleoatmospheric record from peatlands accumulating during the Cretaceous-Paleogene boundary event, Western Interior Basin, Canada. *GSA Bulletin*, 127, 1564-1582.

Keeley J. E. & Sandquist D. R. (1992). Carbon: freshwater plants. *Plant, Cell, and Environment*, 15, 1021-1035.

Kupsch W. O. (1957). Frenchman Formation of Eastern Cypress Hills, Saskatchewan, Canada. *Bulletin of the Geological Society of America*, 68, 413-420.

Labandeira C. C., Johnson K. R., & Lang P. (2002). Preliminary assessment of insect herbivory across the Cretaceous-Tertiary boundary: Major extinction and minimal rebound. *Geological Society of America Special Paper*, 361, 297-327.

Liu H. & Liu W. (2016). *n*-Alkane distributions and concentrations in algae, submerged plants and terrestrial plants from the Qinghai-Tibetan Plateau. *Organic Geochemistry*, 99, 10-22.

Liu H., Liu Z., Zhao C., & Liu W. (2019). *n*-Alkyl lipid concentrations and distributions in aquatic plants and their individual δD variations. *Science China Earth Science*, 62, https://doi.org/10.1007/s11430-019-9370-8

Lomax B., Beerling D. Upchurch G Jr, & Otto-Bliesner B. (2001). Rapid (10-yr) recovery of terrestrial productivity in a simulation study of the terminal Cretaceous impact event. *Earth and Planetary Science Letters*, 192, 137-144.

Macleod K. G., Quinton P. C., Sepúlveda J., & Negra M. H. (2018). Postimpact earliest Paleogene warming shown by fish debris oxygen isotopes (El Kef, Tunisia). *Science*, 360, 1467-1469.

Markovetz A. J., Cazin J. Jr., & Allen J. E. (1968). Assimilation of alkanes and alkenes by fungi. *Applied Microbiology*, 16, 487-489.

Maruoka T., Koerberl C., & Bohor B. F. (2007). Carbon isotopic compositions of organic matter across continental Cretaceous–Tertiary (K-T) boundary sections: Implications for paleovenvironment after the K-T extinction event. *Earth and Planetary Science Letters*, 253, 226-238.

Mason E., Edmonds M., & Turchyn A. V. (2017). Remobilization of crustal carbon may dominate volcanic arc emissions. *Science*, 357, 290-294.

McIver E. E. (1989). Fossil Flora of the Paleocene Ravenscrag Formation, Southwestern Saskatchewan, Canada. *University of Saskatchewan*.

McIver E. E. (1999). Paleobotanical evidence for ecosystem disruption at the Cretaceous-Tertiary boundary from Wood Mountain, Saskatchewan, Canada. *Canadian Journal of Earth Sciences*, 36, 775-789.

McIver E. E. (2002). The paleoenvironment of *Tyrannosaurus rex* from southwestern Saskatchewan, Canada. *Canadian Journal of Earth Sciences*, 39, 207-221.

McElwain J. C. & Punyasena S. W. (2007). Mass extinction events and the plant fossil record. *TRENDS in Ecology and Evolution*, 22, 548-557.

McFarlin J. M., Axford Y., Masterson A. L., & Osburn M. R. (2019). Calibration of modern sedimentary $\delta^{2}H$ plant wax-water relationships in Greenland lakes. *Quaternary Science Reviews*, 225, [105978]. https://doi.org/10.1016/j.quascirev.2019.105978.

Moore N., Arima E., Walker R., & Silva R. R. (2007). Uncertainty and the changing hydroclimatology of the Amazon. *Geophysical Research Letters*, 34, doi:10.1029/2007GL030157.

Nichols, G. (2013). Sedimentology and Stratigraphy. Somerset: Wiley.

Niedermeyer E. M., Schefuß E., Sessions A. L., Mulitza S., Mollenhauer G., Schulz M., & Wefer G. (2010). Orbital- and millennial-scale changes in the hydrologic cycle and vegetation in the western African Sahel: insights from individual plant wax δD and $\delta^{13}C$. *Quaternary Science Reviews*, 29, 2996-3005.

Norris R. D., Huber B. T., & Self-Trail J. (1999). Synchroneity of the K-T oceanic mass extinction and the meteorite impact: Blake Nose, western North Atlantic. *Geology*, 27, 419-422.

Odgaard B. V. (1999). Fossil pollen as a record of past biodiversity. *Journal of Biogeography*, 26, 7-17.

1074 Petersen S. V., Dutton A., & Lohmann K. C. (2016). End-Cretaceous extinction in Antarctica
1075 linked to both Deccan volcanisms and meteorite impact via climate change. *Nature*
1076 *Communications*, DOI: 10.1038/ncomms12079.-a
1077
1078 Petersen S. V., Tabor C. R., Lohmann K. C., Poulsen C. J., Meyer K. W., & Carpenter S. J.
1079 (2016). Temperature and salinity of the Late Cretaceous Western Interior Seaway. *Geology*, 44,
1080 903-906.-b
1081
1082 Polissar P. J. & D'Andrea W. J. (2014). Uncertainty in paleohydrologic reconstructions from
1083 molecular δD values. *Geochimica et Cosmochimica Acta*, 129, 146-156.
1084
1085 Pope K. O., Baines K. H., Ocampo A. C., & Ivanov B. A. (1994). Impact winter and the
1086 Cretaceous/Tertiary extinctions: Results of a Chicxulub asteroid impact model. *Earth and*
1087 *Planetary Science Letters*, 128, 719-725.
1088
1089 Rach O., Brauer A., Wilkes H., & Sachse D. (2014). Delayed hydrological response to
1090 Greenland cooling at the onset of the Younger Dryas in western Europe. *Nature Geoscience*, 7,
1091 109-112.
1092
1093 Redman C. M., Gardner J. D., Scott C. S., & Braman D. R. (2015). Geological setting of
1094 vertebrate microfossil localities across the Cretaceous-Paleogene boundary in southwestern
1095 Saskatchewan, Canada. *Canadian Journal of Earth Sciences*, 52, 846-862.
1096

1097 Renne P. R., Deino A. L., Hilgen F. J., Kuiper K. F., Mark D. F., Mitchel III W. S., Morgan L.
1098 E., Mundil R., & Smit J. (2013). Time scales of critical events around the Cretaceous-Paleogene
1099 boundary. *SCIENCE*, 339, 684-687.
1100
1101 Rozanski K., Araguás- Araguás L., Gonfiantini R. (1993). Isotopic Patterns in Modern Global
1102 Precipitation. *Climate change in continental isotopic records*, 78, 1-36.
1103
1104 Sachse D., Billault I., Bowen G. J., Chikaraishi Y., Dawson T. E., Feakins S. J., Freeman K. H.,
1105 Magill C. R., McInerney F. A., van der Meer M. T. J., Polissar P., Robins R. J., Sachs J. P.,
1106 Shmidt H. L., Sessions A. L., White J. W. C., West J. B., & Kahmen A. (2012). Molecular
1107 Paleohydrology: Interpreting the Hydrogen-Isotopic Composition of Lipid Biomarkers from
1108 Photosynthesizing Organisms. *Annual Review of Earth and Planetary Sciences*, 40, 221-249.
1109
1110 Schoene B., Eddy M. P., Samperton K. M., Keller C. B., Keller G., Adatte T., & Khadri S. F. R.
1111 (2019). U-Pb constraints on pulsed eruption of the Deccan Traps across the End-Cretaceous mass
1112 extinction. *Science*, 363, 862-866.
1113
1114 Sepúlveda J., Alegret L., Thomas E., Haddad E., Cao C., & Summons R. E. (2019). Stable
1115 isotope constraints on marine productivity across the Cretaceous-Paleogene mass extinction.
1116 *Paleoceanography and Paleoclimatology*, 34, 1195-1217.
1117

Setegn S. G., Rayner D., Melesse A. M., Dargahi B., & Srinivasan R. (2011). Impact of climate change on the hydroclimatology of Lake Tana Basin, Ethiopia. *Water Resources Research*, 74, doi:10.1029/2010WR009248.

Smit J. & Hertogen J. (1980). An extraterrestrial event at the Cretaceous-Tertiary boundary. *Nature*, 285, 198-200.

Sprain C. J., Renne P. R., Vanderkluysen L., Pande K., Self S., & Mittal T. (2019). The eruptive tempo of Deccan volcanism in relation to the Cretaceous-Paleogene boundary. *Science*, 363, 866-870.

Srivasta S. K. (1981). Fossil pollen genus Kurtzipites Anderson. *Journal of Palaeontology*, 55, 868-879.

Super J. R., Chin K., Pagani M., Li H., Tabor C., Harwood D. M., & Hull P. M. (2018). Late Cretaceous climate in the Canadian Arctic: Multi-proxy constraints from Devon Island. *Palaeoceanography, Palaeoclimatology, Palaeoecology*, 504, 1-22.

Sweet A. R., & Braman D. R. (1992). The K-T boundary and contiguous strata in western Canada: interactions between paleoenvironments and palynological assemblages. *Cretaceous Research*, 13, 31-79.

Sweet A. R., Braman D. R., & Lerbekmo J. F. (1999). Sequential palynological changes across the composite Cretaceous-Tertiary (K-T) boundary claystone and contiguous strata, western Canada and Montana, U.S.A. *Canadian Journal of Earth Sciences*, 36, 743-768.

Therrien F., Eberth D. A., Braman D. R., & Zelenitsky (2007). High-resolution organic carbon isotope record across the Cretaceous-Tertiary boundary in south-central Alberta: implications for the post-impact recovery rate of terrestrial systems and use of $\delta^{13}C$ as a boundary marker. *Canadian Journal of Earth Sciences*, 44, 529-542.

Tierney J. E. & deMenocal P. B. (2013). Abrupt shifts in Horn of Africa hydroclimate since the last glacial maximum. *Science 342.6160*, 843-846.

Vajda V., Raine J. I., & Hollis C. J. (2001). Indication of global deforestation at the Cretaceous-Tertiary boundary be New Zealand fern spike. *Science*, 294, 1700-1702.

Vajda V. & Raine J. I. (2003). Pollen and spores in marine Cretaceous/Tertiary boundary sediments at mid-Waipara River, North Cantebury, New Zealand. *New Zealand Journal of Geology & Geophysics*, 46, 255-273.

Vajda V. & McLoughlin S. (2007). Extinction and recovery patterns of the vegetation across the Cretaceous-Paleogene boundary – a tool for unraveling the causes of the end-Permian mass-extinction. *Review of Paleobotany and Palynology*, 144, 99-112.

1163 Varricchio, D. J., C. Koeberl, R. F. Raven, W. S. Wolbach, W. C. Elsik, and D. P. Miggins.
1164 (2010). Tracing the Manson impact event across the Western Interior Cretaceous Seaway. P. in
1165 Large Meteorite Impacts and Planetary Evolution IV. *Geological Society of America Special*
1166 *Paper*, 465, 269-299.
1167
1168 Vellekoop J., Sluijs A., Smit J., Schouten S., Weijers J. W. H., Sinninghe Damsté J. S., &
1169 Brinkhuis H. (2014). Rapid short-term cooling following the Chicxulub impact at the
1170 Cretaceous-Paleogene boundary. *PNAS*, 111, 7537-7541.
1171
1172 Vellekoop J., Esmeray-Senlet S., Miller K. G., Browning J. V., Sluijs A., van der Schootbrugge
1173 B., Sinninghe Damasté J. S., & Brinkhuis H. (2016). Evidence for Cretaceous-Paleogene
1174 boundary bolide "impact winter" conditions from New Jersey, USA. *Geology*, 44, 619-622.
1175
1176 Vellekoop J., Woelders L., van Helmond N. A. G. M., Galeotti S., Smit J., Slomp C. P.,
1177 Brinkhuis H., Claeys P., & Speijer R. P. (2018). Shelf hypoxia in response to global warming
1178 after the Cretaceous-Paleogene boundary impact. *Geology*, 46, 683-686.
1179
1180 Walls R. A., Mountjoy E. W., & Fritz P. (1979). Isotopic composition and diagenetic history of
1181 carbonate cements in Devonian Golden Spike reef, Alberta, Canada. *Geological Society of*
1182 *America Bulletin*, 90, 963-982.
1183

Wilf P., Johnson K. R., & Huber B. T. (2003). Correlated terrestrial and marine evidence for global climate changes before mass extinction at the Cretaceous-Paleogene boundary. *PNAS*, 100, 599-604.

Wolfe J. A. & Upchurch Jr. G. R. (1986). Vegetation, climactic, and floral changes at the Cretaceous-Tertiary boundary. *Nature*, 324, 148-152.

Yamamoto S., Hasegawa T., Tada R., Goto K., Rojas-Consuegra R., Díaz-Otero C., García-Delgado D. E., Yamamoto S., Sakuma H., & Matsui T. (2010). Environmental and vegetational changes recorded in sedimentary leaf wax *n*-alkanes across the Cretaceous-Paleogene boundary at Loma Capiro, Central Cuba. *Palaeogeography, Palaeoclimatology, Palaeoecology*, 295, 31-41.

Zhao B., Zhang Y., Huang X., Qiu R., Zhang Z., & Meyers P. A. (2018). Comparison of *n*-alkane molecular, carbon and hydrogen isotope compositions of different types of plants in the Dajiuhu peatland, central China. *Organic Geochemistry*, 124, 1-11.


Figure 1, comprising of a map showcasing the
W110°
W108°
W106°
W104°
W102°
N52°
N51°
N50°
N49°
Saskatchewan
Highway 37
Chambery Coulee
Google Earth
© 2018 Google
Image Landsat / Copernicus
100 km
N

Figure 2, comprising of three field photos with annotations

a)

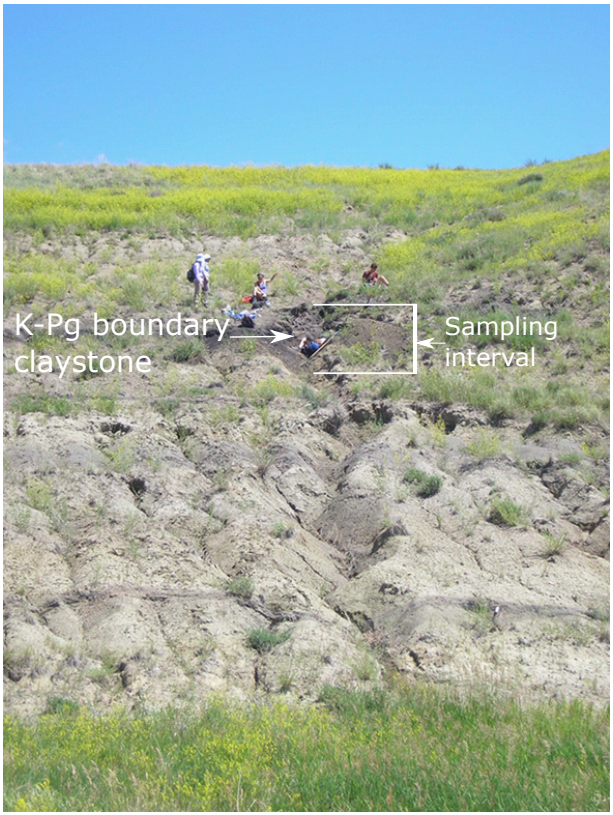

b)

c)

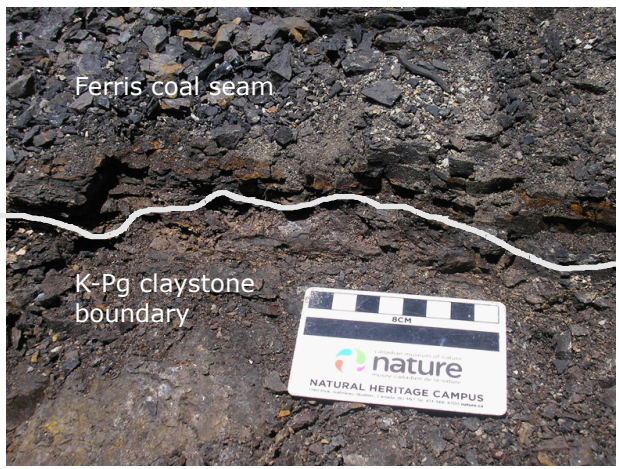

Figure 3, comparing the bulk δ13C and organic carbon percentages from both sites

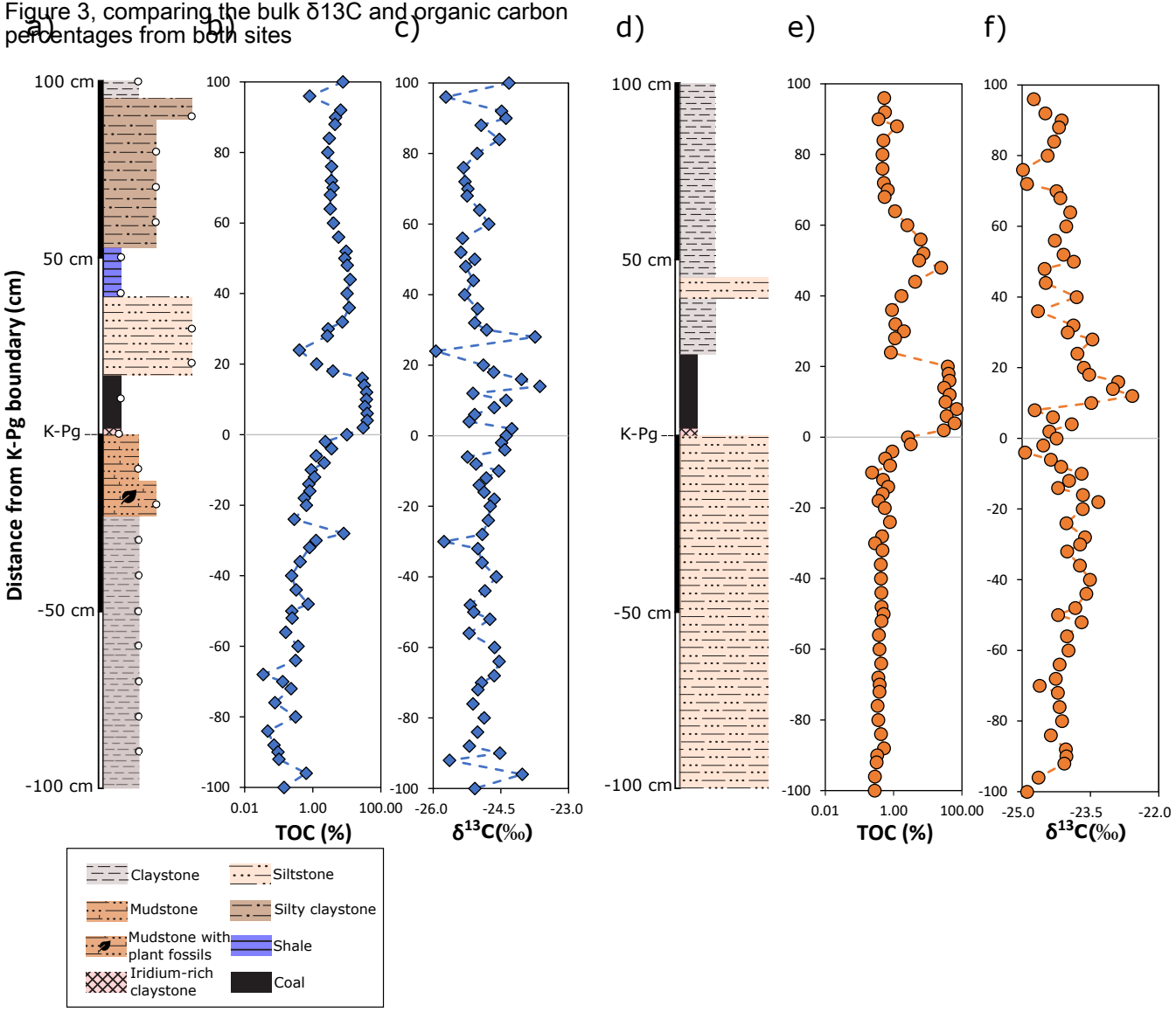

Figure 4, a comparison of several measurements for the HW37 data

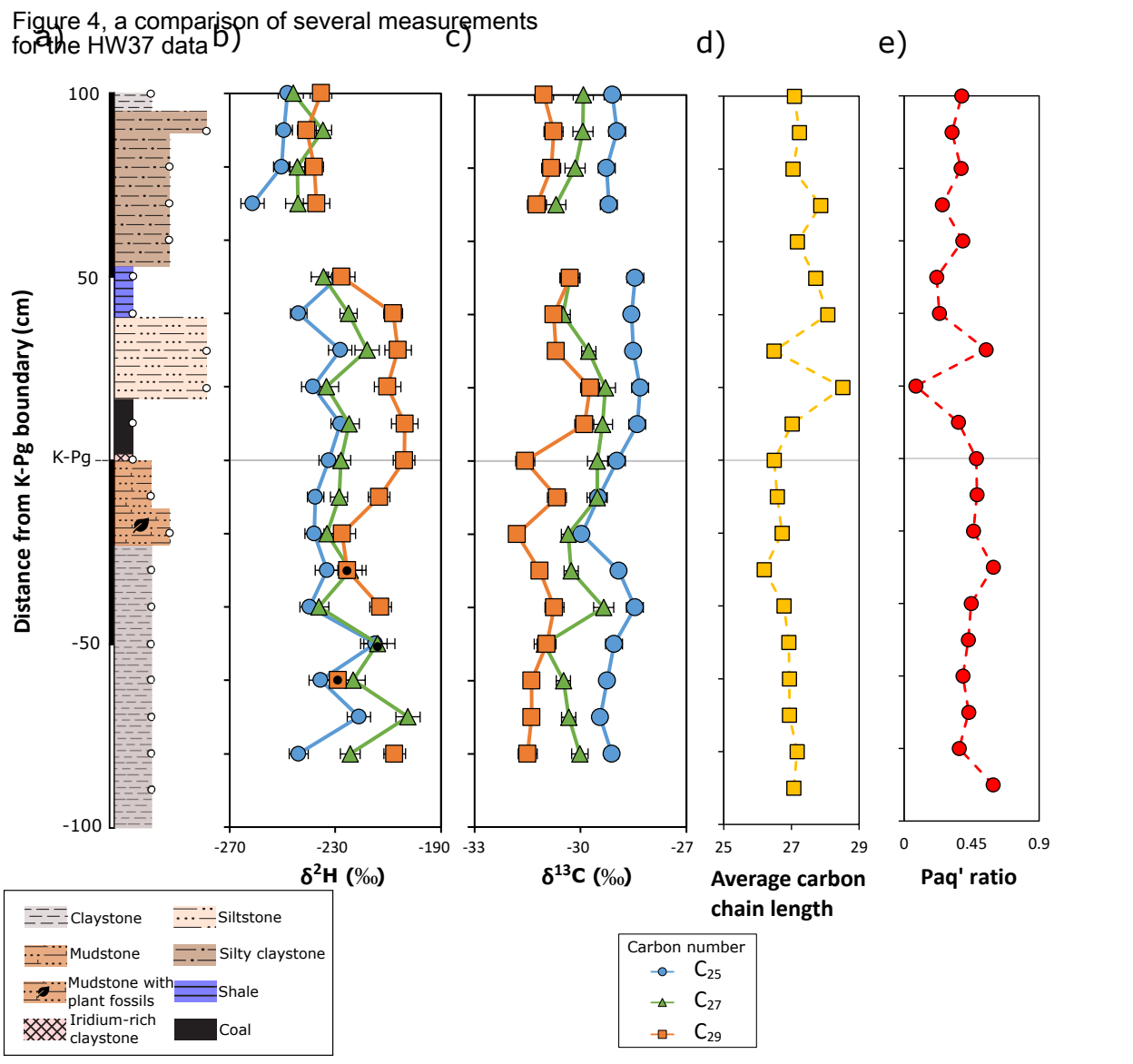

Figure 5, a comparison of several measurements for the CC data

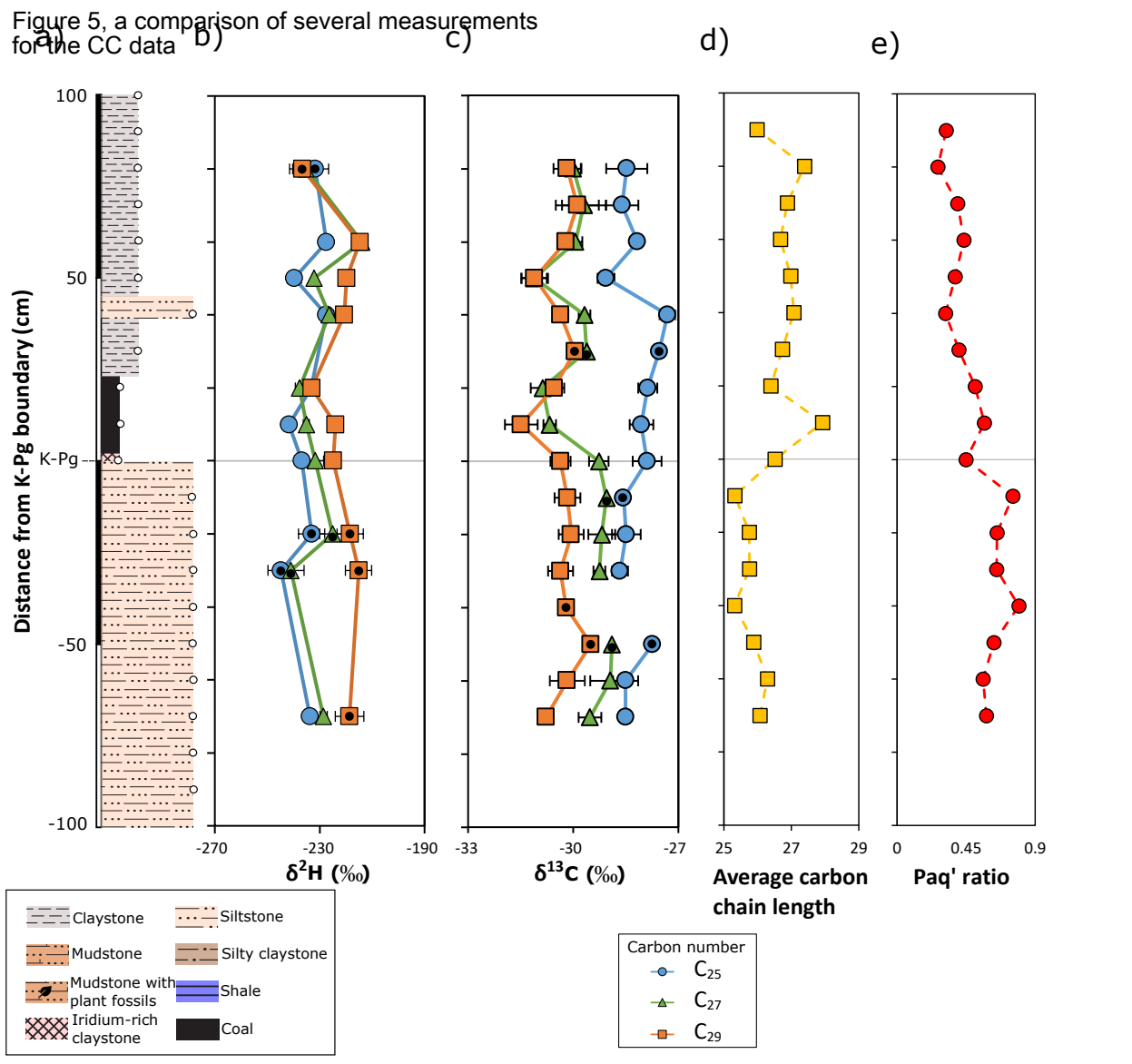

Figure 6: results for the modeled δ13C

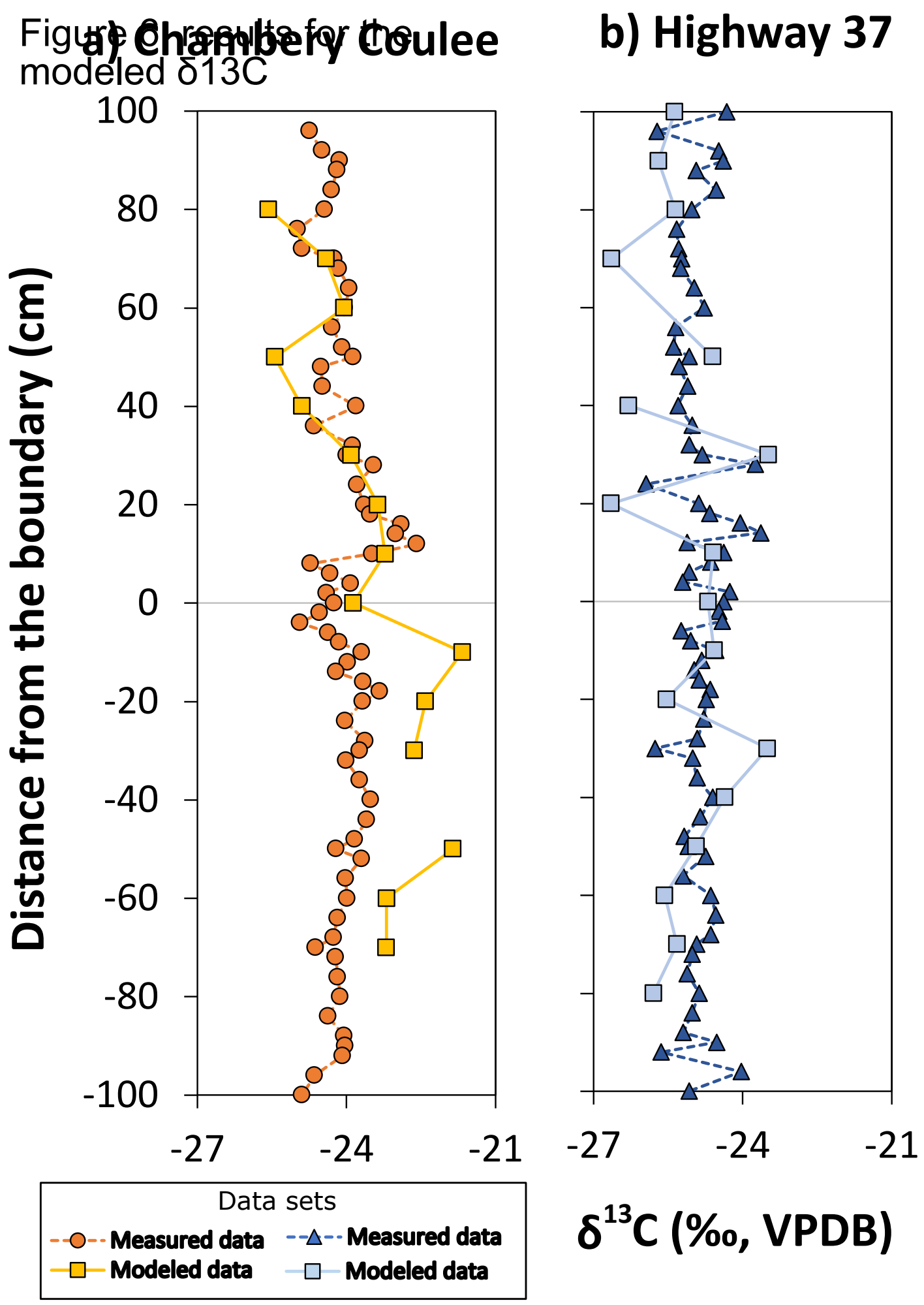

Figure 7. comparing the measurements of chain

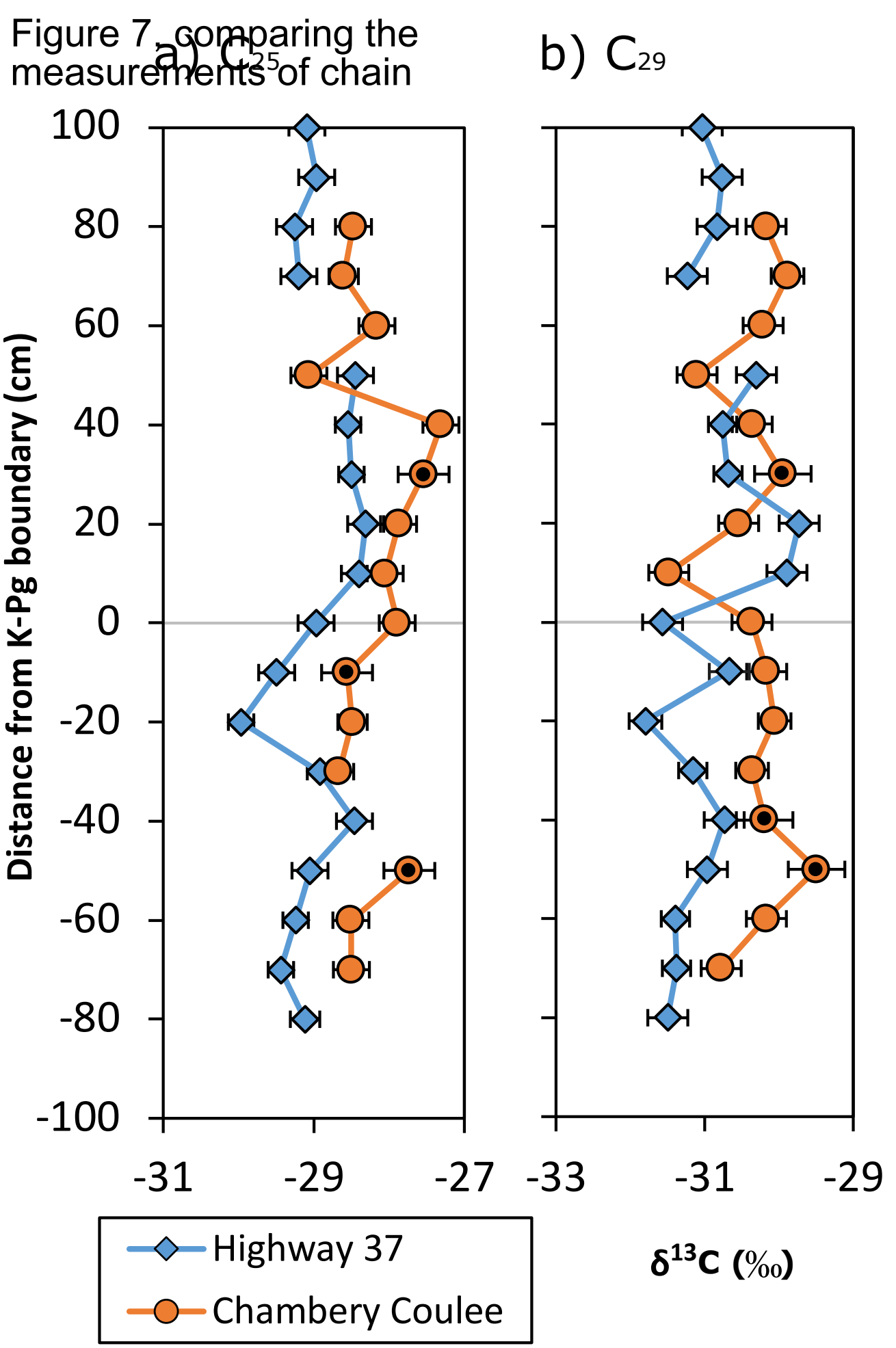

Table of bulk δ13C and organic carbon percentage

Table of Paq' and ACL results

Table of hydrogen stable isotope measurements from Chambery Coulee

Table of hydrogen stable isotope measurements from Highway 37

Table of carbon stable isotope measurements from Chambery Coulee

Table of carbon stable isotope measurements from Highway 37

Declaration of interests

☒ The authors declare that they have no known competing financial interests or personal relationships that could have appeared to influence the work reported in this paper.

☐The authors declare the following financial interests/personal relationships which may be considered as potential competing interests:

Supplementary table on lab standards

Supplementary table on n values and standard deviation for hydrogen stable isotope measurements from Chambery Coulee

Supplementary table on n values and standard deviation for hydrogen stable isotope measurements from Highway 37

Supplementary table on n values and standard deviation for carbon stable isotope measurements from Chambery Coulee

Supplementary table on n values and standard deviation for carbon stable isotope measurements from Highway 37

Captions for 7 figures

Captions for 6 tables